DIPLOMARBEIT

Automatic Segmentation of Contrast Enhanced Cardiac MRI for Myocardial Perfusion Analysis

ausgeführt am Institut für Computergraphik und Algorithmen
der Technischen Universität Wien
in Kooperation mit dem
VRVis, Zentrum für Virtual Reality und Visualisierung

unter Anleitung von
Ao.Univ.Prof. Dipl.-Ing. Dr.techn. Eduard Gröller
in Kooperation mit
Dipl.-Math. Dr.techn. Katja Bühler
Dipl.-Ing. Sebastian Zambal

durch
Andreas Schöllhuber
Matr. Nr.: 0226055
A - 1040 Wien, Wiedner Gürtel 24

Wien, im März 2008

Abstract

Cardiovascular diseases are the major cause of death in the developed world. About half of these are due to ischemia heart diseases. The high death rate caused by coronary artery diseases increases the need for preliminary detection. Perfusion magnetic resonance imaging has turned out to be very promising for this purpose. A contrast agent is injected intravenously to visualize the perfusion. Due to the extremely time-consuming manual analysis of these relatively large datasets, efforts for automatic approaches have been introduced. Most of these proposed methods focus on parts of the analysis process. The present thesis identifies four steps for an automatic analysis approach: localization of the heart, suppression of motion artifacts, segmentation of the myocardium, and perfusion analysis.

This thesis presents a method covering all these subtasks in an automatic manner with no need for any user interaction. First the acquired MR images are analyzed to roughly detect the heart. A registration step compensates motion artifacts based on the breathing of the patient. The segmentation step provides the contour of the myocardium at every time step. Based on these segmentations the perfusion is quantified.

This thesis gives a detailed description of the implementation. Furthermore the algorithm was tested on 11 datasets. The obtained results are presented and discussed. Inspection of the results indicates that this method is very promising for an efficient perfusion analysis.

Kurzfassung

Die häufigsten Todesfälle in den Industrienationen basieren auf Erkrankungen des Herz-Kreislauf-Systems. Davon entfallen in etwa die Hälfte auf ischämische Herzerkrankungen. Die hohe Sterblichkeitsrate bei Herzkranzgefäßerkrankungen macht eine effiziente Früherkennung solcher Krankheiten nötig. Hierfür hat sich die Perfusionsdiagnostik mittels Magnet-Resonanz-Tomographie (MRT) als sehr vielversprechend herausgestellt. Um die Durchblutung der Herzkranzgefäße sichtbar zu machen, wird ein Kontrastmittel intravenös appliziert. Da die manuelle Analyse solch großer Datenmengen sehr zeitaufwändig ist, wird eine Automatisierung angestrebt. Derzeit existieren allerdings nur Teillösungen einer automatischen Analyse. In dieser Diplomarbeit wurden vier Schritte für die Implementierung einer solchen Anwendung identifiziert: Lokalisierung des Herzens in den Daten, Unterdrückung bzw. Kompensation von Bewegungsartefakten, Segmentierung des Herzmuskels sowie die Analyse der Perfusion des Herzmuskels.

Im Rahmen dieser Diplomarbeit wurde eine vollständig automatisierte Methode zur Analyse von Perfusionsdaten entwickelt. Diese Methode berücksichtigt dabei alle oben angeführten Teilbereiche: Zu Beginn wird durch Datenanalyse das Herz grob lokalisiert. Ein nachfolgender Registrierungsschritt kompensiert die durch die Atmung des Patienten entstandenen Bewegungsartefakte. Im Segmentierungsschritt wird die Kontur des Herzmuskels in jedem Bild bestimmt. Abschließend wird die Perfusion im segmentierten Bereich bestimmt und quantifiziert.

Diese Diplomarbeit liefert eine detaillierte Beschreibung der Implementierung. Der vorgeschlagene Algorithmus wurde an elf Datensätzen getestet. Die erzielten Ergebnisse werden präsentiert und diskutiert. Eine Kontrolle der Ergebnisse läßt darauf schließen, dass die vorgestellte Methode zur automatischen Analyse von Perfusionsdaten geeignet ist.

Acknowledgments

I would like to thank Professor Eduard Gröller for accepting me as his master student and reviewing my work.

This master thesis was carried out at the VRVis Center for Virtual Reality and Visualization in Vienna. I would like to thank the VRVis for supporting my work and providing me the necessary working facilities. I would like to thank AGFA Health Care for their financial support of this thesis.

I thank Katja Bühler for giving me the chance to write my thesis at the VRVis.

I want to express my great gratitude to Sebastian Zambal. This work would not have been possible without him. He introduced me into the topic, supported me with literature, gave me important hints during many interesting discussions, and he always encouraged me in doing my work.

Finally I would like to thank my girlfriend Gudrun for her support. Especially I would like to thank my parents Theresia and Georg Schöllhuber who always did their best in supporting me.

Contents

List of Figures

List of Tables

Chapter 1

Introduction

Cardiovascular diseases are the major cause of death (∼40%, [Austria, 2006]). About half of these are due to ischemia heart diseases. The high death rate caused by coronary artery diseases leads to an increased demand of preliminary detection. Myocardial perfusion diagnosis has turned out as a promising tool therefore. This method of diagnosis allows to identify ischemic areas of the myocardium. Several imaging methods for myocardial perfusion exist: Single Photon Emission Computer Tomography (SPECT), Positron Emission Tomography (PET), Myocardial Contrast Echocardiography (MCE), and Perfusion Magnetic Resonance Imaging (Perfusion MRI). Perfusion MRI has turned out as a very promising method. Unlike SPECT and PET, MRI does not work with radiation. Additional, attenuation problems known from MCE do not occur with MRI.

By perfusion MRI the distribution of an injected contrast agent is observed over a time period (figure 1.1). This distribution is an indicator for the perfusion. Many different measurements for quantifying the perfusion exist. All these measurements are based on the progression of the contrast agent in the myocardium. Manual analysis of the huge perfusion datasets (up to 70 time steps and 5 slices per time step) is a very time-consuming task. Furthermore, distinguishing between areas

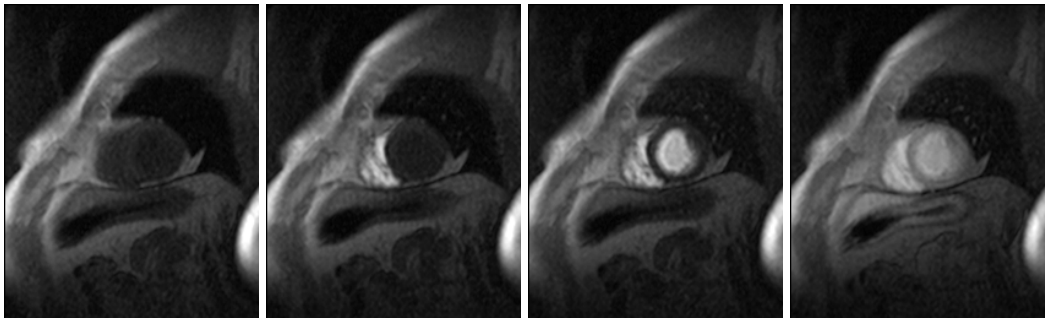

(a) (b) (c) (d)

Figure 1.1: Perfusion MRI Sequence. At the beginning no contrast agent is observed (a). After some seconds it appears in the right ventricle (b). Then it appears in the left ventricle (c) and finally in the myocardium (d).

of normal and ischemic tissue is very challenging and an expert is necessary for analysis of the image data. So the request for an automatic analysis of these datasets has risen. This thesis presents a method for an automatic segmentation and analysis of perfusion MRI datasets without any human interaction.

1.1 Problem Statement

Perfusion MRI datasets are mostly four dimensional (3D + time). Manual analysis of these huge datasets is very time consuming.

This thesis presents an automatic method to analyze these datasets. An automatic analysis method has to deal with several problems:

- *Operator:* No standards for acquiring MRI datasets are available. Therefore several parameters for adjusting a MR equipment exist which may lead to varying results.
- *Patient:* During the acquisition period the patient is asked to hold the breath. However, not all patients are able to do so during the whole long acquisition period (up 40 seconds and more). This causes motion artifacts based on breathing which have to be detected and compensated.
- *Anatomy:* The arrangement of coronary arteries varies from patient to patient.
- *Pathology:* A pathological heart may have another appearance than a healthy one.
- *Imaging:*
  - Poor spatial resolution
  - Noise
  - The poor contrast between myocardium and surrounding tissues makes it difficult to distinguish between them.
  - The Contrast Agent leads to varying intensities.

This work addresses all of these problems and presents a method to analyze the perfusion in the myocardium. At the beginning a region of interest (ROI) covering the left cardiac ventricle (LV) is determined. Rigid image registration is performed to minimize motion artifacts. The myocardium is segmented at all time steps. Finally the contrast agent distribution in the myocardium is analyzed based on the segmentation.

1.2 Thesis Overview

This thesis shows a fully automatic method for the analysis of perfusion MRI datasets.

First a detailed overview of the anatomy, physiology, and pathology of the human heart and the coronary arteries is given in chapter 2. Furthermore this overview includes therapeutic interventions and early diagnosis methods for coronary artery diseases. Additional an overview of perfusion MRI and analysis methods for the perfusion are given.

Chapter 3 shows a summary of related work dealing with perfusion MRI datasets. Furthermore related work dealing with non-perfusion MRI datasets is shown which can be adapted to perfusion MRI datasets by considering some restrictions.

Chapter 4 gives a detailed description of a method for a fully automatic analysis of perfusion MRI datasets. This chapter is divided into the four major tasks of the analysis process:

- ROI Selection
- Registration
- Segmentation
- Analysis

Chapter 5 illustrates the results obtained from the presented method. This chapter shows the results separately for the four tasks and gives a performance analysis.

Finally a conclusion and a discussion for future work is given in chapter 6.

Chapter 2

Medical Background

For a better understanding how perfusion images are generated and why the analysis is so important an overview of the anatomy, physiology and pathophysiology of the heart is given in this chapter. Furthermore an overview of perfusion analysis is given.

2.1 Anatomy

Heart

The heart is the pump of the human body. It is a rhythmically contracting muscle which pumps blood all over the body supplying all body parts and organs with oxygen. It is shaped like an upside down cone with rounded off apex. The anatomic axis of the heart looks sloping down. It runs relatively to the patient from the top right back side to the bottom left front side of the thorax. As illustrated in figure 2.1 the heart is in the direct neighborhood of the lung. Due to breathing both position and shape of the heart are changing. The weight of the heart is about 250-300g for women and about 300-350g for men [Lippert *et al.*, 2002]. The size corresponds approximately to that of the fist.

The heart is divided by the septum into a left and a right part. Every part consists of two chambers. The smaller chamber is called atrium and the bigger one ventricle. The ventricle and the atrium are separated by an atrioventricular valve. In addition both chambers are closed by a valve. These valves define the flow direction of the blood and prevent a backward flow. The inner surface of the ventricles is irregular and can be covered by spongy muscle bars (trabeculae carneae). In addition the papillary muscles extend into the ventricle. Figure 2.2 shows a schematic illustration of a cross-section of the heart.

Cardiac Wall

The cardiac wall consists of three layers: endocardium (inner layer), myocardium (center layer) and epicardium (outer layer). The thickness of the cardiac wall varies

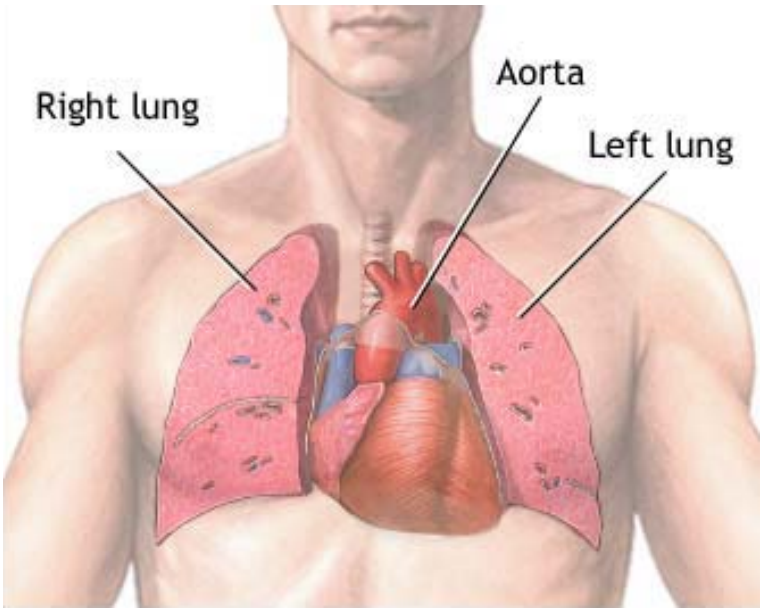

Figure 2.1: Heart Location. [refer health, 2008] Spatial relation of the heart and the lung.

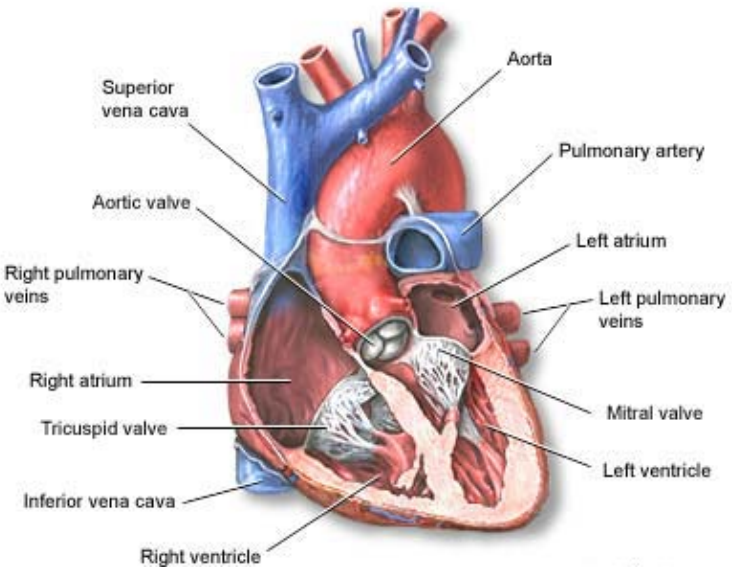

Figure 2.2: Cross-section of the heart. [refer health, 2008]

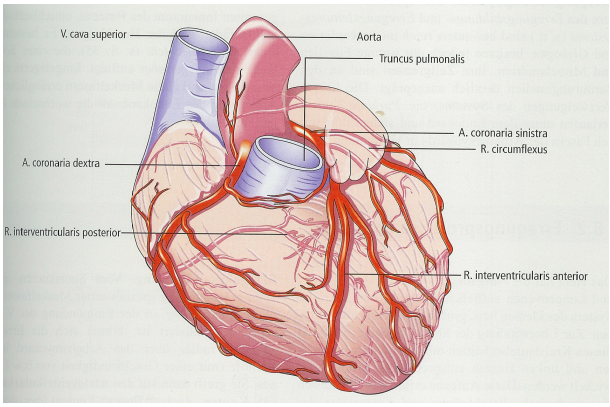

Figure 2.3: Coronary arteries. [Thews *et al.*, 1999] Schematic illustration of the coronary arteries.

for the four chambers. The cardiac wall of the ventricles is thicker than the wall of the atria. Furthermore the cardiac wall of the left ventricle is thicker than the wall of the right ventricle. This is a consequence of the higher activity of the left ventricle which pumps the blood into the circulation. The myocardium is the muscle layer of the cardiac wall and therefore it represents largest part of its mass.

The heart muscle fibers are arranged facilitating concentrical contraction. This concentrical contraction maintains the circulation of blood. The myocardium requires large amounts of oxygen and nutrients. These requirements are supplied by the coronary arteries. To keep the heart fully functional an adequate blood circulation (perfusion) of the coronary arteries is required.

Coronary Arteries

The heart itself is supplied with oxygen by the coronary arteries which have its origin in the aorta. They are divided into a left (A. coronaria sinistra) and a right (A. coronaria dextra) coronary artery. The left coronary artery splits into Ramus circumflexus and Ramus interventricularis anterior. Both branches achieve approximately the same thickness as the right coronary artery.

The left coronary artery provides about 80% of the total heart supply [Thews *et al.*, 1999]. It supplies the bigger part of the left ventricle wall, the left atrium wall, a small part of the right ventricle wall, and large areas of the septum. The right coronary artery supplies the bigger part of the right ventricle wall, right atrium wall, and a small part of the septum and the left ventricle wall. A schematic illustration of the coronary arteries is given in figure 2.3. The venous system is like the artery system. For diagnostic purpose of coronary artery diseases both branches of the left coronary artery are considered as separate vessels. Therefore coronary artery diseases are divided into one, two, or three vessels diseases. The distribution pattern of the coronary arteries have a high variation between different persons. Accordingly an assignment of vessels to myocardial areas is only possible to a limited extent.

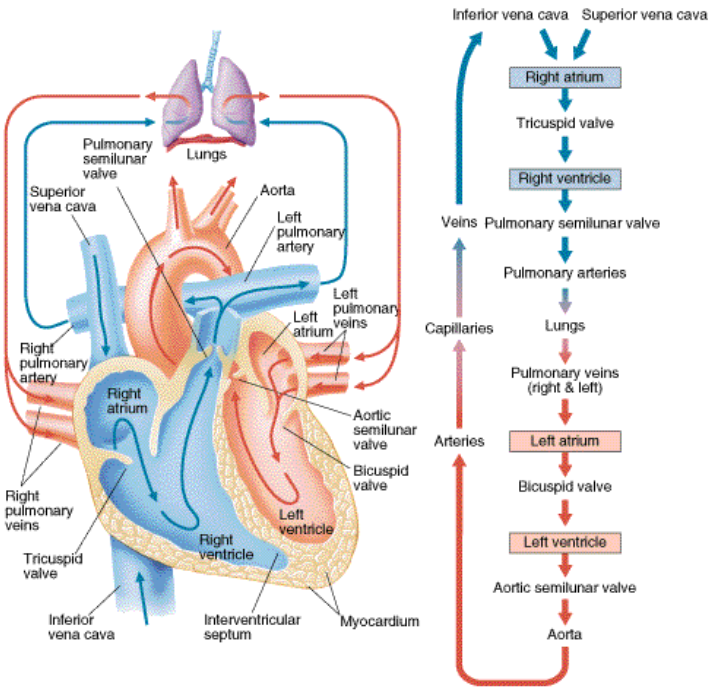

Figure 2.4: Schematic illustration of the blood flow. [Allyn & Bacon, 2004]

2.2 Physiology

The blood flow is generated by rhythmic contraction and relaxation of the heart muscle. The direction of blood flow is regulated by the valves. First the atrium contracts and the blood is pushed into the ventricle. Then the ventricle contracts and ejects blood into the arteries. In one cycle the oxygen poor blood flows from the cava (vena cava superior and vena cava inferior) into the right atrium. By contraction of the right atrium it is pumped into the right ventricle which ejects the blood into the truncus pulmonalis. In this vessel the blood flows to the lung and becomes oxygenated. After passing the four lung veins the blood enters the left atrium. It is pumped into the left ventricle and afterward it is ejected into the aorta. Starting from the aorta the oxygen rich blood reaches all regions of the human body. The blood flow is illustrated in figure 2.4.

Under stress e.g. physical strain more energy and thereby more oxygen is needed by muscles and organs. For providing more oxygen heartbeat and stroke volume have to increase. Accordingly the heart has to work harder and needs more oxygen too. To compensate this requirement the coronary arteries dilate. The coronary reserve measures the possibility of compensating oxygen requirement. It is defined as [Thews *et al.*, 1999]:

$$coronary\_reserve = \frac{O_2\_usage_{max} - O_2\_usage_{act}}{O_2\_usage_{act}} \tag{2.1}$$

Whereas $O_2\_usage_{max}$ is the maximal possible and $O_2\_usage_{act}$ the actual available O_2_usage. A fully adaptive heart under rest conditions has a coronary artery reserve of about 4.5.

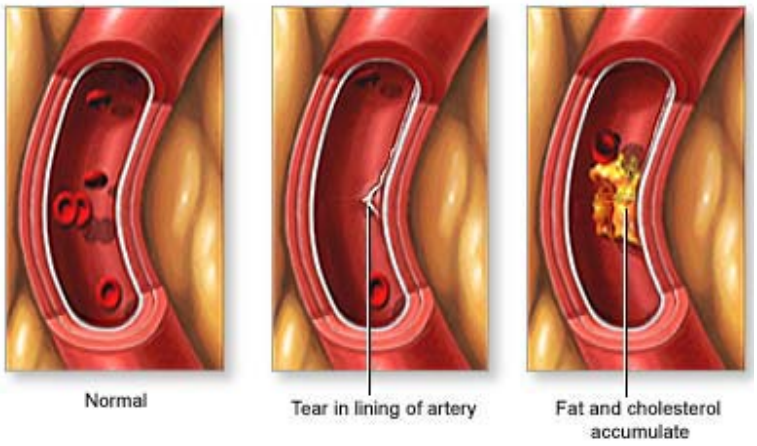

Figure 2.5: Progressive build-up of Plaque. [refer health, 2008]

2.3 Pathophysiology

Like other arteries coronary arteries can get arteriosclerosis. This is called a coronary artery disease. Arteriosclerosis is an accumulation of plaque at the vessel wall (figure 2.5). This accumulation causes a narrowing of the vessel and leads to reduced blood flow. The coronary reserve offers a compensation of this reduced blood flow. It is possible to compensate a stenosis of 85-90% under rest and a stenosis of 50-85% under stress conditions [Thews *et al.*, 1999]. If the reduction of the coronary flow reserve is too large no more compensation is possible. Risk factors for coronary artery diseases are:

- hypercholesterolemia
- smoking
- hypertension
- overweight
- tautness and stress
- sleep apnea
- heritable handicap
- diabetes

By a coronary artery disease a imbalance between delivered and needed oxygen may occur. Such a imbalance leads to angina pectoris which is classified into four types [Thews *et al.*, 1999]:

- stable angina pectoris

- unstable angina pectoris
- rest angina pectoris
- mute myocardial ischemia

Symptoms for an angina pectoris [Pschyrembel, 2002] are a suddenly beginning pain in the chest radiating to the left shoulder, arm, neck, hand, and back. Often a tightness in the chest combined with choking fit and dyspnea to the point of agony occur.

The characteristic of a stable angina pectoris is that the symptoms are stress-dependent. For unstable angina pectoris the symptoms sometimes occur at stress but can occur at rest too. If the symptoms occur already at rest it is called rest angina pectoris. Sometimes it is possible that a bad blood circulation of the heart does not cause any specific symptoms. This is called mute myocardial ischemia.

Angina pectoris is the preliminary stage of a heart attack. A heart attack has similar symptoms like the angina pectoris. Unlike an angina pectoris in case of a heart attack the artery is completely barred (e.g. by a thrombus). So the imbalance of delivered and needed oxygen becomes that big that an irreversible myocardial damage occurs which leads to necrosis. (A necrosis is an accidental death of cells.) The size of the necrosis depends on the area which was supplied by the blocked vessel. Early complications of a heart attack are [Thews *et al.*, 1999]:

- cardiac arrhythmias
- mechanical collapse of the myocardium
- mitral regurgitation

Cardiac arrhythmias may cause cardiac death based by ventricular fibrillation. A mechanical collapse of the myocardium may cause a pulmonary edema or a cardiac shock. Later complications of a heart attack are [Thews *et al.*, 1999]:

- myocardial aneurysm
- myocardial rupture
- papillary muscle rupture

A formation of myocardial aneurysm can lead to a stroke. A myocardial rupture is mostly lethal. A rupture of papillary muscles leads to a mitral regurgitation and an impossible treat of pulmonary edema.

If such complications do not occur or are survived the necrotic area scares over. Such scares can shorten the functionality of the heart. The limitation depends on the size of the scar. If a large area is concerned a heart failure emerges.

A heart failure causes a steadily insufficiently oxygen and blood supply to the human body. The WHO (World Health Organisation) [WHO, 2007] defines heart failure as follows: *A person has heart failure when his heart is unable to pump enough blood around to supply the oxygen the body needs.* In succession a pulmonary edema or a cardiac shock can appear.

2.4 Therapy

At an early stage of coronary artery disease a medical treatment is induced. Secondary to a medical treatment a behavior modification is advised. If advanced stenosis exists an intervention is necessary to avoid a possible heart attack. This intervention may be a balloon angioplasty, a stent implantation, or a bypass operation.

2.5 Early Diagnosis

Diseases affecting the blood circulation system are the major causes of death. The following statistics are collected by Statistik Austria [Austria, 2006] in the year 2006 and are valid for Austria. About 40% of all cases of death result from diseases of the blood circulation system. About half of these are caused by ischemia heart diseases. 8% of all cases of death are caused by a heart attack. Due to this high death rate the elimination of the risk factors and an early diagnosis for angina pectoris are desirable. First order risk factors are smoking, hypertension, hyperlipoproteinemia, diabetes mellitus, homocysteinemia and overweight. Secondary order risk factors, like lack of physical movement, stress, or psychological frustrations, can also prefer coronary heart diseases. Because coronary artery diseases may cause cardiac arrhythmias an electrocardiogram (ECG) is the first choice for detection. But ECG under rest conditions only leads to significant results if the coronary artery disease is advanced. So a rest ECG is not suitable for an early diagnosis. Better results are achieved by using a stress ECG. Therefore the patient is requested using an ergometer during the ECG measurement. Modifications in the ECG may indicate a coronary artery disease. Although this kind of examination delivers a high false positive rate, it indicates this disease. This means that many people with a positive coronary artery disease diagnosis do not have one. Therefore further examinations should be performed.

A coronary angiography leads to a certain diagnosis but it is an invasive examination method which can lead to complications. Therefore some other image based examination methods exist to validate or exclude a possible coronary artery disease. If still a coronary artery disease is indicated a coronary angiography can be applied to detect the location of the stenosis. Some image based examination methods are [Bogaert *et al.*, 2005]:

- Single Photon Emission Computer Tomography (SPECT)
- Positron Emission Tomography (PET)
- Myocardial Contrast Echocardiography (MCE)
- Perfusion Magnetic Resonance Imaging (Perfusion MRI)

All these methods enable myocardial perfusion measurement.

Generally, perfusion is the flow of liquid through a hollow organ or a blood vessel [Pschyrembel, 2002]. The amount of blood flow per time unit in a body tissue is also called perfusion. The perfusion has a dimension of $\frac{ml}{g \cdot min}$.

SPECT

SPECT is a nuclear medicine tomographic imaging technique. The radionuclides are injected intravenously. The administered radionuclides decay and emit gamma-rays which are detected by a gamma-camera (figure 2.6(a)). Lower counts of gamma-rays indicate an abnormal myocardial perfusion. If the patients have a balanced ischemia it can not be detected, because of the constraint that only the relative distribution of radionuclides can be obtained. On the other hand this method can also fail to distinguish between viable and nonviable myocardium tissue. An additional problem is the lack of spatial resolution.

PET

PET is like SPECT a nuclear medicine tomographic imaging technique. Radionuclides are injected intravenously. Unlike SPECT radionuclides emitting positrons (β-radiation) are used. A positron interacts with an electron in the human body and emits two photons moving in opposite directions. These photons are detected and show the distribution of the radionuclides (figure 2.6(b)). PET has a higher spatial resolution than SPECT and the absolute myocardial perfusion can be measured. So it is possible to detect balanced ischemia. Due to the use of radionuclides with very low half-life (down to minutes and seconds) they have to be produced locally. This makes the method so expensive and therefore not widely available.

Both methods (SPECT and PET) belong to functional imaging techniques. That means only information about the metabolism and not about morphology will be received. So no spatial relationship between the position of the emitted radiation and the different tissues exists. To overcome this problem SPECT and PET are combined with computer tomography (CT). The radiation on the patient represents a big disadvantage of these techniques which may lead to long-term consequences.

MCE

MCE is a real-time imaging tool. It allows to observe the heart function at real-time. An intravenous of intracoronary injection of micro bubbles is applied. The echo characteristics are different for the micro bubbles and the tissue and therefore they can be visualized (figure 2.6(c)). The echocardiography can lead to shadowing artifacts. They can be reduced by using a low dose of echo contrast agent. The advantages of this method are the real-time mode, the good spatial resolution and the absence of radiation.

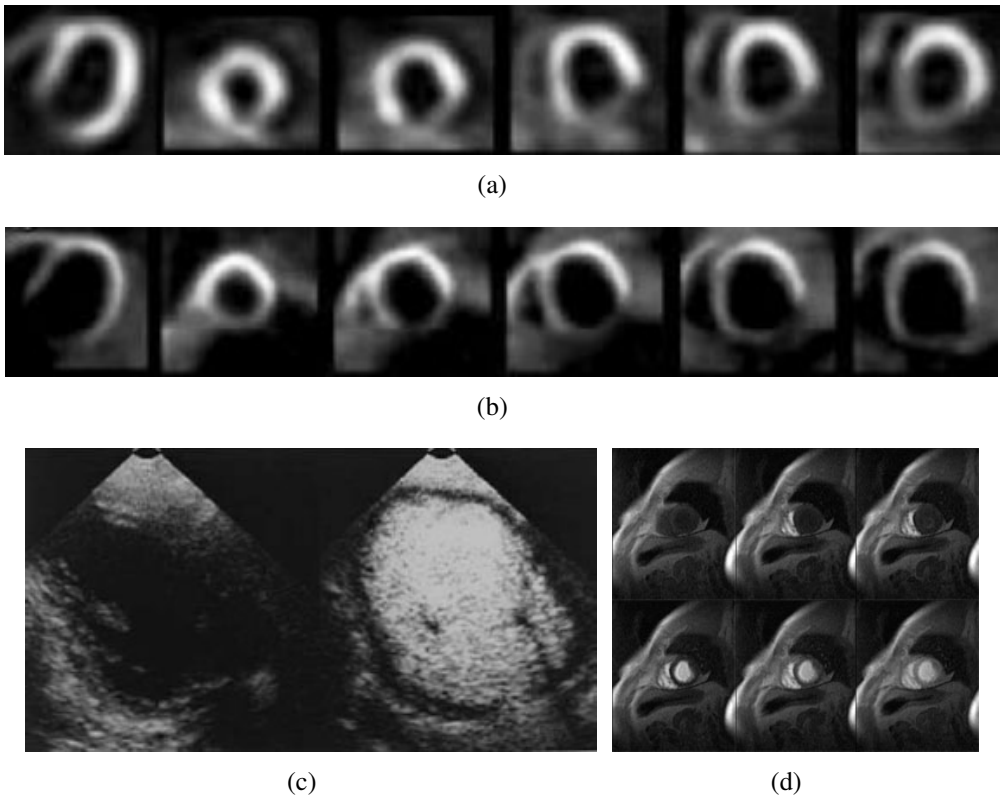

(a) (b) (c) (d)

Figure 2.6: Different Series of Perfusion Images. (a) SPECT [Graf *et al.*, 2006] and (b) PET [Graf *et al.*, 2006] shows a whole serial. (c) [Mulvagh *et al.*, 2000] shows only one snapshot a MCE real-time measurement. (d) shows some samples of a perfusion MRI serial.

Perfusion MRI

Perfusion MRI is very similar to MRI, but uses a contrast agent to visualize the blood circulation (figure 2.6(d)). Therefore the contrast agent is injected intravenously and then catabolized by the body. Advantages are the possibility of multislice measurements along different axes, no radiation exposure, no attenuation problems and the wide availability of MRI.

Figure 2.6 shows results obtained from the different methods explained above. Table 2.1 gives a summary of the most important characteristics of the different methods to measure myocardial perfusion.

This work focuses on the analysis of cardiac perfusion images obtained by perfusion MRI. Therefore the next sections will go into detail how the images are acquired, what kind of problems occur, and how the images can be interpreted.

SPECT	radiation exposure only relative distribution low spatial resolution only functional measurement
PET	radiation exposure higher spatial resolution than SPECT expensive only functional measurement not widely available
MCE	cheap no radiation exposure real-time mode shadowing artifact good spatial resolution attenuation problems
perfusion MRI	better resolution than PET and SPECT no radiation exposure widely available slices along different axes no attenuation problems

Table 2.1: Characteristics overview of different perfusion measurement techniques

2.6 Cardiac perfusion MRI

Physical Background

Cardiac MRI is fundamentally the same as MRI techniques at other body parts. MRI is a technique based on the physical fundament of nuclear magnetic resonance. The fact that elementary particles have a magnetic momentum and an angular momentum is essential. Particle systems, like atom nuclei, have an intrinsic magnetic momentum and angular momentum if they have an odd number of protons and/or neutrons. As a result of this property the atom nuclei rotate around their axes (figure 2.7(a)) and generate an intrinsic low magnetic field. Applying an external magnetic field causes the rotation axes of the atom nuclei align in a precession (2.7(b)). The alignment can be either in the same direction (figure 2.7(c)) or in the opposite direction of external magnet field. The frequency of the precession f_0 is proportional to the applied magnetic field B_0 and the gyro-magnetic ratio of the element:

$$f_0 = \frac{\gamma}{2\pi} B_0 \tag{2.2}$$

Where γ is the gyro-magnetic ratio of the element and is a constant for every isotope. These properties allows to measure the distribution of the different elements.

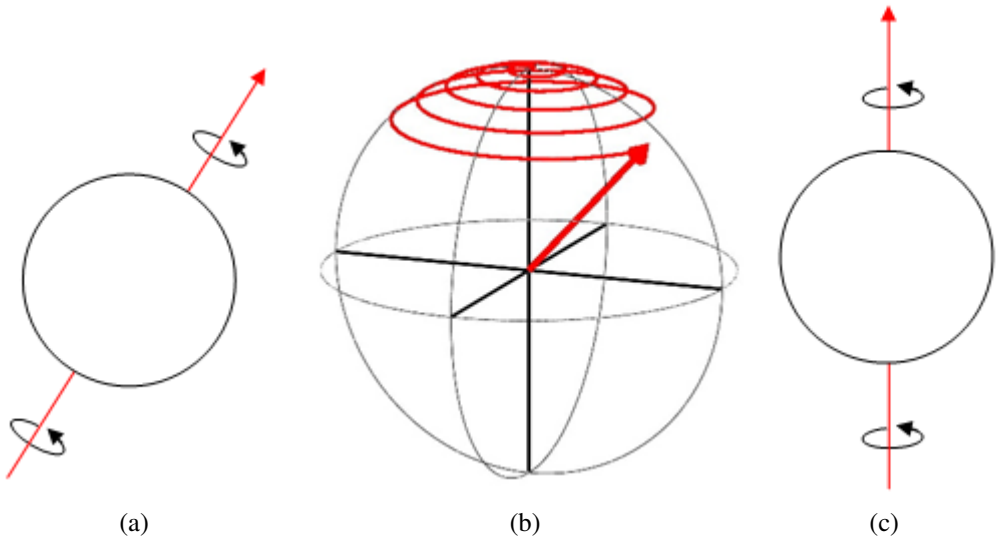

Figure 2.7: Precession. Atom nuclei with an odd number of protons and/or neutrons have a magnetic momentum and therefore rotate around their axes (a). After applying an external magnetic field the axes align by a precession (b) to the direction of the external field (c)

Measurement Procedure

In the human body the directions of the low magnetic fields are random and compensate each other. Therefore, no magnetic field can be measured. When the body is brought into a high magnetic field B_0 all rotating axes of the atom nuclei get aligned either the same or the opposite direction of B_0. Oppositely aligned atom nuclei compensate their magnetic field. The magnetic field measured along B_0 is called longitudinal magnetization.

A second (high-frequency) magnetic field B_1 is applied perpendicular to B_0. Atom nuclei precess away from the longitudinal alignment to the direction of B_1. Therefore, the longitudinal magnetization decreases and the transversal magnetization increases. Turning off B_1 effects the atom nuclei to precess back to the longitudinal alignment until the equilibrium is reached. During the relaxation - precession back to the equilibrium - two measurements can be carried out:

- T_1-Relaxation
- T_2-Relaxation

T_1-Relaxation defines the time until the equilibrium is reached. In the ideal case all atom nuclei precess synchronously (in phase). After turning off B_1 the rotations dephase and the strength of the transversal magnetic field decreases. If all of the atom nuclei precess independently the transversal magnetization becomes zero. The time until the transversal magnetization becomes zero is defined as T_2. T_2 is significantly shorter than T_1.

Imaging

The resonance signal needed for the imaging process is measured by coils. This signal is a high-frequency magnetic signal occurring after turning off B_1. It has the same frequency as B_1. The strength is proportional to the number of excited atoms whereby a conclusion to the density is possible. The length of the resonance signal gives information about the physical interaction between the atoms. Due to the fact that different atoms have different T_1 and T_2 times it is possible to distinguish between different tissues. For a better contrast between interesting tissues a pulse repetition of B_1 can be applied (e.g. at moments where T_1 is only reached for one tissue). This leads to T_1 and/or T_2 weighted images.

Organs can often be visualized better with MRI than with other imaging techniques. For some tissues like nerves and the brain a suitable visualization is only achievable with this technique. The adjustment of the repetition time allows to visualize interesting details. Thereby no standards for the measurement exist. This leads to varying results depending on the operator. This fact makes it difficult to realize an automatic interpretation of the results. A very big advantage of MRI is the possibility to acquire images of slices of arbitrary directions.

Cardiac Perfusion MRI

The goal of cardiac perfusion MRI is to visualize and analyze the perfusion of the myocardium. For getting an overview of the blood flow a contrast agent is injected intravenously. As a result of the blood flow (described in a previous section) the contrast agent first appears in the right ventricle then in the left ventricle and finally in the myocardium. Some images of a perfusion MRI serial are shown in figure 2.6(d). Figure 2.6(d) shows a so called short-axis view. This work focuses on such short-axis views. A short-axis view is a slice perpendicular whereas a long-axis view is a slice parallel to the anatomy heart axis. Figure 2.8 shows different slices of the heart.

All images of a serial are acquired at corresponding points in time of a heart cycle. This is called ECG-gated and prevents motion artifacts based on the heart beat. To minimize the motion artifacts based on respiration the patient is asked to hold the breath. Acquiring images under rest conditions only allows to detect advanced vessel narrowings. Small narrowings can be compensated because of coronary reserve and therefore they can not be detected. For still seeking out small narrowings the images must be acquired under stress conditions. Furthermore a comparison of the rest and stress results may indicate a preliminary perfusion reduction.

The next section shows how to make use of perfusion data to detect myocardial areas with diminishing perfusion.

2.7 Analysis of perfusion data

To analyze perfusion data the progress of the contrast agent has to be examined at every position. Typical curves of the progress are shown for the right ventricle, left

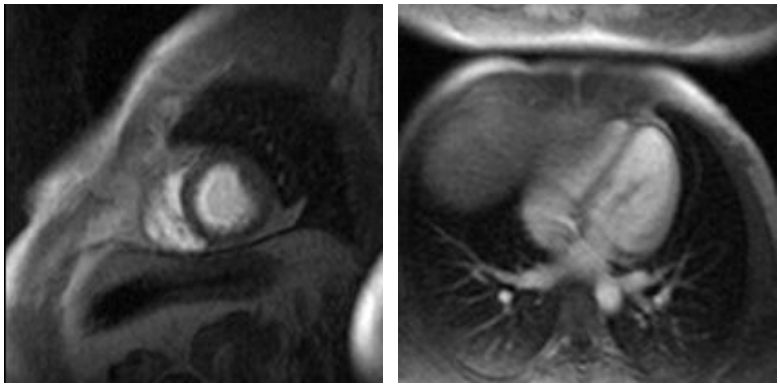

(a) (b)

Figure 2.8: Difference short-axis long-axis view. Different slices of the heart in a short-axis (a) and long-axis (b) view

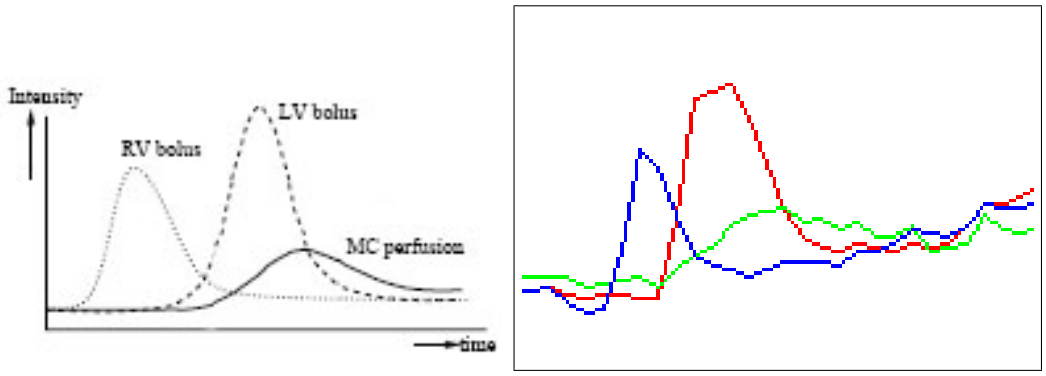

(a) (b)

Figure 2.9: Progression of contrast agent. (a) ideal case [Spreeuwers and Breeuwer, 2001] (b) a real case.

ventricle, and the myocardium in Fig. 2.9. The left figure shows the ideal case. The right figure shows example curves. These example curves were obtained from a dataset analyzed in this work.

There exist different measurements to quantify myocardial perfusion. All of them are based on the curve of the contrast agent progression (intensity time curve) of the myocardium. These measures are:

- *Peak Enhancement (PE):* Maximum value normalized with the baseline [Al-Saadi *et al.*, 2000; Oeltze *et al.*, 2007].

- *Contrast Appearance Time (CAT):* Time difference between contrast agent (CA) arrival time in the left ventricle and in the myocardium [Al-Saadi *et al.*, 2000; Oeltze *et al.*, 2007].

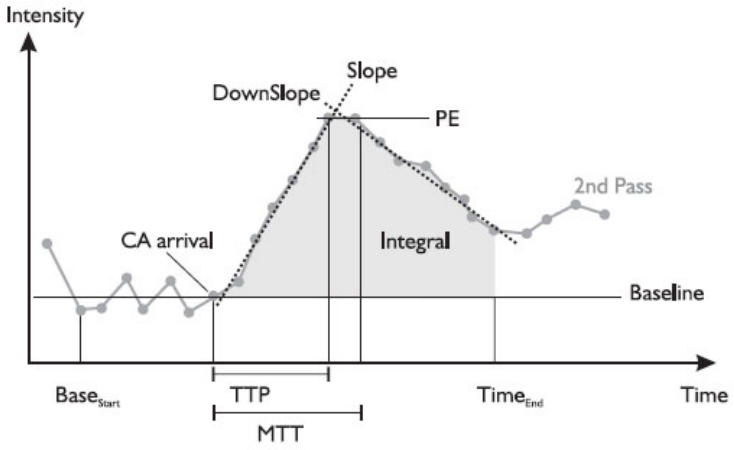

Figure 2.10: Signal Intensity Time Curve measurements. [Oeltze *et al.*, 2007] A typical signal intensity time curve for myocardial perfusion and possible measurements.

- *Time To Peak (TTP):* Time until PE is reached starting from the contrast agent arrival time [Al-Saadi *et al.*, 2000].
- *Integral:* Area under the curve between CA arrival time and the end of the first pass [Oeltze *et al.*, 2007].
- *Mean Transit Time (MTT):* Time until the half of the Integral is reached [Oeltze *et al.*, 2007].
- *Upslope:* Steepness of the curve before PE [Al-Saadi *et al.*, 2000; Schwitter *et al.*, 2001].
- *Downslope:* Steepness of the curve after PE [Oeltze *et al.*, 2007].

Figure 2.10 shows a typical signal intensity time curve for a single voxel belonging to the myocardium. Furthermore some possible measurements for myocardial perfusion are included.

These measurements allow a diagnosis. It turns out that regions with diminishing perfusion can be identified by upslope and peak enhancement. Furthermore the upslope of the signal intensity time curve linearly fits to the myocardial perfusion reserve [Al-Saadi *et al.*, 2000; Al-Saadi *et al.*, 2001; Christian *et al.*, 2004; Schwitter *et al.*, 2001; Nagel *et al.*, 2003].

Chapter 3

Related Work

The previous chapter has given an overview of the anatomy, physiology and pathophysiology of the heart. Additional methods for detecting coronary artery diseases prematurely were presented. Furthermore therapeutic interventions for coronary artery diseases were discussed.

This chapter will give an overview of related work in the area of segmentation and analysis of perfusion MRI data. For detecting coronary artery diseases based on perfusion MRI data various key issues have become apparent:

- Region of Interest (ROI) detection
- Registration
- Segmentation
- Analysis

Now an overview of related work dealing with these key issues is given.

3.1 Region of Interest (ROI) detection

The ROI is the region covering the examined anatomical structure. There exists no related work focusing on the automatic ROI detection in cardiac perfusion MRI. In many published methods - focusing on the segmentation of cardiac perfusion MRI - the ROI has to be defined manually. Sometimes some assumptions are made like that the interesting structures are located in the center of the images.

However, some methods exist focusing on automatic ROI detection in non-perfusion MRI. Non-perfusion images are taken at different stages of the cardiac cycle. Furthermore at least one cardiac cycle is imaged.

Sörgel et al. [Sörgel and Vaerman, 1997] have shown a method to localize the heart in non-perfusion MRI. This method is used to initialize an active contour approach for segmenting the heart. The images show the heart at different stages of the cardiac cycle. By observing gray value variations over time it is possible to

detect the heart. Areas with high variations can be identified as belonging to the heart. Their method works as follows: First the gray value variances are calculated for every voxel over time. This leads to a variance volume. Second a threshold is applied at every slice. This threshold is defined to keep at least a given amount of voxels. Third a morphological cleaning is applied. Fourth all slices are summed up and a thresholding is applied again. Finally the remaining area is identified as the region covering the heart.

Zambal et al. [Zambal *et al.*, 2008] have adapted this method to initialize an Active Appearance Model (AAM). Gering [Gering, 2003] has shown a very similar approach to initialize a Contextual Dependency Network (CDN).

There are fundamental differences between perfusion and non-perfusion MRI. Nevertheless the above approaches can be adapted to work for perfusion MRI as well. In perfusion MRI no heart motion is present, but the contrast agent leads to high gray value changes were it passes. Therefore the gray value variations of perfusion MRI and non-perfusion MRI are very similar. So it is possible to use the above-mentioned methods for perfusion data.

3.2 Registration

Different registration methods for perfusion images were presented.

Yang et al. [Yang *et al.*, 1997] have presented a method for compensating translational motion. They conclude to the translational motion using phase differences between successive images.

Approaches based on Active Appearance Models (AAMs) were presented by Stegman et al. [Stegmann and Larsson, 2003; Stegmann *et al.*, 2005] and Ólafsdóttir [Ólafsdóttir, 2004; Ólafsdóttir, 2005]. They analyze the variances and cluster an annotated training set off-line. Additional image intensity changes caused by the contrast agent are modeled by a slice coupled AAM. These approaches do not only focus on registration. They are a combination of registration and model based segmentation.

Wong et al. [Wong *et al.*, 2005] have shown a registration method based on normalized mutual information. Milles et al. [Milles *et al.*, 2007] use an independent component analysis approach to extract image features for registration.

3.3 Segmentation

Automatic segmentation of the myocardium in perfusion images is a quite difficult challenge. The complexity of this task is based on a wide range of image variabilities which are caused by patient movement, anatomical variations, pathologies, imaging noise, limited resolution, as well as artifacts.

There exist only a few methods for segmenting the myocardium in cardiac perfusion MRI. All of them ignore some variabilities or require some human interventions.

Spreeuwers and Breeuwer [Spreeuwers and Breeuwer, 2001] have presented a method detecting myocardial boundaries based on image gray values. This method assumes that no motion artifacts are present or that the images are already registered to each other. They are searching for local maxima in time and space to detect pixels identifying the left and right ventricle. Afterward region growing is applied to extract areas for both ventricles. Then two maximum intensity projections (MIPs) are determined: One for the images before the contrast agent appears in the myocardium, and the other one for the rest of the images. Then these MIP images are subtracted and the myocardium appears as a bright region. Then the image is transformed into polar coordinates and a five node snake is fitted to maximize the contrast ratio.

Spreeuwers et al. [Spreeuwers *et al.*, 2002a; Spreeuwers *et al.*, 2002b] have further presented a method to improve the myocardial contour. Therefore they vary the contours of the segmented myocardium. Then they analyze the upslope of the intensity time curves of myocardial segments and compare them to the original. If there are significant differences adaptations are applied.

Pluempitiwiriyawej and Sotthivirat [Pluempitiwiriyawej and Sotthivirat, 2005] have presented another method for segmenting the myocardium in perfusion MRI data. This method ignores heart motions too. It is based on active contours and extracts an initial contour which is passed to their so called Stochastic Active Contour Scheme (STACS) [Pluempitiwiriyawej *et al.*, 2005]. First they calculate difference images for adjacent images in the whole dataset. After thresholding these images they apply morphological closing to merge pixels that are close together. Then a median filter is applied to remove scattering pixels. The largest area is determined and two concentric circles centered on the largest area are created. These circles are the initial contour for the myocardium. Finally STACS is applied. STACS uses an energy minimization approach to segment the heart and its structures. The used energy function consists of four different terms:

- region based term
- edge based term
- global property term
- local property term

The global property term defines the global contour shape which is an ellipse. The local property term defines the smoothness of the contour.

Adluru et al. [Adluru *et al.*, 2006] have shown another method. This method is based on level sets including an image registration step to reduce motion artifacts. This method however assumes that the heart is roughly located at the center of the images. The registration step uses the temporal center of the sequence as reference image. Then all other images are registered to this reference image by minimizing the mean square difference. A Hanning-Window filter is used to penalize the center region of the image more than the outer region. A variance image is generated to locate the heart. The highest value in the variance image is used as a seed point

for the left ventricle. Then the original image is transformed into polar coordinates according to this seed point. This polar map is thresholded and seed points for the myocardium are defined. These seed points have to lie three pixels outside of the left ventricle. The seed points are converted back into cartesian coordinates and used as an input of a level set based framework.

Sun et al. [Sun *et al.*, 2004] have presented a combination of contrast-invariant affine registration and segmentation. This method requires human intervention to select a region of interest (ROI) and a reference image. The registration step is based on edge informations. Therefore edge informations (gradient direction, gradient magnitude) are extracted inside the ROI. A similarity measurement based on these informations is minimized and leads to the final registration. Then for every image the gray value differences to the reference image are calculated. This leads to difference images. Only the ROI is used to gain these difference images. Finally an energy minimization approach is applied to extract the contours of the myocardium.

Postiano et al. [Positano *et al.*, 2003] segment the myocardium at a single slice. A user has to select the ROI where the myocardium is located. Furthermore the slice has to be selected where the myocardium should be segmented. Then a registration using Mutual Information is applied. The myocardium is segmented at the selected slice using a gradient vector flow approach ([Xu and Prince, 1997]). Finally the intensity time curves for the myocardial segments are determined which can be used to analyze the perfusion.

There exist many other approaches for segmenting the heart but they are designed for non-perfusion MRI data. However, some of them can be applied on perfusion MRI data if some restrictions are introduced. Especially, perfusion images with contrast agent appearing in the left and right ventricle but not yet in the myocardium, can be segmented similar to non-perfusion MRI images. If such images are identified, one of the following methods can is applicable: Active Contours, Active Shape Models, Active Appearance Models. This is outlined in the following:

Active Contours

Active contours are only based on image features and shape-constraints. The goal is to place a contour gaining a trade-off between shape-constraints and edge information.

Luuk Spreeuwers and Marcel Breeuwer [Spreeuwers and Breeuwer, 2001; Spreeuwers and Breeuwer, 2003] have introduced a method to extract the myocardial boundary using coupled active contours. In contrast to active contours a coupled active contours approach evaluates two contours simultaneously. This method needs a good manual initial definition of these contours at a single slice. Then the initialization is propagated to the other slices. Furthermore this method needs a good contrast between the segmenting tissues because active contours are an edge based approach.

Pluempitiwiriyawej et al. [Pluempitiwiriyawej *et al.*, 2005] have introduced an extended version of active contours. This method combines stochastic-region based

and edge-based information with shape priors of the heart and local properties of the contour. The stochastic-region information allows to segment images with low texture contrast. Additional the combination of region and edge information leads to a higher robustness to noise and the initial contours. The initial contours still have to be defined manually.

Yeh et al. [Yeh *et al.*, 2005] have introduced a branch-and-bound dynamic programming approach to reduce the high computational costs for extracting the endocardial boundary. After manually defining a ROI by a circle that includes the whole left ventricle the region is converted into polar coordinates. The axes of this retrieved polar map are: the distance from the center and the radial direction. For extracting the endocardial features (edges) a Prewitt-operator is applied. Afterward a network is generated ensuring that the detected border is a closed curve. Then a dynamic programming approach is applied to the network. Thereby the endocardial boundary that optimizes the objective function within specified constraints is determined. Finally, the determined contour is mapped back to the original image data. This approach only deals with the task of segmentation of the left ventricle at a single slice whereby no registration is needed. Additional the ROI has to be defined manually and the features for detecting the contour of the left ventricle are only based on edges.

Active Shape Models

Active Contour is a segmentation technique only based on image features. Better results can be established by using prior knowledge about the shapes of the interesting structures. Therefore some methods based on ASM were suggested for cardiac perfusion segmentation.

2D-ASMs were introduced by Cootes et al. [Cootes *et al.*, 1995] for the first time. For ASMs a model comprises a set of landmark points. Therefore a training set is segmented manually by placing points on the boundary of the interesting object. Then all images of the training set are aligned. Statistics for the training set are calculated such as the mean shape and the principle components. The principle components are calculated by the principle component analysis (PCA) and gives the 'mode of variation'. Only the principle components with the highest 'mode of variation' are kept to reduce the model complexity without loss of highly significant information. Now this model can be used to find similar shapes in unseen images.

This 2D-ASM approach inspired the extension to 3D-ASM. Van Assen et al. [van Assen *et al.*, 2003a] and Kaus et al. [Kaus *et al.*, 2004] showed such 3D-ASMs and their matching based on edges. Van Assen et al. [van Assen *et al.*, 2003b] presented an extended approach leading to better results. This approach uses fuzzy interference for the edge detection. They [van Assen *et al.*, 2005] also presented a 3D-ASM dealing with sparse and arbitrarily oriented cardiac MRI data and called it SPASM.

There exists an approach of 4D models too presented by Montagnat et al. [Montagnat and Delingette, 2005]. This 4D deformable model contains all stages of a

cardiac cycle with temporal constraints. This model was used to segment synthetic SPECT datasets.

Active Appearance Models

AAMs are an extension of ASMs [Cootes *et al.*, 1998]. Additional to contour information, texture information was taken into account. The shape model is calculated in the same way as ASMs. After obtaining the mean shape of the model, all training datasets are warped to the mean shape so that the control points matches. Then gray values are sampled over the whole region covered by the shape and PCA is applied to get the principle axes. So the model exists of two parts: one for the shape and one for the gray values. Because of possible correlations of these models they are combined and PCA is applied again. This model allows to find objects with similar shapes and gray values in unseen images. Mitchell et al. [Mitchell *et al.*, 2002] extended this approach to a 3D-AAM.

Alternative Approaches

Additional to these three methods alternative approaches exist. A virtual exploring robot traveling around the left ventricle was presented by Behloul et al. [Behloul *et al.*, 2001]. The start position of the robot has to be defined outside the left ventricle. The target position has to be defined inside the left ventricle. The robot navigates around the left ventricle in a wall tracking mode to find a way to the target position. If no path to the target is found the robot accomplish a complete loop which leads to the contour of the myocardium.

An automatic segmentation approach using a contextual dependency network (CDN) was presented by Gering [Gering, 2003]. This work also contains an automatic search of the ROI. Thereby the variance for every voxel is calculated and thresholded. After applying morphological operations the greatest three dimensional structure is identified as the ROI where the CDN is applied.

3.4 Analysis

Some work exists focusing on the analysis and visualization respectively of the perfusion.

As introduced in the previous chapter the analysis is based on the intensity time curve of the myocardium. Different measurements as mentioned in the previous chapter are (figure 2.10): Peak Enhancement (PE), Contrast Appearance Time (CAT), Time To Peak (TTP), Integral, Mean Transit Time (MTT), Upslope, and Downslope (section 2.7).

To visualize these measurements and retain a spatial correlation different techniques are introduced. These techniques visualize perfusion data in combination with morphological image data [Oeltze *et al.*, 2006]. Figure 3.1 illustrates a method

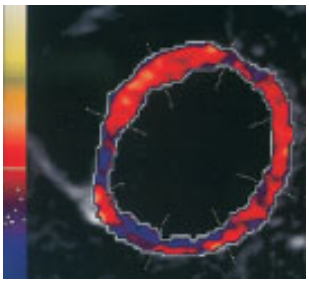

Figure 3.1: 2D-Perfusion Plot. [Schwitter *et al.*, 2001] Color-coded upslope of a single slice. Blue indicates a small upslope which indicates a low perfusion. Red indicates a normal perfusion.

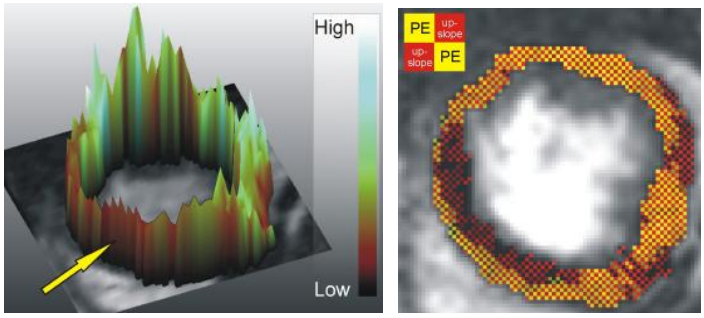

(a) (b)

Figure 3.2: Two parameter visualization. (a) Three dimensional visualization of upslope (color) and PE (height) (b) Visualization of upslope and PE as color icons. [Oeltze *et al.*, 2007]

to visualize the upslope in a 2D-plot. Figure 3.2 illustrates two techniques visualizing two different measurements concurrently. This leads to better results if a combination of these two parameters indicates a bad perfusion.

The above-mentioned techniques are voxel based. Therefore for each voxel the measurements are calculated and visualized separately. If the images are very noisy or not registered to each other wrong measurements may be obtained. A common technique is to average the gray values over the segments and then calculate the measurements.

For a treatment plan it is important to identify the vessels causing a bad perfusion. Therefore the American Heart Association (AHA [AHA, 2007]) has defined a standardization for myocardial segmentation [Cerqueira *et al.*, 2002] which divides the myocardium into 17 segments (figure 3.3). The heart is divided into three slices (basal, mid-cavity and apical). The basal and mid-cavity slices are divided into six and the apical slice into four segments. The 17th segment is the apex. Projecting all segments into a single plane leads to the so-called bull's eye plot. The bull's eye plot is shown in figure 3.4. It also shows the supply areas of the coronary branches which are coded by different colors.

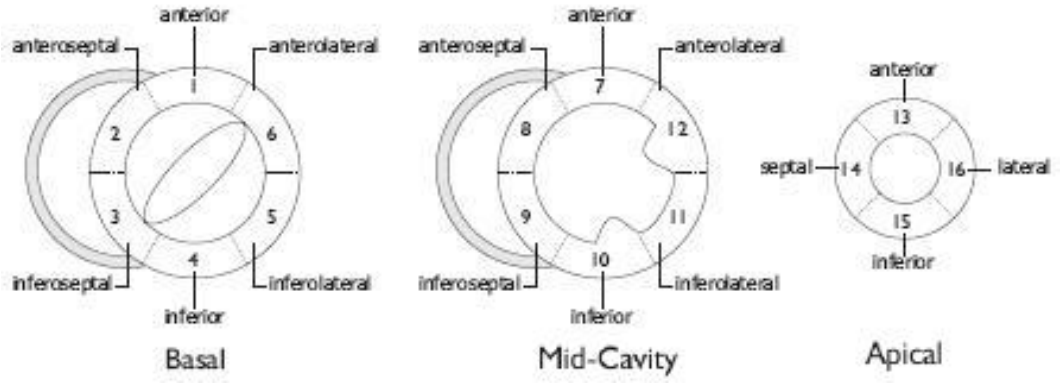

Figure 3.3: Standardized myocardial segmentation. Short axis views of the segments. The apex (the 17th segment) is not visualized. [Kuß, 2006]

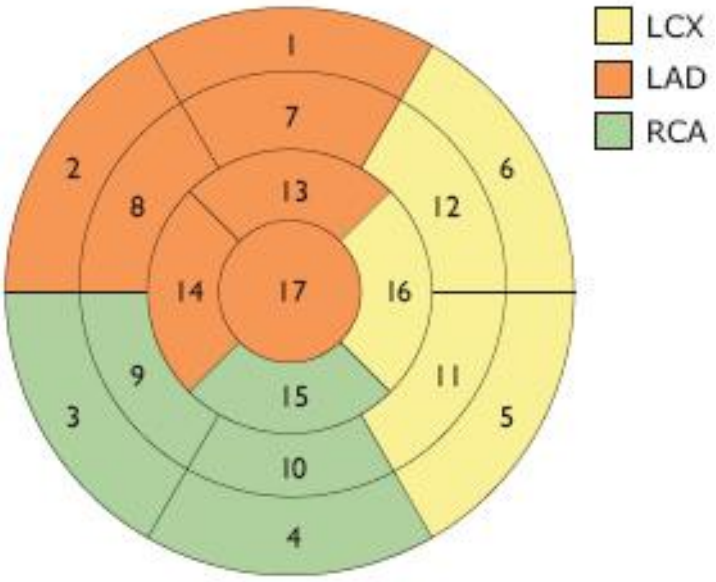

Figure 3.4: Bull's-Eye Plot and AHA-conform nomenclature. 1. basal anterior 2. basal anteroseptal 3. basal inferoseptal 4. basal inferior 5. basal inferolateral 6. basal anterolateral 7. mid anterior 8. mid anteroseptal 9. mid inferoseptal 10. mid inferior 11. mid inferolateral 12. mid anterolateral 13. apical anterior 14. apical septal 15. apical inferior 16. apical lateral 17. apex. The segments are colored according to the supplying coronary branch (LCX - left circumflex artery, LAD - left anterior descending artery, RCA - right coronary artery) [Kuß, 2006]

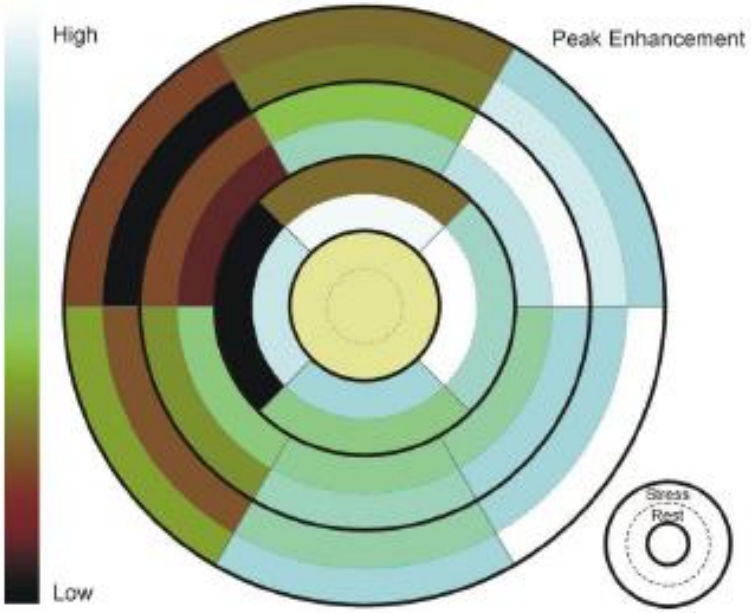

Figure 3.5: Refined Bull's-Eye Plot. Every segment is divided into two segments and visualizes the perfusion under rest and stress conditions. [Oeltze *et al.*, 2007]

To visualize the perfusion difference between rest and stress condition Oeltze et. al. [Oeltze *et al.*, 2007] have introduced a refined bull's eye plot. This is shown in figure 3.5. This refined bull's eye plot divides every segment into two separately parts, one for rest and one for stress conditions. So it is possible to identify regions with a different perfusion under rest and stress conditions. This leads to an indication of preliminary perfusion reduction.

This chapter has given an overview of related work focusing on different tasks in the analysis process of cardiac perfusion MRI. The next chapter will give a detailed description of how these tasks are realized in this thesis.

Chapter 4

Image Processing Pipeline

Cardiac perfusion MRI was identified as a promising approach for preliminary detection of coronary artery diseases [Al-Saadi *et al.*, 2000; Al-Saadi *et al.*, 2001; Edelman, 2004; Kaiser *et al.*, 2003; Wilke *et al.*, 1997; Wolff *et al.*, 2004]. Currently the analysis of such perfusion images is done by manual inspection which is a very time-consuming and tedious task. Therefore a need for a robust and automatic analysis tool exists. Such a tool first has to segment the myocardium in all images and then to calculate meaningful parameters quantifying the perfusion. Automated segmentation of the myocardium in perfusion images is quite a difficult challenge. The complexity of this task is based on a wide range of image variabilities. These variabilities are caused by patient movement, anatomy variations, pathologies, imaging noise, limited resolution, as well as artifacts.

An automatic analysis tool has to cope with all these difficulties to provide acceptable and significant results. This work presents a method for automatic analyzing cardiac perfusion MRI data. The designed method is divided into four parts. These parts identify the main issues for analysis of cardiac perfusion MRI data:

- Region of Interest (ROI) Selection
- Image Registration
- Segmentation
- Analysis

Every single task is based on the output of the preceding task. This composition represents an image processing pipeline which is illustrated in figure 4.1.

First this pipeline locates the heart and defines a ROI covering it (section 4.1). Therefore two approaches are investigated: a variance based approach and a model based approach. The variance based method is adapted from Sörgel et al. [Sörgel and Vaerman, 1997] whereas the model based method represent a novel approach for locating the ROI.

After locating the ROI a rigid registration is applied to minimize artifacts caused by patient motion (section 4.2). The registration uses Mutual Information [Viola and Wells, 1997] and is like other methods restricted to the ROI.

Figure 4.1: Image Processing Pipeline. In the 4D dataset (3D+T) (a) first a region of interest is located (b). Then the images are registered to each other (c) and the myocardium is segmented (d) at every slice. Based on these segmentations the perfusion of the myocardium is determined (e).

Then the contours of the myocardium are extracted at every single time step (section 4.3). Therefore a new two step approach is introduced. It first extracts characteristic intensity time curves for the different regions (LV, RV and myocardium) and then determines myocardial boundaries for every single time step based on these curves. This approach uses an adapted algorithm for finding a path with minimal costs in a polar map [Yeh *et al.*, 2005].

Finally, the perfusion of the myocardium is quantified and visualized (section 4.4). The quantification is done as recommended by Al-Saadi et al. [Al-Saadi *et al.*, 2000]. The results are visualized in a bull's eye plot [Cerqueira *et al.*, 2002] which is extended by the characteristic intensity time curves.

All these steps are performed automatic without any user interaction. Now this chapter goes into detail how these issues are treat in a fully automatic manner without any user interaction.

4.1 ROI Selection

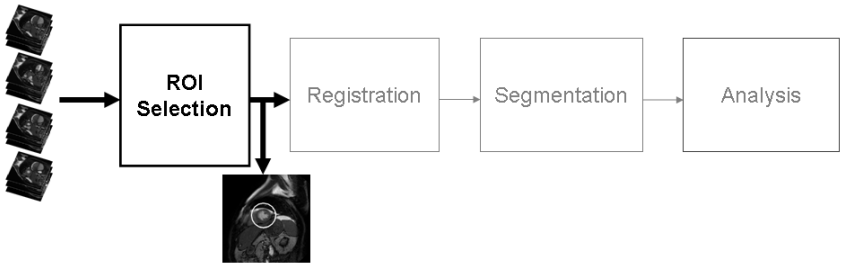

The first key task is to determine the region of interest (ROI). The ROI considered here is the image region covering the left ventricle and the myocardium.

As mentioned in the previous chapter (chapter 3) ROI selection is often done manually. Typically the user has to define an area including the left ventricle by drawing a contour around it. The problem of automatic localization of the heart in non-perfusion MR images has been tackled by several authors by exploiting gray value variation over time [Gering, 2003; Sörgel and Vaerman, 1997; Zambal *et al.*, 2008]. In this thesis experiments were performed using gray value variances on perfusion data. For some datasets the method operated very well. However it failed when larger motion artifacts appeared.

Therefore a new approach for detecting the heart in perfusion MRI is introduced. This novel method is based on a incremental pattern matching approach of a very simple pattern of the left ventricle and the myocardium. By observing each time separately motion artifact problems are avoided. This method identifies possible candidates in every single time step using only spatial information. In a final step the most likely candidate is identified.

Then the successive tasks (registration and segmentation) are exclusively performed on this ROI. This leads to better results and saves computation time.

A detailed discussion of the two investigated methods for ROI selection follows in sections 4.1.1 and 4.1.2.

4.1.1 Variance based ROI Selection

This method is based on the related work of Gering, Sörgel et al., and Zambal et al. [Gering, 2003; Sörgel and Vaerman, 1997; Zambal *et al.*, 2008]. These methods operate on non-perfusion functional MR heart datasets containing at least one cardiac cycle. The motion of the heart causes very high gray value variations over time. Therefore the heart can be located by using information of these variations.

Perfusion studies differ from functional MR because the heart is captured at equal stages of the cardiac cycle (the imaging sequence is ECG-gated). Thus no heart motion based on the heart beat appears. However, the injected contrast agent causes high gray value changes in areas where it passes. So, it is possible to identify the heart as the region with maximum variation of the gray values.

The method works as follows: At the beginning all images are filtered by a 5×5 mean filter (figure 4.2(a) to suppress noise. Then the gray value variance for every single voxel is calculated as follows:

$$\sigma^2(x, y, z) = \frac{1}{N-1} \sum_{t=0}^{N-1} (I(x, y, z, t) - \mu(x, y, z))^2 \tag{4.1}$$

where $I(x, y, z, t)$ indicates the gray value at spatial position (x, y, z) at time step t. $\mu(x, y, z)$ represents the mean value of a voxel at position (x, y, z). N indicates the number of time steps. The mean value for a voxel is calculated as:

$$\mu(x, y, z) = \frac{1}{N} \sum_{t=0}^{N-1} I(x, y, z, t) \tag{4.2}$$

The calculation of the variances for every single voxel over time leads to a so-called variance volume (figure 4.2(b)). To achieve the heart region which is identified by high variances a threshold operation is applied (figure 4.2(c)). The threshold is adaptively selected so that the summed area of all voxels makes at least $80cm^2$. This corresponds to the area of an average human heart in the datasets considered in this thesis. This threshold is applied to every slice of the variance volume.

The heart region is assumed to be a single connected area. Therefore the largest four-connected components are identified and extracted in each slice (figure 4.2(d)). It can be observed that this leads to good results. Anyway, it is still possible that misleading pixel sets appear in some slices. To increase the robustness all slices are summed up (figure 4.2(e)) and again the greatest component is extracted (figure 4.2(f)). Finally, the bounding box containing the whole extracted area defines the region of interest (ROI) (figure 4.2(g)). Algorithm 1 outlines the whole procedure as pseudo code.

Datasets containing huge motion artifacts or datasets with misaligned image sequences may lead to a false identification of the ROI (figure 4.3(g)). To overcome this problem a new method based on pattern matching was developed.

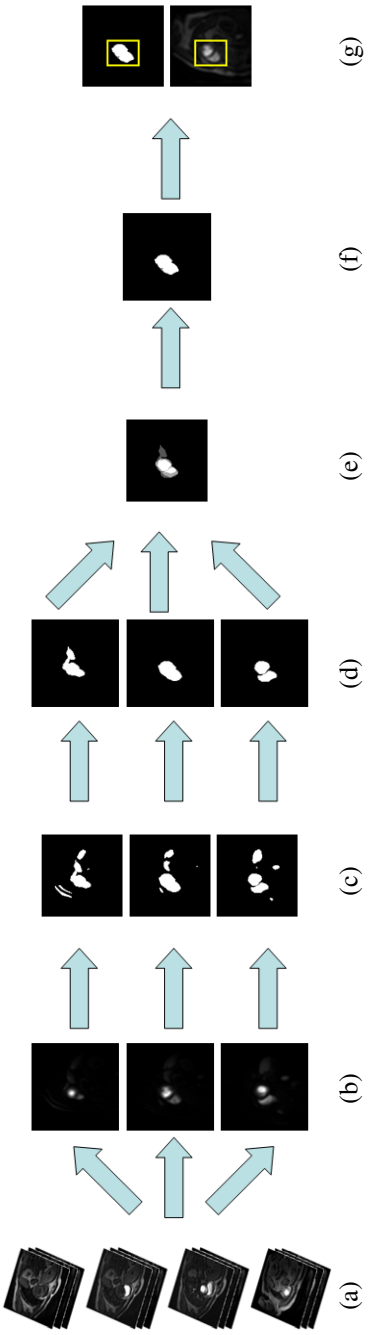

Figure 4.2: From the filtered images (a) the variance volume (b) is calculated. After thresholding this volume (c) the greatest connected components are extracted (d). Afterward the slices are summed up (e) and again the greatest connected component is extracted (f). The bounding box covering this component identifies the ROI (g)

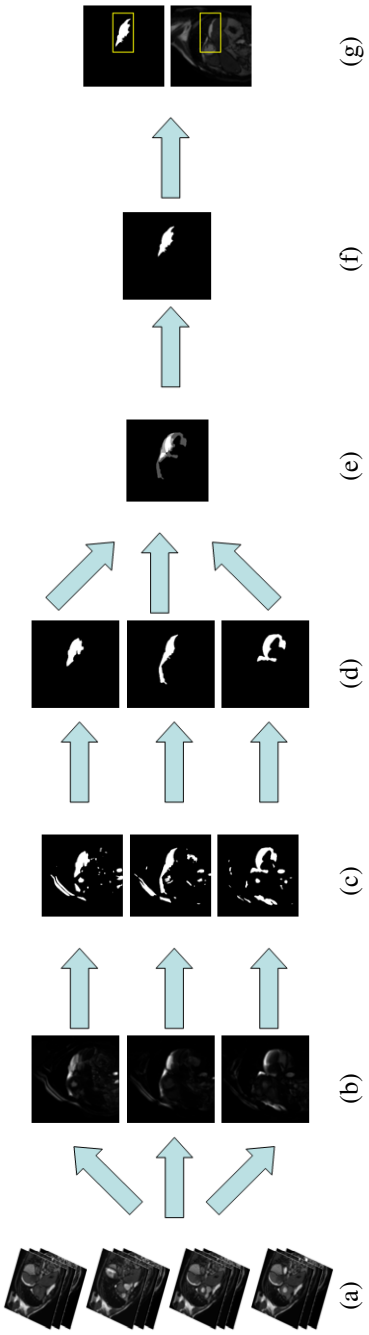

Figure 4.3: This dataset contains huge motion artifacts. Therefore large areas with high values appear (b) where no perfusion occur. This results in a wrong extraction of the greatest connected component (f) and therefore to an incorrect ROI (g).

Algorithm 1 Variance based ROI detection

```
1: input: 4D dataset
2: output: ROI
3: filter every image by a 5 × 5 mean filter
4: calculate variance volume
5: for every slice of the variance volume do
6:     threshold image
7:     extract greatest connected component
8: end for
9: accumulate all slices
10: extract greatest connected component
11: identify bounding box
```

4.1.2 Pattern Matching

In experiments it was observed that motion artifacts and misaligned datasets are the major reasons disqualifying the mentioned variance based method for locating the heart in cardiac MRI perfusion data. Therefore an alternative method is introduced. This new method does not rely on gray value variations over time. Instead, it tries to locate the heart in separate time steps. First the method filters out multiple candidates at every time step. Then the best matching candidate is determined.

Pattern Definition

The new approach is based on pattern matching and pattern searching respectively in the whole dataset. The pattern, the algorithm is looking for, represents the region of left ventricle and myocardium. Basically the pattern is a circle of homogeneous gray values surrounding a homogeneous region with different, brighter gray values. The myocardium is seen as a circle with a range of possible diameters. It is assumed that the circle that has to be detected has a diameter between 40mm and 80mm. This reflects the range of possible diameters for the left ventricle as observed in the available datasets. The inner area of the circle represents the left ventricle.

Both areas - myocardium and left ventricle - are homogeneous regions and therefore it is assumed that the according gray value variances are minimal. To ensure that these two homogeneous regions have different gray values an additional constraint is added: the inner area has to be brighter than the circle itself. This leads to a detection of candidates where the contrast agent appears in the left ventricle and not yet in the myocardium.

Pattern Matching (Multiple Candidates)

An exhaustive search of such a pattern would lead to unacceptable computation time. To reduce computational time the pattern matching algorithm is designed in a hierarchical structure. This hierarchical structure constricts the given pattern bit by bit and the amount of possible candidates decreases at every step.

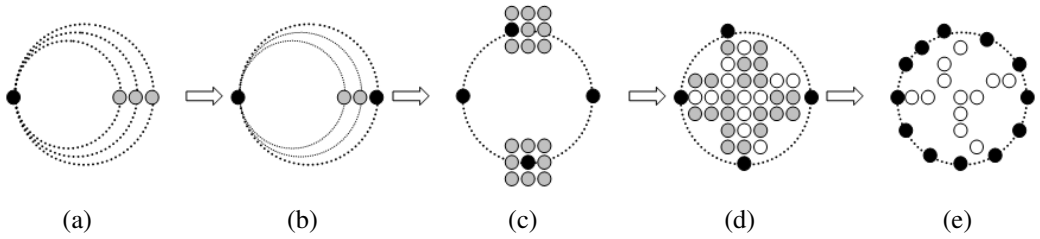

Figure 4.4: Pattern Matching. Pattern to match LV candidates. First the most left point of the model is fixed (a). Then corresponding most right points are located (b). After identifying corresponding highest and lowest points (c) candidates with a high texture variance within these four points are discarded. For the remaining candidates the inner area is observed (d). Finally, more points on the circle are considered 4.4(e) to refine the texture variance measurement.

The individual constraints which are checked one after the other as the algorithm proceeds are:

1. At the beginning every possible circle with a diameter between 40mm and 80mm is treated as a candidate. First the most left point of a candidate is fixed (figure 4.4(a)).

2. The fixed point is compared to the most right point (figure 4.4(b)). If the texture difference between these two pixels is lower or equal a given threshold (1% of gray value range) the candidate is kept otherwise it is discarded.

3. Now the highest and lowest pixels of the candidates are considered. Since the left ventricle is not necessarily a perfect circle some variations of the position of the highest and lowest pixels are allowed. A 3×3 neighborhood of these pixels is taken into account and the pixel with the highest similarity to the most left and most right pixel is treated as highest and lowest pixel respectively (figure 4.4(c)). The most left and most right pixels as well as the determined highest and lowest pixels define the outer samples of the candidate. If the texture variance of these outer samples lies above a given threshold (0.1% of gray value range) the candiate is discarded.

4. After inspecting the contours of the candidates the inner areas are considered: samples in the neighborhood along the horizontal and the vertical axis are selected (figure 4.4(d)). These sample points (inner samples) must have a very high texture difference to the mean value of the outer samples to guarantee a good contrast.

   To fulfill the constraint that the inner area (left ventricle) has to be brighter than the contour (myocardium) all candidates having a smaller texture mean value of the inner samples than the outer samples are discarded. To satisfy the other constraint - the inner area has to be homogeneous - all candidates with a high texture variance of the inner samples are discarded. This threshold is set to 0.5% of the gray value range which is clearly higher than the texture

variance threshold for the outer samples. Due to the fact that the inner area of the matching model may include papillary muscles appearing darker than the contrast enhanced left ventricle.

To further reduce the amount of candidates the difference between the texture mean values of the inner and outer samples has to be greater than a given threshold (30% of gray value range). Otherwise the candidate is discarded. This threshold seems to be very high but therefore only candidates having a very high contrast between outer (myocardium) and inner (left ventricle) samples will remain.

5. After identifying possible candidates more samples on the circle are taken (figure 4.4(e)). The texture variance of these outer samples is recalculated to get a more robust measurement of the texture variance. This texture variance is used to indicate how well a candidate matches the pattern. A lower texture variance indicates a higher probability for being the correct candidate.

Figure 4.5 shows the progress of the candidates reduction when the model is restricted step by step.

This hierarchical procedure filters out multiple candidates for each time step. Some of them do not represent the left ventricle correctly due to misleading appearances of the pattern in the dataset (figure 4.6). Therefore all candidates are sorted according to the texutre variance of the outer samples and the ten candidates with lowest texture variance are kept (4.7). Typically some false positives remain.

Pattern Matching (Best Candidate)

To finally identify the correct location of left ventricle and myocardium, a model matching approach is used introducing additional anatomical information. The shape of the model is defined by properties observed in the available datasets. The model consists of two concentric circles and an attached circle segment (figure 4.8).

The area inside the inner circle represents the left ventricle. The area between the two concentric circles represents the myocardium. The attached circle segment represents the lung and has an opening angle of $90°$.

This model is placed on every candidate to identify the best one. It is placed in such a way that the centers of the candidate and the left ventricle of the model match. The radius of the model's left ventricle is set equal to the radius of the candidate. The thickness of the myocardium is chosen as half the radius of the candidate and the radius of the circle segment is set to 2.5 times the radius of the candidate. These model parameters are chosen based on the observed properties in the available datasets.

To compare the candidates a difference measurement has to be defined. The error rate according to the following classification is used: The assumption is made that the placed model correctly defines the different regions (classes) in the unseen images. The probabilities for gray values observed in a certain class is calculated.

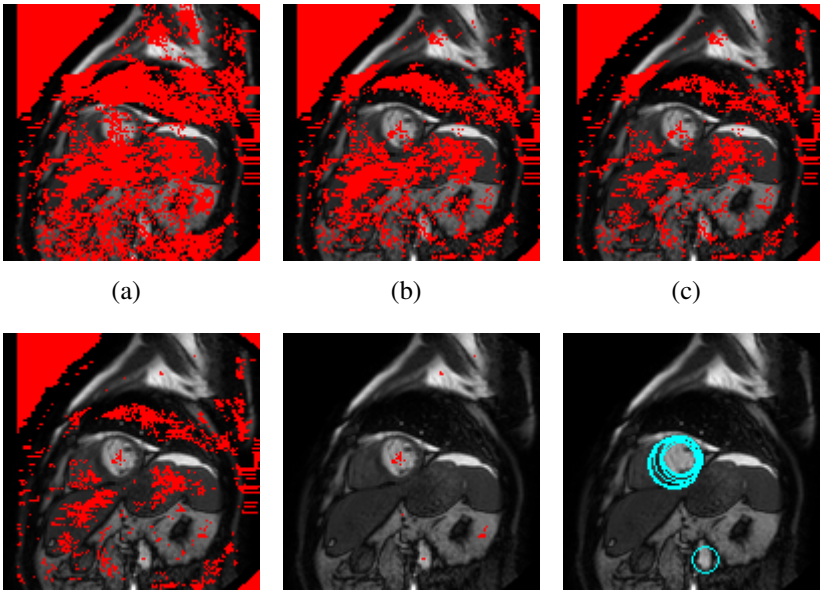

Figure 4.5: Candidates Reduction. A red pixel indicates the center of a remaining candidate. At the beginning every pixel represents a center of a possible candidate. First, the most left point of the candidate is fixed. (a) shows remaining candidates after inspecting the most right point. (b) shows remaining candidates after inspecting the highest and lowest point. Then it is checked if the inner area is brighter than the circle (c). Afterward the requirement for a homogeneous inner area is concerned (d). Finally, the difference of the gray values of the inner and outer points is checked if it is above a given threshold. (e) shows the remaining candidates. (f) shows the contours of the ten candidates with minimal gray value variance of the outer points.

Afterward for every pixel under the model the expected class based on the probabilities of the gray values is determined. For each pixel this gray value based classification is compared to the classification according to the region of the model that overlaps the pixel. All pixels for which the two classifications differ increase the difference measure between model and data. The error rate is defined as:

$$error\_rate = \frac{\#falsely\_classified\_samples}{\#samples} \tag{4.3}$$

Considering only one of the three different regions c_i and the gray values of pixels observed there, the probability of a gray value g_k observed in this region is defined as:

$$p(g_k|c_i) \quad = \quad \frac{H_{c_i}(g_k)}{\sum_{j=1}^{N} H_{c_i}(g_j)} \tag{4.4}$$

where $H_{c_i}(g_k)$ is the absolute frequency of the appearance of the gray value g_k in the region of c_i and N indicates the number of available gray values. For a specific

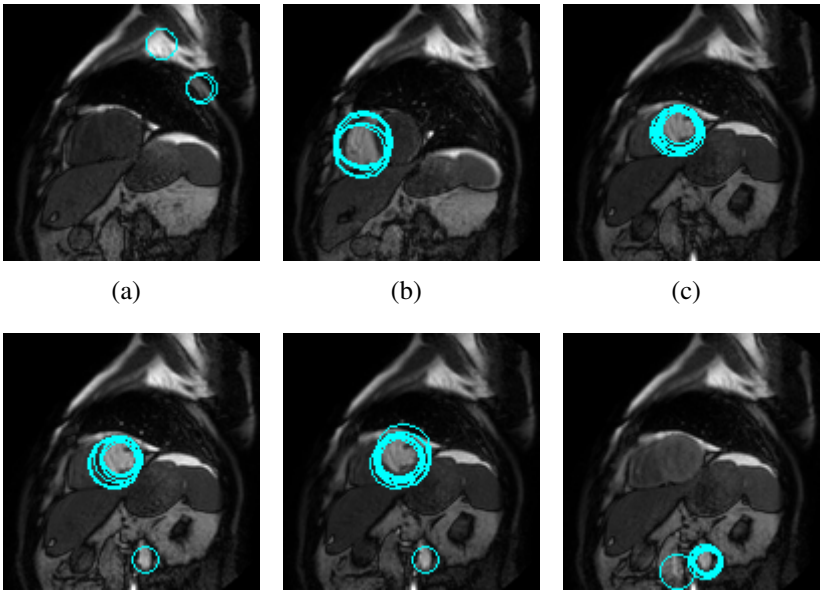

(a) (b) (c)

(d) (e) (f)

Figure 4.6: Multiple Candidates for different time steps. In cases where the contrast agent neither appears in the left ventricle nor in the right ventricle only false candidates are identified (a). If the contrast agent only appears in the right ventricle, it may be identified being a possible candidate (b). Correct candidates are identified if the contrast agent appears in the left ventricle (c). Sometimes still false candidates are found if the contrast agent appears in the left ventricle (d), (e). If no more contrast agent appears in the left ventricle, again only false candidates are identified (f).

gray value g_k the maximum likely assignment to a class c^* defines the gray value based class:

$$c^* = \arg\max_{c_i} p(g_k|c_i) \tag{4.5}$$

To deal with rotation the model is placed on the candidates and rotated in 20° steps. Finally the candidate with the lowest error rate is identified as the best candidate. The bounding box covering the whole candidate is defined as the region of interest. Algorithm 2 outlines the method for ROI extraction based on model matching.

Algorithm 2 Model based ROI detection

```
input: 4D dataset
output: most probably candidate
for all time steps do
    for all pixel do
        for all pixels along horizontal axis within distance 40-80mm do
            if gray value difference ≥ 0.01 then
                discard candidate
            else
                locate upper and lower pixel
                if gray value variance of outer pixels > 0.01 then
                    discard candidate
                else
                    locate inner pixels
                    if inner pixels darker than outer pixels then
                        discard candidate
                    else if gray value variance of inner pixels > 0.05 then
                        discard candidate
                    else if difference of inner and outer gray values < 0.3 then
                        discard candidate
                    else
                        recalculate outer variance with more pixels
                    end if
                end if
            end if
        end for
    end for
end for
sort candidates by outer gray value variance
keep 10 candidates with lowest variance
for all candidates do
    initialize model
    for all 20° model rotation do
        calculate error rate
    end for
end for
sort candidates by error rates
keep candidate with lowest error rate
```

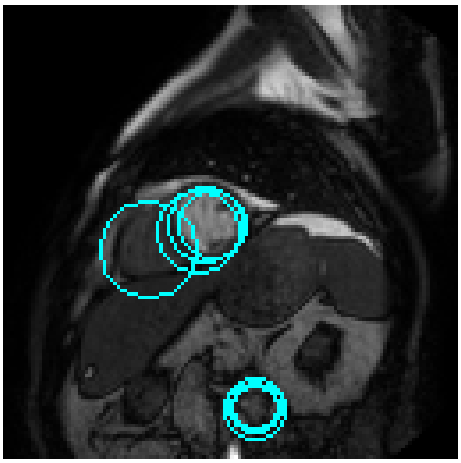

Figure 4.7: Most probably candidates. Ten candidates with lowest variance of the outer points. There still exist some false positives.

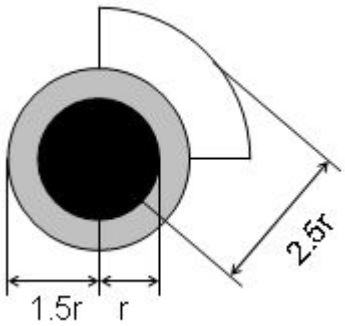

Figure 4.8: Model. Left ventricle (black), myocardium (gray), lung (white)

4.2 Registration

The relative long data acquisition time of perfusion data - up to 40 seconds and more - leads to one major problem in the segmentation process: breathing artifacts. During the data acquisition process the patient is asked to hold the breath. However, not all patients are able to do so during the whole acquisition time. Breathing causes the lung to expand and contract. Due to the fact that the heart lies directly next to the lung it will change its position and shape. Since the following segmentation step relies on spatial and temporal information, it is essential to correct these motion artifacts as much as possible.

In order to eliminate motion artifacts the images of different time steps need to be registered. For this a similarity metric is required. Gray value difference, mean square error, or cross correlation only lead to good results if all images exhibit similar gray values in corresponding regions. Perfusion images have time-dependent gray values due to the enhancement caused by the contrast agent. For such images mutual information [Viola and Wells, 1997] as difference measure is much better suited. Mutual information of two discrete random variables X and Y is defined as:

$$I(X,Y) = \sum_{y \in Y} \sum_{x \in X} p(x,y) \cdot \log \frac{p(x,y)}{p(x) \cdot p(y)} \tag{4.6}$$

Here the two random variables X and Y are the two images to be compared. $p(x)$ and $p(y)$ are the marginal probability distribution functions of the gray values of X and Y. They are defined as the normalized histograms for each of the two images. $p(x,y)$ is the joint probability distribution function for the gray values of both images and is defined as the normalized two dimensional joint histogram of the images.

The higher the mutual information, the higher the probability that the two compared images are well aligned. To minimize the computational costs and get better results the mutual information is not calculated for the whole images, but only at a discoidal region covering the candidate identified in the previous step (section 4.1). A reference image is chosen to which all other images are registered. This reference image is defined as the image at the time step where the previously detected candidate is located.

All other images, the so-called floating images, are placed on the reference image and shifted in all directions. The mutual information is calculated at every shifted position. The shift that leads to the maximum mutual information is considered as the optimal registration. The shift of the floating images is restricted by $\pm 2r$ whereas r is the radius of the candidate. The registration process is outlined in algorithm 3.

Algorithm 3 Registration

```
1: input: Reference Image R, Floating Image F, Candidate x, y, r
2: output: x-Shift, y-Shift
3: for dx := −2r to dx ≤ 2r do
4:     for dy := −2r to dy ≤ 2r do
5:         mi(dx,dy) ← MutualInformation (R(x,y), F(x+dx, y+dy))
6:     end for
7: end for
8: [x-Shift, y-Shift] ← arg min(mi(dx,dy))
```

4.3 Segmentation

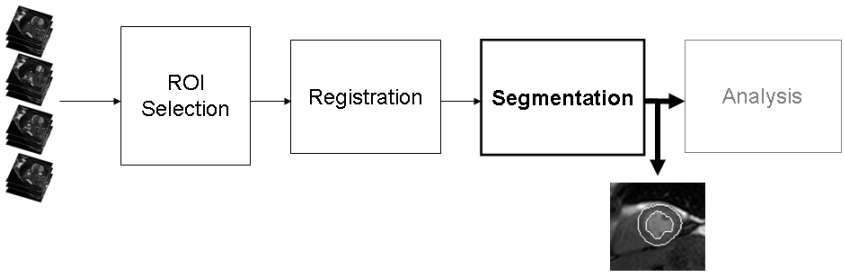

After registration the segmentation is performed: the goal is to detect the inner and outer boundaries of the myocardium in each time step. The fact that the contrast agent arrives at different anatomical regions at different times allows to separate the myocardium from other tissues.

The segmentation is done in two steps. In the first step characteristic intensity time curves for four different regions (left ventricle, myocardium, right ventricle, and background) are calculated (section 4.3.1). In the second step these curves are used to derive contours for the individual time steps (section 4.3.2).

4.3.1 Estimation of characteristic intensity time Curves

In perfusion images four regions can be identified by their characteristic intensity time curves: left ventricle, right ventricle, myocardium, and background. The goal is to estimate these four characteristic intensity time curves. Therefore, four steps are carried out to estimate them:

1. Initial Estimation
2. Classification
3. Classification Refinement
4. Final Estimation

Initial Estimation

Based on the model fitted to the data in the localization step and the rigid registration an initial estimate for the characteristic intensity time curves is made.

The outline of the initially detected circular candidate (section 4.1) identifies pixels of the myocardium. By observing the intensities of these pixels over time an initial approximation of the characteristic intensity time curve of the myocardium is set up (figure 4.9 (a)).

The characteristic intensity time curve of the left ventricle is considered next. To do so the pixels inside the circle defining the myocardium are observed. It is not guaranteed that the whole inner area of this circle corresponds to the left ventricle.

Therefore only pixels lying within a disc of half the myocardium's radius are used for a more robust estimation of the curve. Within this region fewer misleading pixels (as caused by papillary muscles) disturb the result. This leads to an initial characteristic intensity time curve of the left ventricle (figure 4.9 (b)).

Algorithm 4 Right Ventricle Detection

1: input: Candidate (x, y, r), Characteristic LV Curve c
2: output: RV Mask
3: create ring shaped mask with radii $\frac{3}{2}r$ and $2r$ centered at (x, y)
4: split mask into 8 segments with same size
5: determine characteristic intensity time curves for all segments
6: t $\leftarrow$ maximum upslope of c
7: determine maximum upslope for every segment before time step t
8: RV Mask $\leftarrow$ segment with maximum upslope

To estimate the characteristic intensity time curve for the right ventricle a representative region has to be identified first. Therefore the moment of contrast agent arrival in the left ventricle is needed. The greatest intensity increase in subsequent time steps indicates the moment of contrast agent arrival. For better results a linear fit of the gray values of three subsequent time steps is calculated. The slope of the resulting regression line ($y = mx + b$) defines the intensity change. The parameters (m, b) of the regression line are calculated as follows:

$$m = \frac{n\sum xy - \sum x \sum y}{n\sum x^2 - \left(\sum x\right)^2} \tag{4.7}$$

$$b = \frac{\sum y - m\sum x}{n} \tag{4.8}$$

To roughly locate the right ventricle the fact is used that contrast agent first appears in the right ventricle and then in the left ventricle. To locate the right ventricle a circular area around the myocardium is selected and divided into eight segments. For every segment the characteristic intensity time curve is determined (figure 4.9). The curves are determined by calculating the mean gray value of the whole segment for every single time step. The largest intensity increase before contrast agent arrival in the left ventricle is calculated. The segment where this increase is largest is considered to overlap with the right ventricle. Algorithm 4 outlines the procedure for the RV detection. The characteristic intensity time curve of this segment is then a representative curve of the right ventricle (figure 4.9 (c)).

The intensities of the background are assumed to be nearly constant over time. Therefore the characteristic intensity time curve of the background is defined as a curve with a constant value.

Classification

Pixels are classified as belonging either to the left ventricle, myocardium, right ventricle, or background. The characteristic intensity time curves of individual pixels

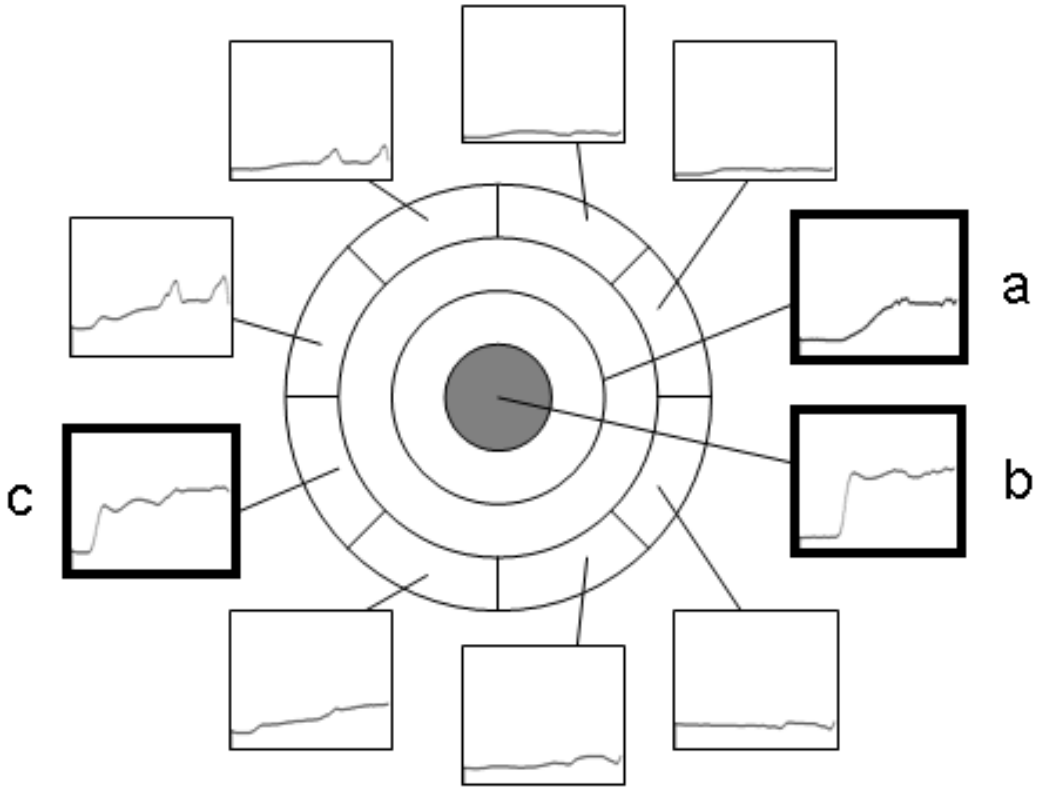

Figure 4.9: Example of segment curves. Pixels on the circle define the curve of the myocardium (a). Pixels inside the circle (gray area) define the curve of the left ventricle (b). Early contrast agent arrival reveals the segment representing the right ventricle (c).

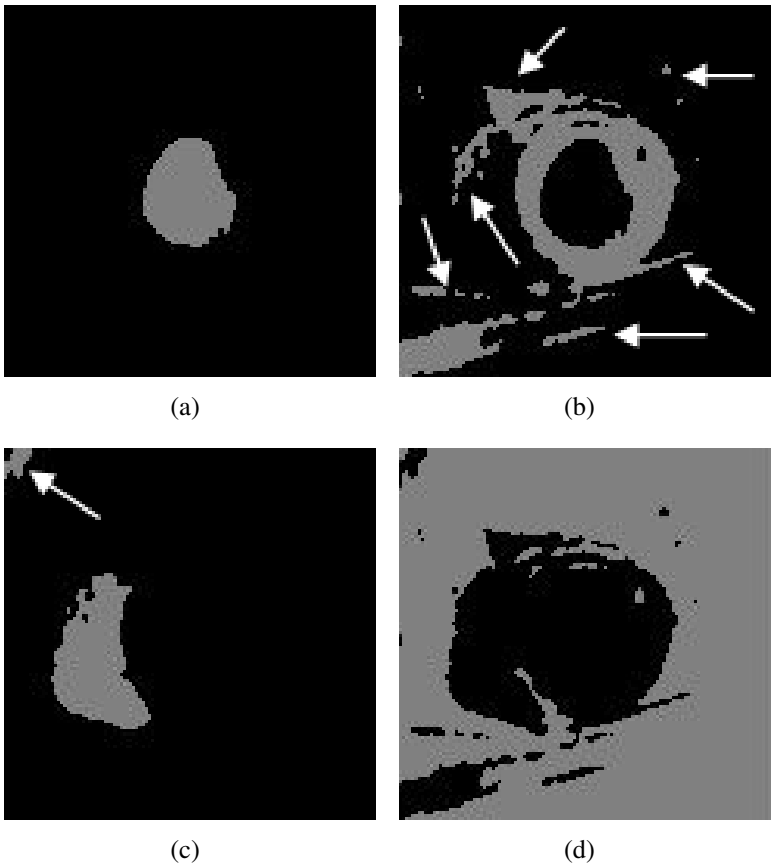

(a) (b)

(c) (d)

Figure 4.10: Initial classification. (a) Left Ventricle, (b) Myocardium, (c) Right Ventricle, (d) Background. Arrows indicates regions not correctly corresponding to the class.

are examined therefore. The characteristic intensity time curve which is most similar defines the class of the pixel. Differences between curves are measured as the mean square differences of the angles of the slopes:

$$d(c_1, c_2) = \sum_{i=0}^{N-1} (\alpha_1(i) - \alpha_2(i))^2 \tag{4.9}$$

$$\alpha_j(i) = \arctan m_j(i) \tag{4.10}$$

where c_1 and c_2 identifies the two curves to compare. $m_j(i)$ is the slope of curve j at position i. The decision for a class is defined as:

$$class_v = \arg\min_i d(c_i, c_v) \tag{4.11}$$

where c_i identifies the different previously calculated characteristic intensity time curves for the classes (left ventricle, right ventricle, myocardium, background) and c_v the characteristic intensity time curve for an individual voxel.

This measurement takes only relative curve changes into account to compensate different intensity offsets.

Classification Refinement

The classification masks obtained in the previous step still contain regions not corresponding to their class (figure 4.10). To get a good final estimation of the characteristic intensity time curves these masks have to be refined. The masks of left ventricle and right ventricle are simply refined by selecting their largest connected components.

The mask of the myocardium is improved based on the branch-and-bound approach from Yeh et al. [Yeh *et al.*, 2005]. It is assumed that the outer contour of the myocardium has approximately a circular shape. The mask of the myocardium is transformed into polar coordinates (angle + radius, figure 4.13 (a)) in respect of the center of the ROI. Every column identifies an angle and every row a radius. A perfectly circular boundary of the myocardium would appear as a straight horizontal line. To find an approximately circular curve a path going from left to right containing every column only once has to be found (figure 4.11). To allow some shape variations the radius is allowed to change by one pixel between adjacent columns. To fulfill the constraint of a closed curve the first and last column are considered adjacent. To find the optimal curve weights are defined for every pixel: At a transition in one column from the myocardium to a different type of tissue the weight is set to zero, from a different tissue to the myocardium to two and in all other cases to one (figure 4.12(b)). Then the path with minimum costs fulfilling the constraints is calculated (figure 4.13 (b)) and the optimized area is extracted (figure 4.13 (c)). Algorithm 5 outlines the process of finding a path with minimal costs in a polar map.

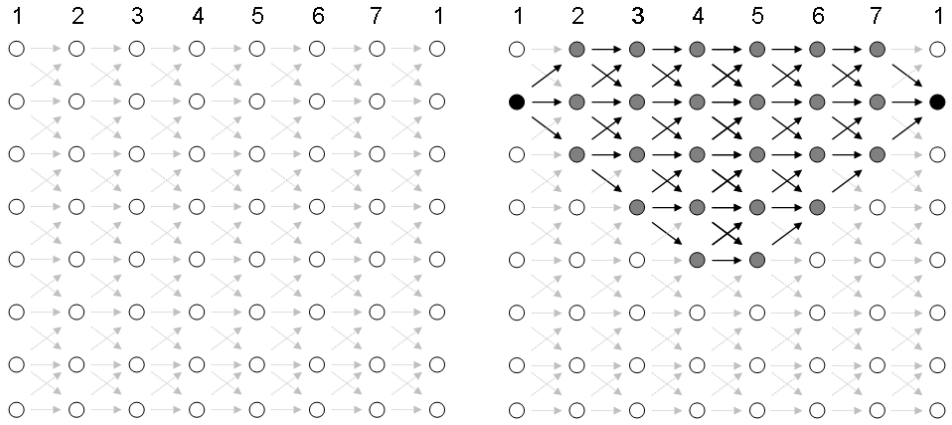

(a) (b)

Figure 4.11: (a) shows all possible connections between adjacent columns. A column identifies an angle and the rows identifies the different radii. The last column is the same as the first column. Fixing a start point constricts the possible paths from left to right (b).

Algorithm 5 Find path with lowest costs in polar map

input: polar map
output: P_i path with lowest costs
append first column to the end of the polar map ▷ closed curve constraint
[width, height] = size(polar map)
calculate weights $w_{i,j}$
for $r = 0$ ... height **do**
  $cost_{i,j} = \infty \forall (0 \leq i \leq width, 0 \leq j \leq height)$
  $cost_{0,r} = w_{0,r}$
  for $c = 1$ to width **do**
    for $k = 0$ to height **do**
      if k lies on valid path starting from r **then**
        $cost_{c,k} = w_{c,k} + \min_{predecessor} cost$
      end if
    end for
  end for
  trace path P_r with lowest costs C_r
end for
determine Path P_i with lowest costs C_i

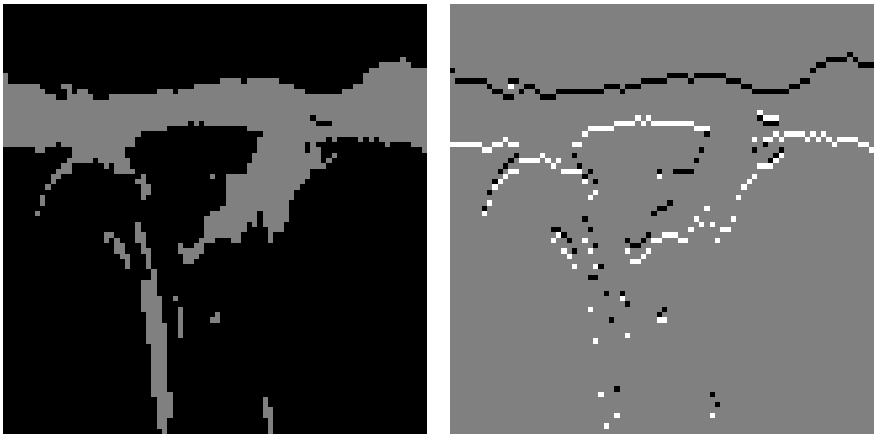

(a) (b)

Figure 4.12: For the polar image of the myocardial mask (a) the weights are calculated (b). The weights are defined as: 2 - black, 1 - gray, 0 - white.

Final Estimation

For the final estimation of the characteristic intensity time curves the refined classification masks are considered. The mean values of the pixels within the masks are observed for every time step. These mean values lead to the final estimation of the characteristic intensity time curves.

4.3.2 Boundary Extraction

In the previous step the characteristic intensity time curves for left ventricle, right ventricle, myocardium, and background are estimated. This is done by focusing on the temporal information. In the boundary extraction step the temporal information is ignored and every individual time step is observed separately. The goal is to extract the inner and outer boundary of the myocardium at every time step. Based on motion artifacts it is problematic to extract the boundaries at a single time step and apply them to the others.

This step has to deal with a great challenge: depending on the progress of the contrast agent highly varying contrasts are observed for different regions. At the beginning of the image sequence contrast agent appears neither in the left ventricle, right ventricle, nor in the myocardium (figure 1.1(a)). Therefore the contrast between these regions is very low. Later the contrast agent appears in the right ventricle whereby a good contrast appears between myocardium and right ventricle (figure 1.1(b)). Then the contrast agent appears in the left ventricle and a good contrast exists between myocardium and left ventricle (figure 1.1(c)). Until now the contrast between myocardium and background especially the lung is very low. If the contrast agent appears in the myocardium this contrast increases (figure 1.1(d)). The contrast between left ventricle and myocardium as well as right ventricle and myocardium simultaneously decreases during contrast agent wash-out. Due to the

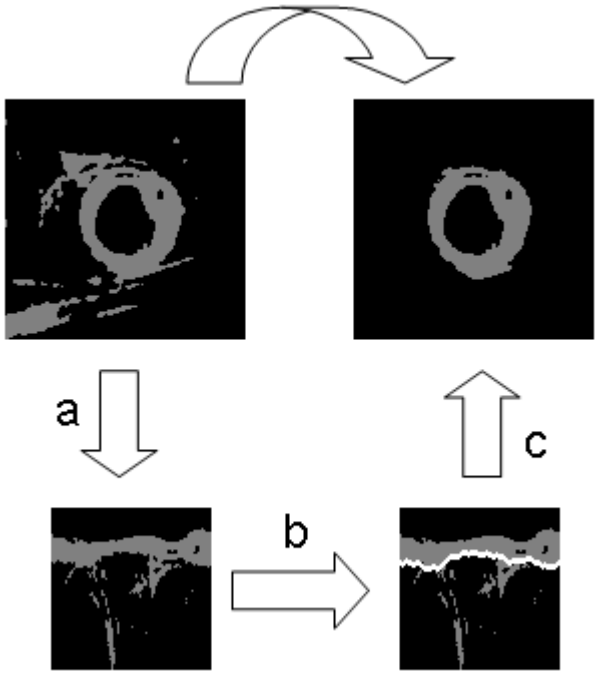

Figure 4.13: Optimization of the myocardial boundary. After transforming the image into polar coordinates (a), the path with minimum costs (white curve) is determined (b) and then transformed back to the spatial domain (c).

varying contrast between myocardium and other tissue the inner and outer boundary of the myocardium are extracted separately.

For extracting the inner boundary a good contrast between myocardium and left ventricle is necessary. Therefore the inner boundary is only clearly determined in time steps where the difference of the characteristic intensity time curves of left ventricle and myocardium is greater than a given threshold (10% of gray value range). At all other time steps a default boundary is assigned. The default boundary is determined at the time step with highest contrast between left ventricle and myocardium. This time step is derived from the characteristic intensity time curves of these regions.

For extracting the outer boundary a good contrast between myocardium and surrounding tissues (right ventricle and background) is necessary. However there exists no image providing this requirement. Therefore the outer boundary is first determined for all time steps and then further refined.

To determine the boundaries the same algorithm as in the previous section (4.3.1) - finding a path with minimal costs - is used. However, the assignment of weights has to be done differently since individual time steps and no time varying gray values are considered now.

(a) (b) (c) (d)

Figure 4.14: Thresholded images based on myocardial characteristic intensity time curve. In (a) contrast agent appears neither in the right ventricle, left ventricle, nor in the myocardium. (b) contrast agent appears in the right ventricle. (c) contrast agent appears in the left ventricle. (d) contrast agent appears in the myocardium.

Weight Definition

For each time step t the mean gray values $\mu_{myo}(t)$ and $\mu_{LV}(t)$ and standard deviations $\sigma_{myo}(t)$ and $\sigma_{LV}(t)$ for the regions of myocardium and left ventricle are calculated. This is done based on the optimized masks as determined in section 4.3.1.

It is assumed that the distribution of gray values for myocardium and left ventricle follow a normal distribution. The intersection point $intersection(t)$ of the curves representing those normal distributions is determined. Each image is thresholded keeping pixels within a specific gray value interval. The interval for thresholding is determined as:

$$interval(t) = \begin{cases} [\mu_{myo}(t) - \sigma_{myo}(t), intersection(t)], & \text{if } \mu_{myo}(t) \leq \mu_{LV}(t) \\ [intersection(t), \mu_{myo}(t) + \sigma_{myo}(t)], & \text{if } \mu_{myo}(t) > \mu_{LV}(t) \end{cases}$$

After thresholding each pixel of the image is assigned either to myocardium (M) or to other tissue (O). Figure 4.14 shows thresholded images at different time steps. White pixels indicate pixels assigned to myocardium and black pixels to other tissue.

Then the thresholded images are transformed into polar coordinates (in respect of the center of the ROI) to detect the boundaries with algorithm 5.

For detecting the boundary as a path with minimal costs weights are assigned to pixels. For the inner boundary the weights are defined as follows: M-M: 20, O-M: 5(n-1), M-O:20, O-O: 10. Whereby n indicates the n-th transition from O to M in one column starting from the center of the left ventricle. This is used to penalize transitions which are farther away from the center and therefore more unlikely correct transitions. For the outer boundary a transition from M to O a weight of zero and for all others a weight of 10 is assigned. To avoid intersections between the inner and outer boundary all pixels inside the inner boundary are assigned infinity. Figure 4.15 shows weights for different time steps. In some time steps (4.15(a),

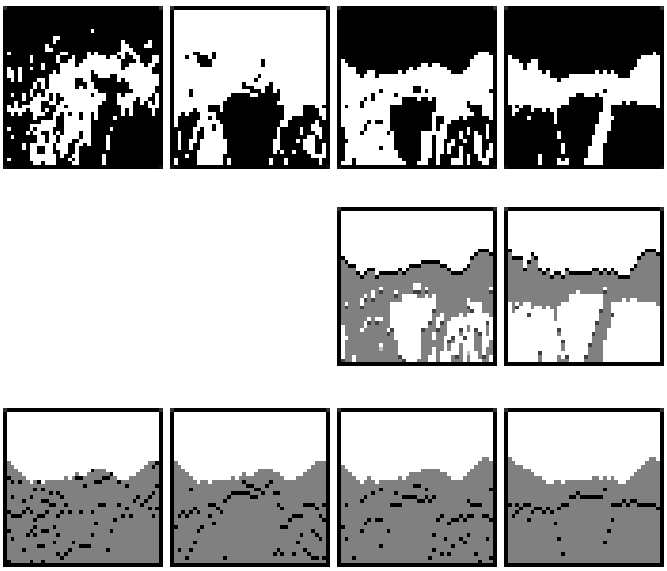

Figure 4.15: Boundary Weights. The top row shows thresholded images transformed into polar map. The center row shows the weights for the inner boundary and the bottom row shows the weights for the outer boundary. The missing two images in the center row indicate that for these time steps the inner contour is not calculated. Because of poor contrast between myocardium and left ventricle the default contour is assigned for these time steps. Black indicates minimal cost and white maximal cost.

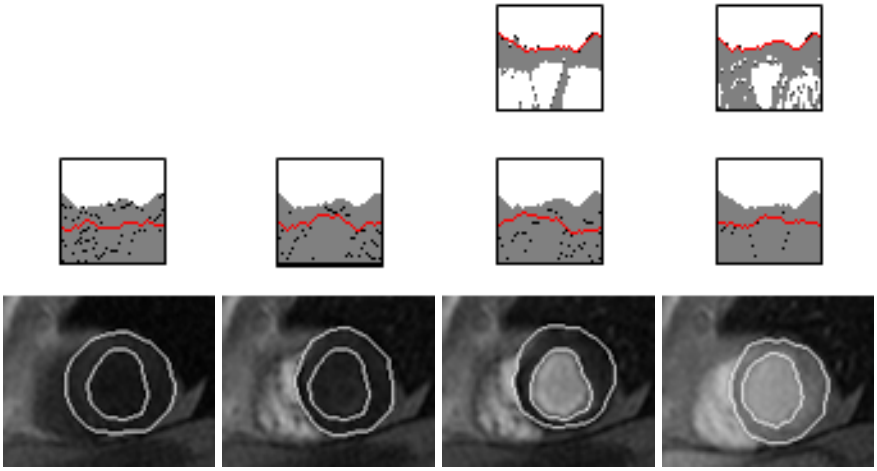

Figure 4.16: Optimal Path for Boundaries. Optimal path for inner boundary (top row) and outer boundary (center row). The bottom row shows the boundaries transformed back to Cartesian coordinates.

4.15(b)) only weights for the outer boundary are defined. Because of poor contrast between myocardium and left ventricle the default contour is assigned there for these time steps. Therefore the inner contour is known and has not to be determined again.

Applying algorithm 5 to the defined weights leads to paths with minimal costs. Transforming these paths back into Cartesian coordinates leads to the myocardial boundaries (figure 4.16). Some of the outer boundaries (figure 4.16(a), 4.16(d)) are inaccurate and do not reside to the edges in the images.

Outer Boundary Refinement

An additional step to refine the outer boundaries follows. It is assumed that no contraction of the myocardium in the perfusion images is observed because the images are ECG-gated. On the other hand it is assumed that the inner boundaries are sufficiently accurately detected. The thickness of the myocardium is determined along rays starting at the center of the left ventricle. The rays are positioned at equidistant angles. This is done separately for every time step. Then the median distances along the rays over time are determined. The outer boundaries are adjusted to be located at the median distance to the inner boundaries (figure 4.17). Algorithm 6 outlines the process for determining the myocardial boundaries.

This section has given a detailed description how the segmentation is performed. In the first part the segmentation process deals with time-dependent information to estimate characteristic intensity time curves for different interesting regions (right ventricle, left ventricle and myocardium). The following part deals with spatial information for every time step separately. The characteristic intensity time curves of the left ventricle and the myocardium allow the definition of an individual thresh-

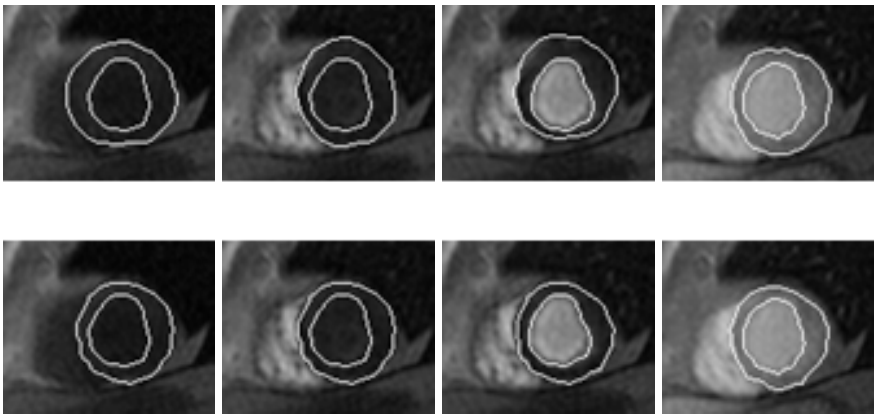

(a) (b) (c) (d)

Figure 4.17: Myocardial Boundaries for different time steps. Before (top row) and after (bottom row) refining the outer boundary.

Algorithm 6 Boundary Determination

input: Characteristic intensity time curves for myocardium c_{myo} and left ventricle c_{LV}, Registered Images I
output: Myocardial Countours for every time step
for all Time steps t **do**
  Threshold image I(t) according to $c_{myo}(t)$ and $c_{LV}(t)$
  transform image into a polar map
  if $|c_{myo}(t) - c_{LV}(t)| > 10\%$ of gray value range **then** ▷ contrast sufficient
    define weights for inner boundary
    find path with minimum costs
  else
    assign default boundary
  end if
  define weights for outer boundary
  find path with minimum costs
  calculate myocardial thickness for different rays
end for
calculate median myocardial thickness over time
add median myocardial thickness to all inner boundaries

old for every time step. Based on these thresholded images the contours of the myocardium are extracted.

The following section uses these segmentations to quantify the myocardial perfusion. Based on this quantification it is possible to make predictions on the health status of the patient.

4.4 Analysis

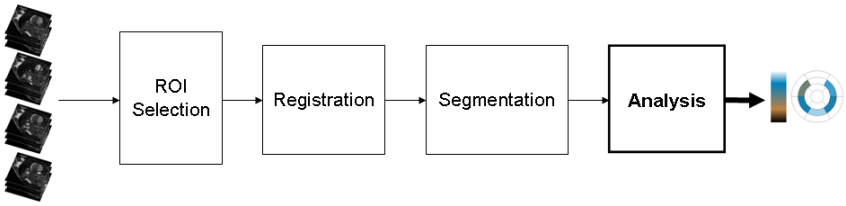

The previous section focused on the segmentation of the myocardium in perfusion MRI datasets. This section focuses on the analysis of myocardial perfusion based on the previously segmentation. The goal is to quantify and visualize the perfusion to offer predictions on the heart functionality of the patient. The quantification is determined for the segments recommended by the American Heart Association (AHA [AHA, 2007; Cerqueira *et al.*, 2002]) (figure 3.3). The perfusion is then visualized in a Bull's Eye plot (figure 3.4). For the analysis and visualization of the different segments it is essential to identify the areas representing them. This leads to a three step analysis procedure: segment definition, segment analysis, visualization.

4.4.1 Segment Definition

As introduced previously (sec. 3.4) the AHA has recommended a standard for partitioning the myocardium. With this partitioning it may be possible to identify narrowed vessels. Therefore it is necessary to divide the myocardium into these recommended segments.

The myocardial area separating left and right ventricle is divided into two segments at the basal (segments no. 2 and 3) and mid-cavity (segments no. 8 and 9) slice. Furthermore the two segments bordering the right ventricle have the same size. The remaining myocardial area is divided into four segments of equal size. At the apical slice the area separating left and right ventricle is a single segment. The remaining myocardial area is divided into three segments of equal size.

To obtain a segment definition holding these requirements it is necessary to detect the area where the right ventricle is attached to the myocardium. After identifying this area the myocardium can be divided into the recommended segments.

Right Ventricle - Myocardium attaching area

To identify the area where the right ventricle is attached to the myocardium the previously obtained right ventricle mask (section 4.3.1) is considered. The mask is

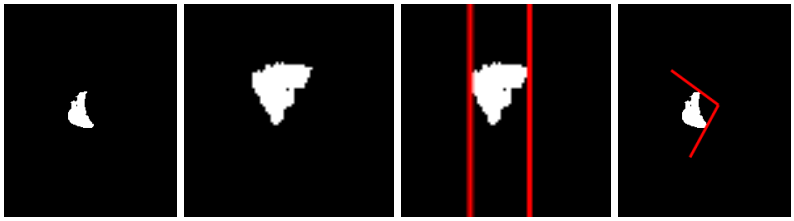

(a) (b) (c) (d)

Figure 4.18: Right Ventricle - Myocardium connection detection. The right ventricle mask (a) is transformed into a polar map (b). The start and end point of the right ventricle are determined (c) to locate the attaching point of the right ventricle to the myocardium (d).

Figure 4.19: Myocardial Segments.

transformed into a polar map (figure 4.18(b)) in respect of the center of the ROI. In the polar map the width and the beginning and ending point of the area are determined (figure 4.18(c). Transforming these points back into Cartesian coordinates the contact area between myocardium and right ventricle is identified.

Segment Partitioning

After locating the area where the right ventricle attaches the myocardium, the myocardium can be divided into its segments. Therefore the attaching area is divided into two segments with same size. Furthermore the remaining myocardial area is divided into four segments with same size. Figure 4.19 shows an example of the determined myocardial segments.

4.4.2 Segment Analysis

After defining the different segments of the myocardium they can be analyzed. For the analysis the characteristic intensity time curves of the segments are considered. Based on these characteristic intensity time curves measurements can be evaluated. As shown in section 2.7 different measurements exist: Peak Enhancement (PE),

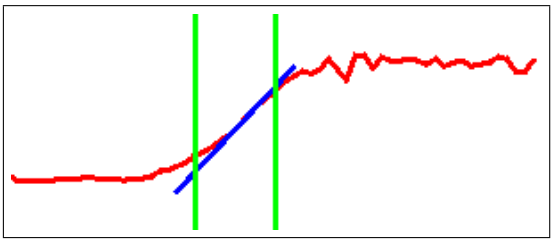

Figure 4.20: Myocardial Intensity Time Curve. The blue line shows the maximum slope of five subsequent points. The green vertical lines delimit the determined contrast agent accumulation period.

Contrast Appearance Time (CAT), Time To Peak (TTP), Integral, Mean Transit Time (MTT), Upslope, and Downslope. It has been shown that regions with bad perfusion can be identified by the measurements upslope and peak enhancement ([Al-Saadi *et al.*, 2000; Al-Saadi *et al.*, 2001; Christian *et al.*, 2004; Schwitter *et al.*, 2001; Nagel *et al.*, 2003]) and that the upslope of the characteristic intensity time curve linearly fits to the myocardial perfusion reserve. Therefore this thesis focuses on determining the upslope for the segments.

Oeltze et al. [Oeltze *et al.*, 2007] characterize the upslope as the maximum slope between two or three subsequent time steps during contrast agent accumulation in the myocardium. Therefore the period of contrast agent accumulation has to be identified. After identifying this period the upslope is evaluated for every segment.

Contrast Agent Accumulation Period

To identify the contrast agent accumulation period the characteristic intensity time curve of the myocardium is investigated. The mean intensity values of the segmented myocardium at every time step define this characteristic intensity time curve. It is assumed that the maximum slope of five (linearly fitted) subsequent points of this curve appears during the contrast agent accumulation period. The accumulation period is assumed to start three time steps before and ends three time steps after the maximum slope appears. The maximum slope of five subsequent points and the accumulation period are shown in figure 4.20.

Segment Analysis

After the contrast agent accumulation period (figure 4.20) is identified, the maximum slope can be calculated for every segment. Therefore the characteristic intensity time curves for every segment are observed. The mean intensity values of a segment at every time step define the characteristic intensity time curve. To identify the maximum slope all possible slopes of three (linearly fitted) subsequent points of these curves within the accumulation period are calculated. The resulting maximum slopes indicate the perfusion quantification of the segments. They are visualized in figure 4.21.

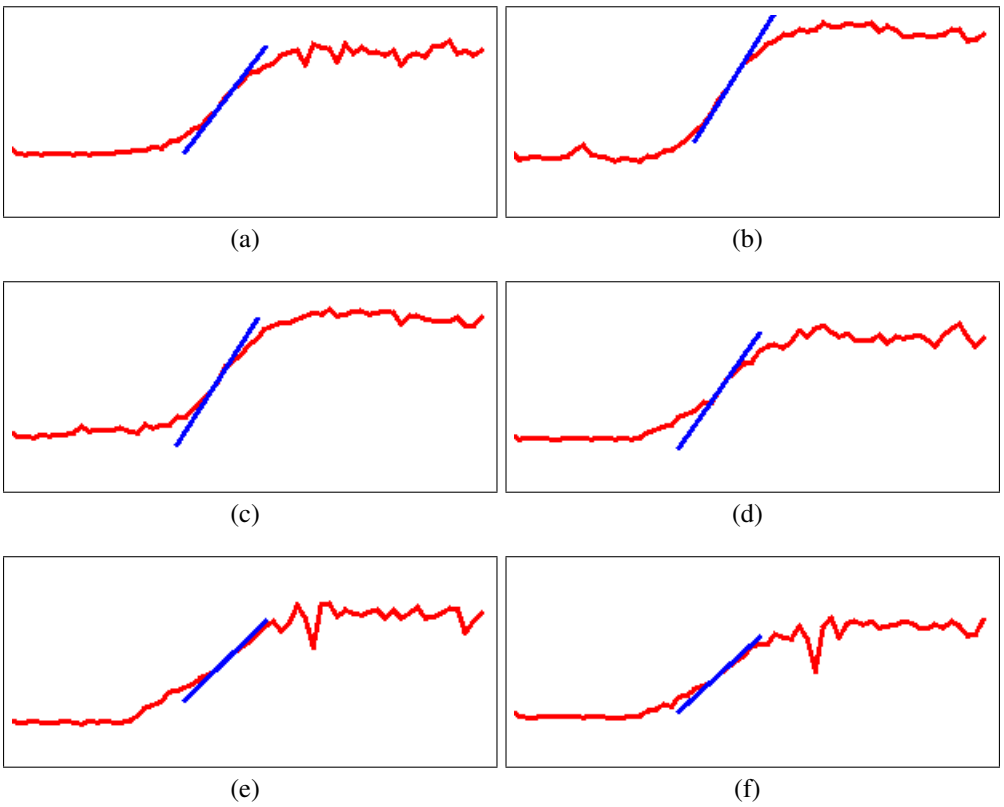

Figure 4.21: Segment Intensity Time Curves. Segment Intensity Time curves for all segments of the myocardium at a mid-cavity slice. The curves represent segments no.7 - no.12. The blue lines show the maximum slopes of three subsequent points inside the determined accumulation period.

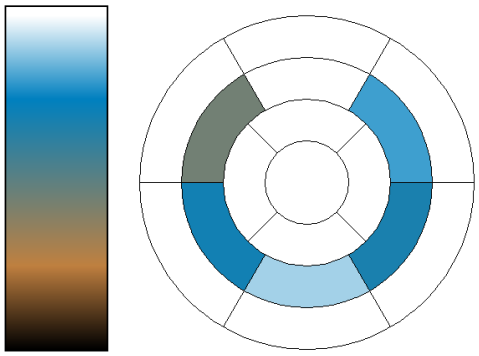

Figure 4.22: Bull's-Eye Plot. Black indicates a bad and white a good perfusion. This Bull's-Eye plot consists only of one ring because the dataset is only segmented at the mid-cavity slice.

4.4.3 Visualization

The previous section has quantified the perfusion for the myocardium. This section will show a method to visualize these quantified measurements to get a visual impression of the perfusion. The quantified perfusion is illustrated using a Bull's-Eye plot (figure 3.4). MRI does not provide absolute measurements as CT, so only a semi-quantitative analysis can be performed. Therefore the previously determined measurements are normalized by the maximum value. These normalized measurements are then color-coded and illustrated in a Bull's-Eye plot (figure 4.22).

4.5 Summary

This section outlines the whole image processing pipeline described in this chapter. Two different methods were introduced for ROI selection. One takes only temporal information into account and the other one only spatial information. The ROI selection is followed by a registration step maximizing the mutual information. The subsequent step first estimates characteristic intensity time curves for different anatomical structures. Based on these curves the myocardial boundaries are extracted. The analysis of perfusion is performed in a concluding step. Therefore the perfusion is quantified and visualized in a Bull's Eye plot. Figure 4.23 outlines this image processing pipeline.

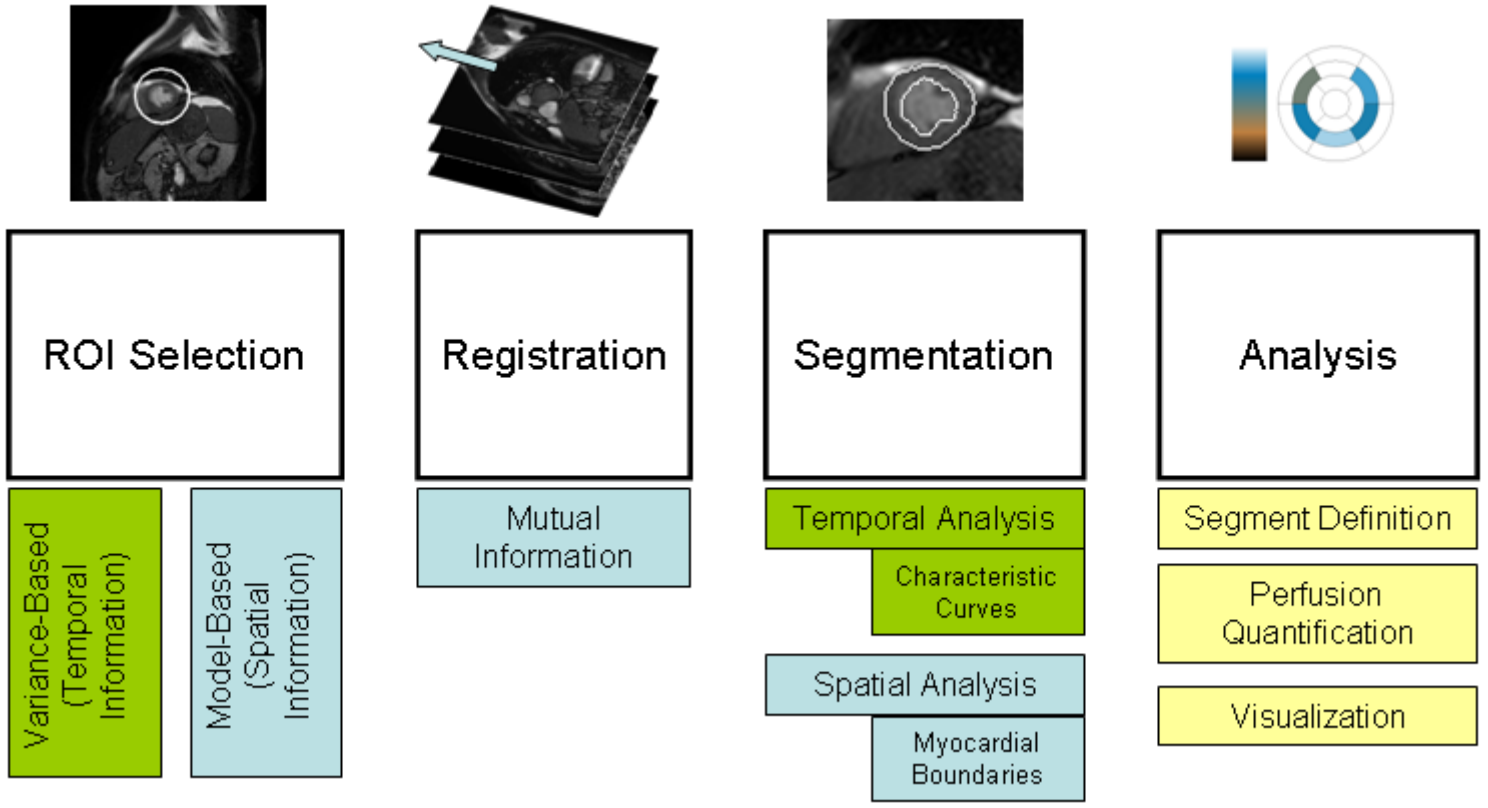

Figure 4.23: Pipeline Overview. Green highlighted areas deals with temporal, blue highlighted with spatial and yellow highlighted with both informations.

Chapter 5

Results

This chapter presents the results obtained with the implementation introduced in the previous chapter. The chapter is organized as follows:

- An overview of the used datasets is given in section 5.1.
- In section 5.2 the results obtained from the ROI selection step are presented.
- The registration results are presented in section 5.3.
- Section 5.4 shows the segmentation results.
- The final analysis results are presented in section 5.5.
- Finally, an overview of the performance of the method is given in section 5.6.

5.1 Dataset Overview

The presented method was tested on eleven cardiac perfusion MRI datasets from nine different patients and three different scanners. Five patients were examined

Patient	*Scanner*	*Resolution*	*R/S*	*Steps*	*Slices*
Patient 1	Philips Gyroscan 1.5T NT Intera	128×128	N/A	17	5
Patient 2	Philips Gyroscan 1.5T NT Intera	128×128	N/A	27	5
Patient 3	Philips Gyroscan 1.5T NT Intera	128×128	N/A	18	5
Patient 4	Philips Gyroscan 1.5T NT Intera	128×128	N/A	29	3
Patient 5	Philips Gyroscan 1.5T NT Intera	128×128	N/A	43	5
Patient 6	Philips 1.5 Intera	256×256	R	77	3
			S	77	3
Patient 7	Philips 1.5 Intera	256×256	R	66	3
			S	59	3
Patient 8	Siemens Symphony 1.5T	208×256	N/A	60	1
Patient 9	Siemens Symphony 1.5T	208×256	N/A	60	1

Table 5.1: Overview of used datasets.

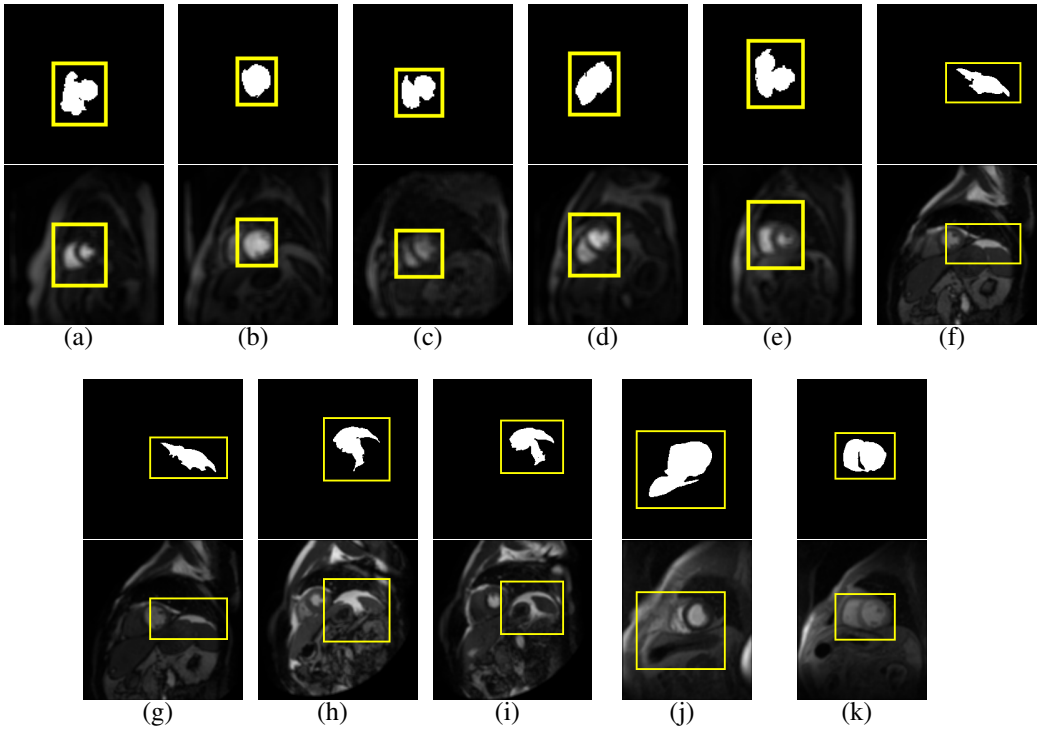

Figure 5.1: Variance Based ROI Selection Results.(a) patient 1, (b) patient 2, (c) patient 3, (d) patient 4, (e) patient 5, (f) patient 6 under rest, (g) patient 6 under stress, (h) patient 7 under rest, (i) patient 7 under stress, (j) patient 8, (k) patient 9. The top row shows the determined bounding box (yellow box) around the greatest connected component (white area). The bottom row shows the bounding box illustrated on a mid-cavity slice.

with a Philips Gyroscan 1.5T NT Intera with a resolution of 128×128 voxels, three to five slices and 17 to 43 time steps. Two patients were scanned with a Siemens Symphony 1.5T with a resolution of 208×256 voxels, only one slice and 60 time steps. Two patients were examined under rest and stress conditions with a Philips 1.5T Intera with a resolution of 256×256 voxels, three slices and 59 to 77 time steps. The datasets are listed in table 5.1.

5.2 ROI Selection Results

Figure 5.1 shows the results obtained from the variance based ROI selection. The ROI is incorrectly determined for patient 6 and patient 7 under rest as well as under stress conditions (5.1(f) - 5.1(i)). This results from huge motion artifacts and poor contrast enhancement caused by the contrast agent.

Figure 5.2 shows the results obtained from the model based ROI selection. The method only fails for patient 3 (figure 5.1(c)). Instead of the left ventricle the right is found. This results from the irregular shape of the left ventricle and the very noisy images.

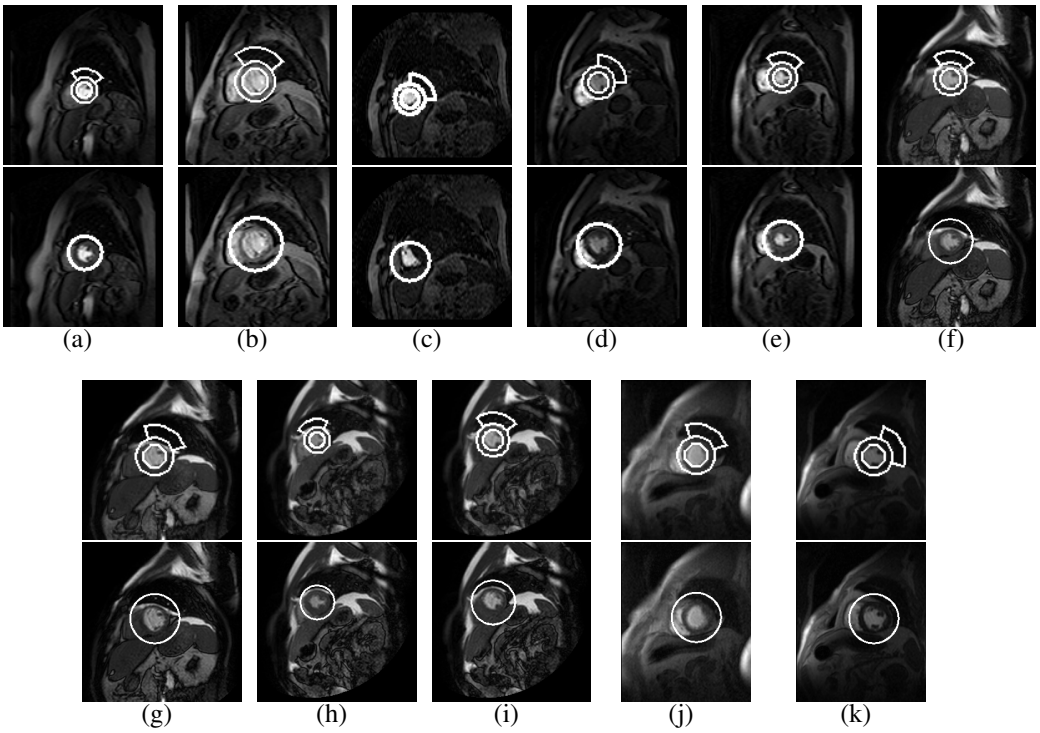

Figure 5.2: Model Based ROI Selection Results.(a) patient 1, (b) patient 2, (c) patient 3, (d) patient 4, (e) patient 5, (f) patient 6 under rest, (g) patient 6 under stress, (h) patient 7 under rest, (i) patient 7 under stress, (j) patient 8, (k) patient 9 The top row shows the best determined candidate identifying the left ventricle. The bottom row shows the ROI surrounding the candidate's left ventricle and myocardium.

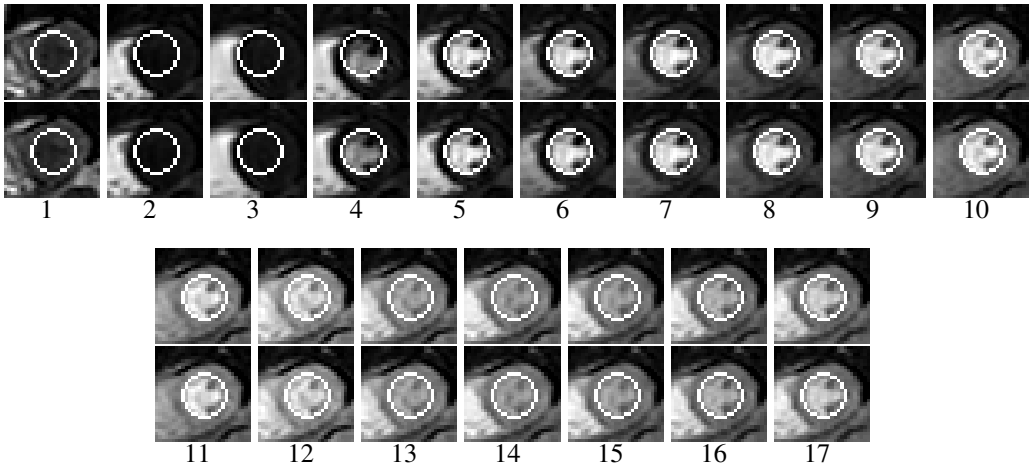

Figure 5.3: Registration Results for Patient 1.

For further examination (registration, segmentation, analysis) the model based ROI selection is used for all datasets. For the dataset from patient 3 the ROI was manually selected to allow a further examination of it.

5.3 Registration Results

Figures 5.3 - 5.13 show the results obtained from the image registration process. For each time step two images are shown. The upper image shows the candidate - identified in the ROI selection step - placed on the unregistered image. The lower image shows the candidate placed on the registered image. For every dataset the whole image sequence is shown. The registered images are compared with the non-registered images to determine an improvement or a decline of motion artifacts. This evaluation is done by visual inspection.

Patient 1 (figure 5.3)

The registration process leads to nearly perfect results and compensates the motion artifact of one image (4). At time step 3 the registration leads to a better but not exactly to the expected result. For all other images equal results like without registration are gained.

Patient 2 (figure 5.4)

The registration process provides better results for three images (3, 15, 27). In one case (21) the registration fails but leads nearly to the same result as without registration. For all other images equal results as without registration are gained.

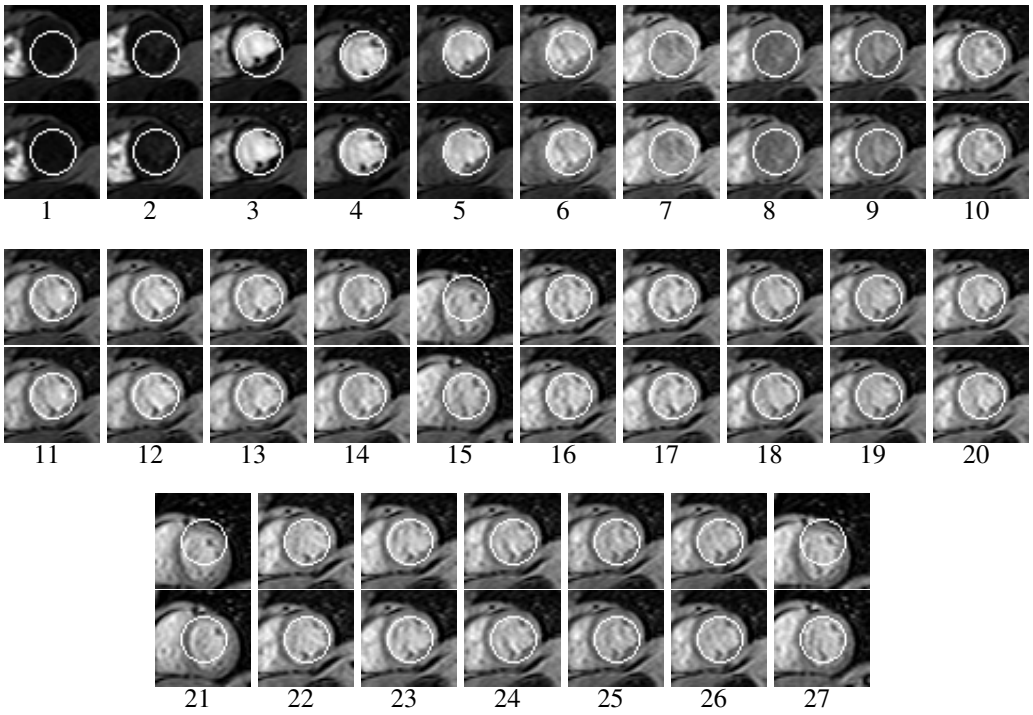

Figure 5.4: Registration Results for Patient 2.

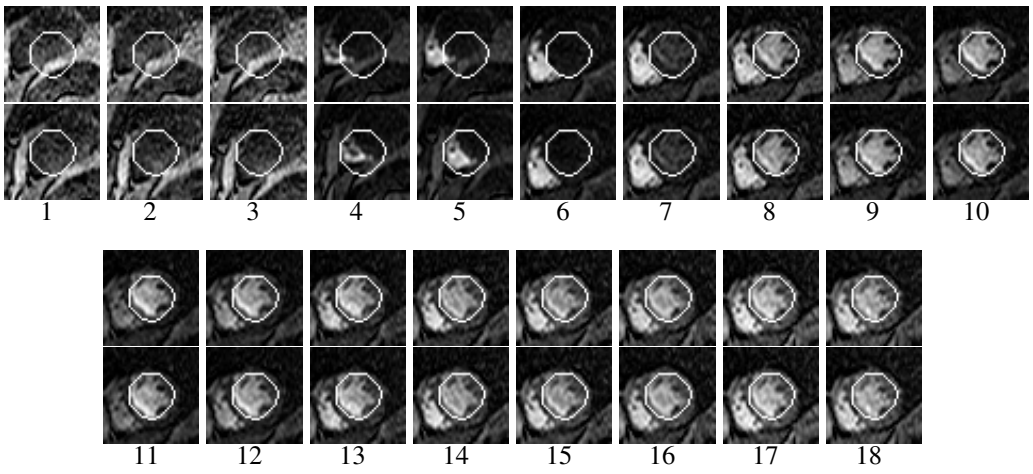

Figure 5.5: Registration Results for Patient 3.

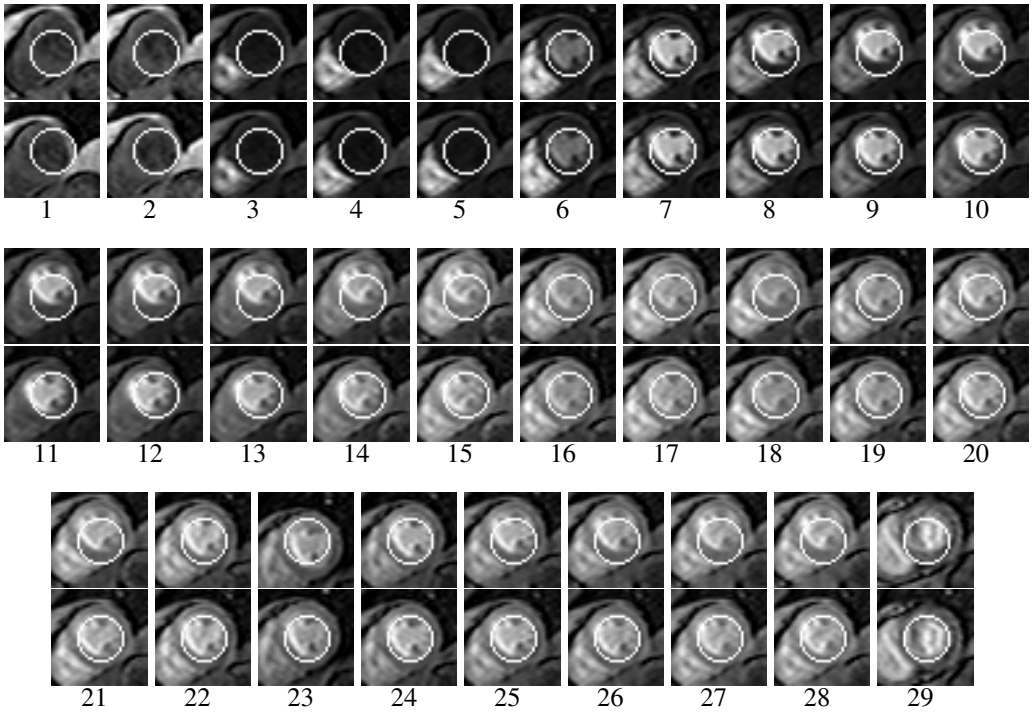

Figure 5.6: Registration Results for Patient 4.

Patient 3 (figure 5.5)

For the first four time steps (1-4) no improvement was achieved although they are clearly unregistered. In one case (5) a decline and in two cases (6,8) an improvement occur. For all other images equal results like without registration are gained.

Patient 4 (figure 5.6)

For two time steps (1,2) no improvements were achieved although they are clearly unregistered. For many other images improvements were achieved (4, 8-29). For all other images equal results like without registration are gained.

Patient 5 (figure 5.7)

The registration process leads to nearly perfect results and compensates the motion artifacts in all images. Improvements (16,25,26,36-38) without any declines are gained.

Patient 6 under rest conditions (figure 5.8)

The registration process leads to nearly perfect results and compensates the motion artifacts in all images. Improvements (8-10,29-33,38-61) without any declines are gained.

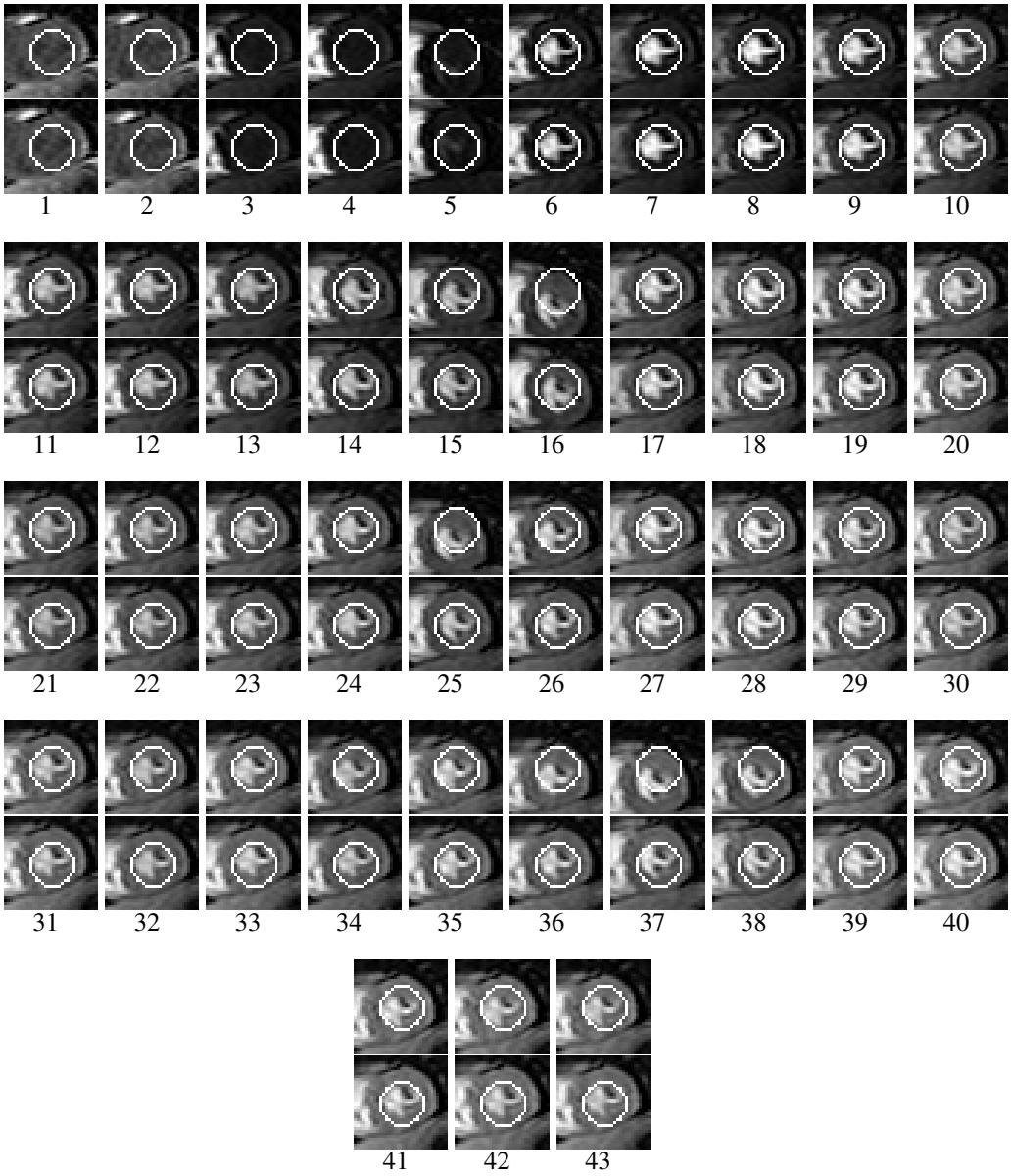

Figure 5.7: Registration Results for Patient 5.

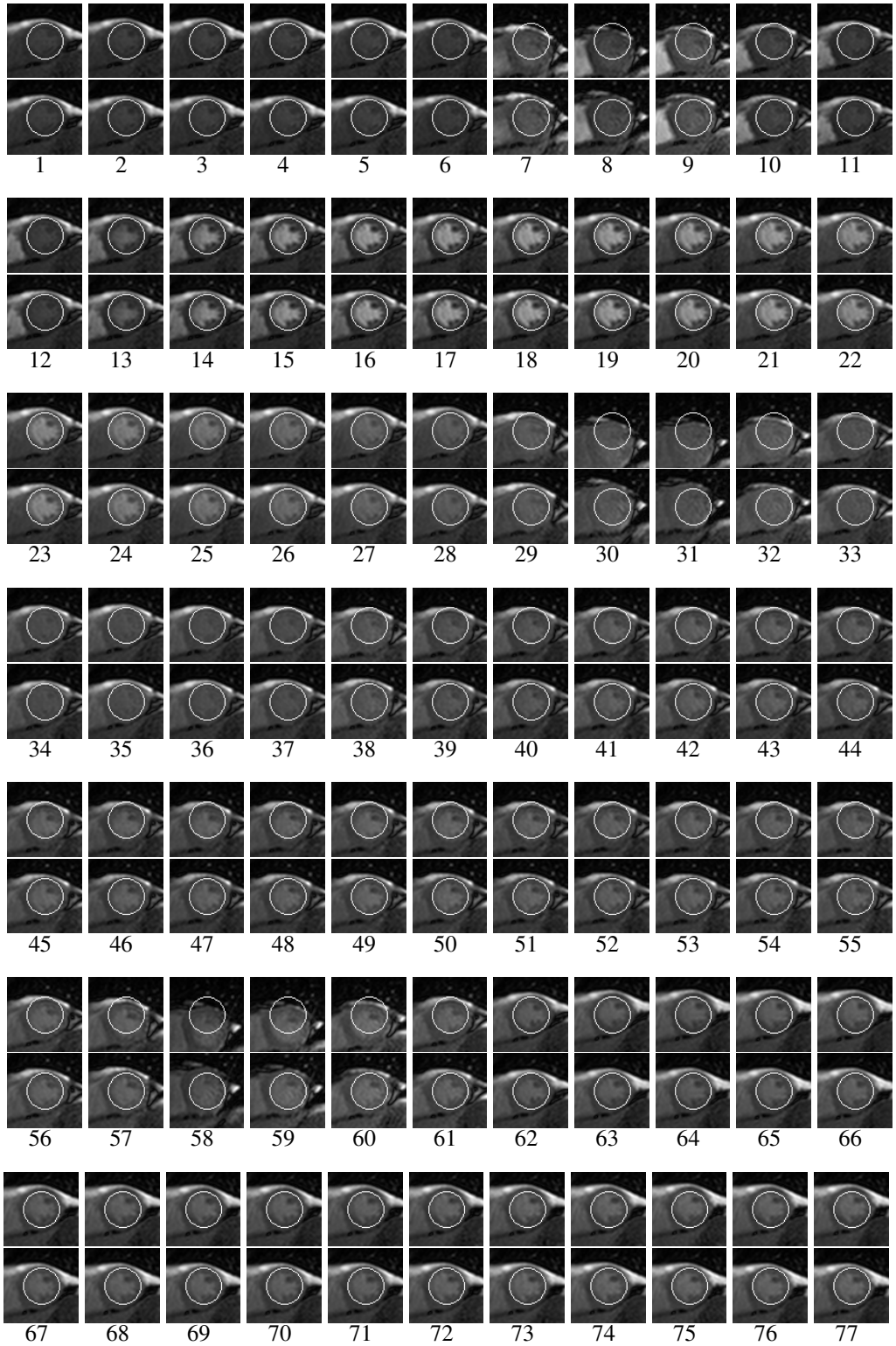

Figure 5.8: Registration Results for Patient 6 under rest conditions.

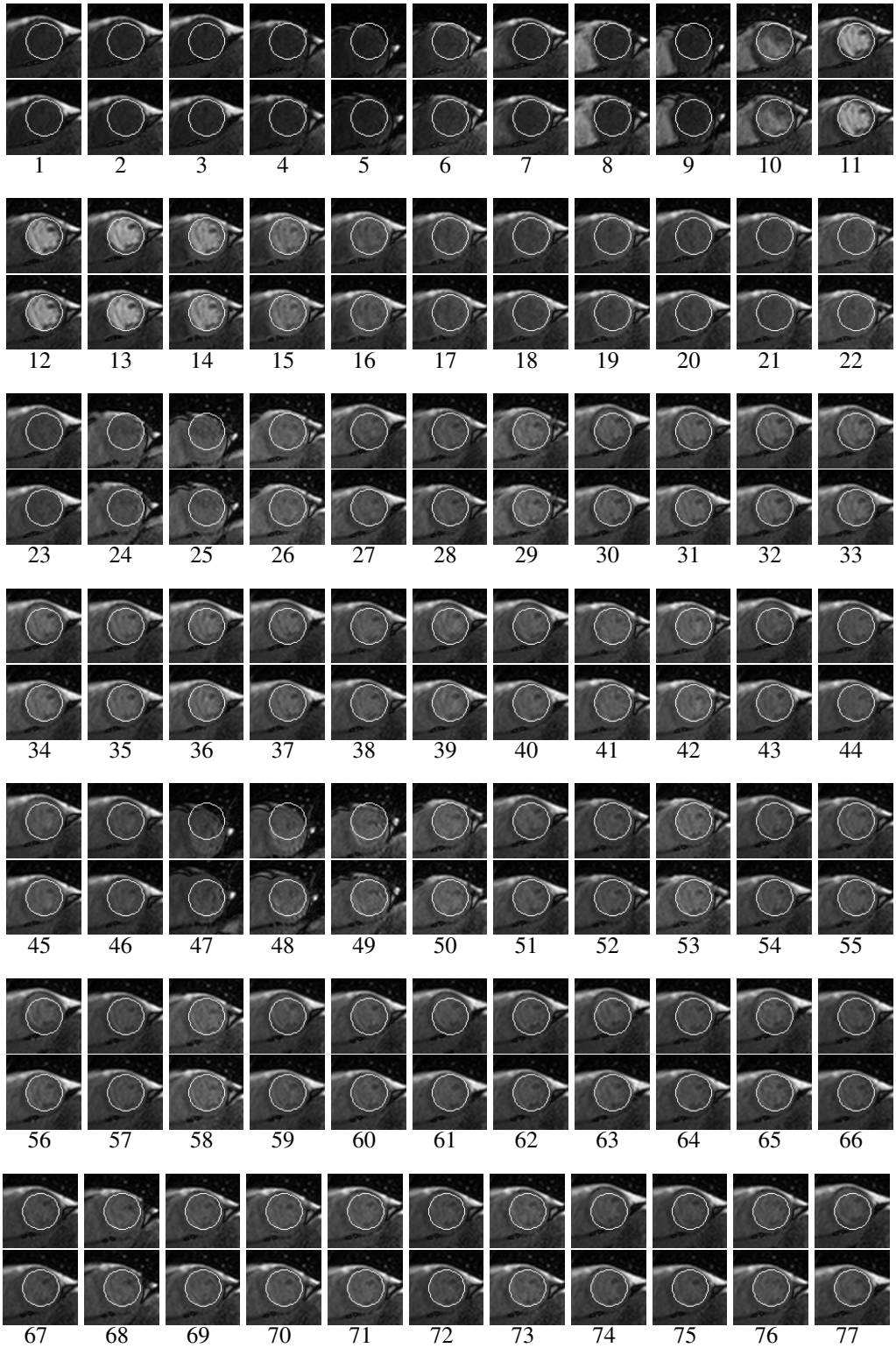

Figure 5.9: Registration Results for Patient 6 under stress conditions.

Patient 6 under stress conditions (figure 5.9)

The registration process leads to perfect results and compensates the motion artifacts in all images. Improvements (6,10,24-27,30,33-40,47-49) without any declines are gained.

Patient 7 under rest conditions (figure 5.10)

The registration process leads to perfect results and compensates the motion artifacts in two images. Improvements (6,36) without any declines are gained.

Patient 7 under stress conditions (figure 5.11)

The registration process leads to good results. It compensates most of the appearing motion artifacts (13,14,31-33, 38-59) but at two time steps (8,9) the results became worse.

Patient 8 (figure 5.12)

The registration process leads to perfect results and compensates the motion artifacts in all images. Improvements (36-41, 55-59) without any declines are gained.

Patient 9 (figure 5.13)

The registration process leads to perfect results and compensates the motion artifacts in all images. Improvements (26-29) without any declines are gained.

Summary

Overall 533 images were registered. In 109 cases ($\sim$20%) an improvement was achieved. For three images ($\sim$0.6 %) the registration result was quenstionable. In these cases no contrast agent is present and a bad contrast between the regions covered by the ROI exists. Therefore it may be possible that the Mutual Information gets very similar values at different positions which may lead to a wrongly decision for the registration shifts. For all other cases neither an improvement nor a decline were achieved.

5.4 Segmentation Results

Figures 5.14 - 5.24 show the results obtained from the segmentation process. The top row shows the segmented myocardium without the final refinement step of the boundary extraction (4.3.2). The bottom row shows the final segmentation of the myocardium.

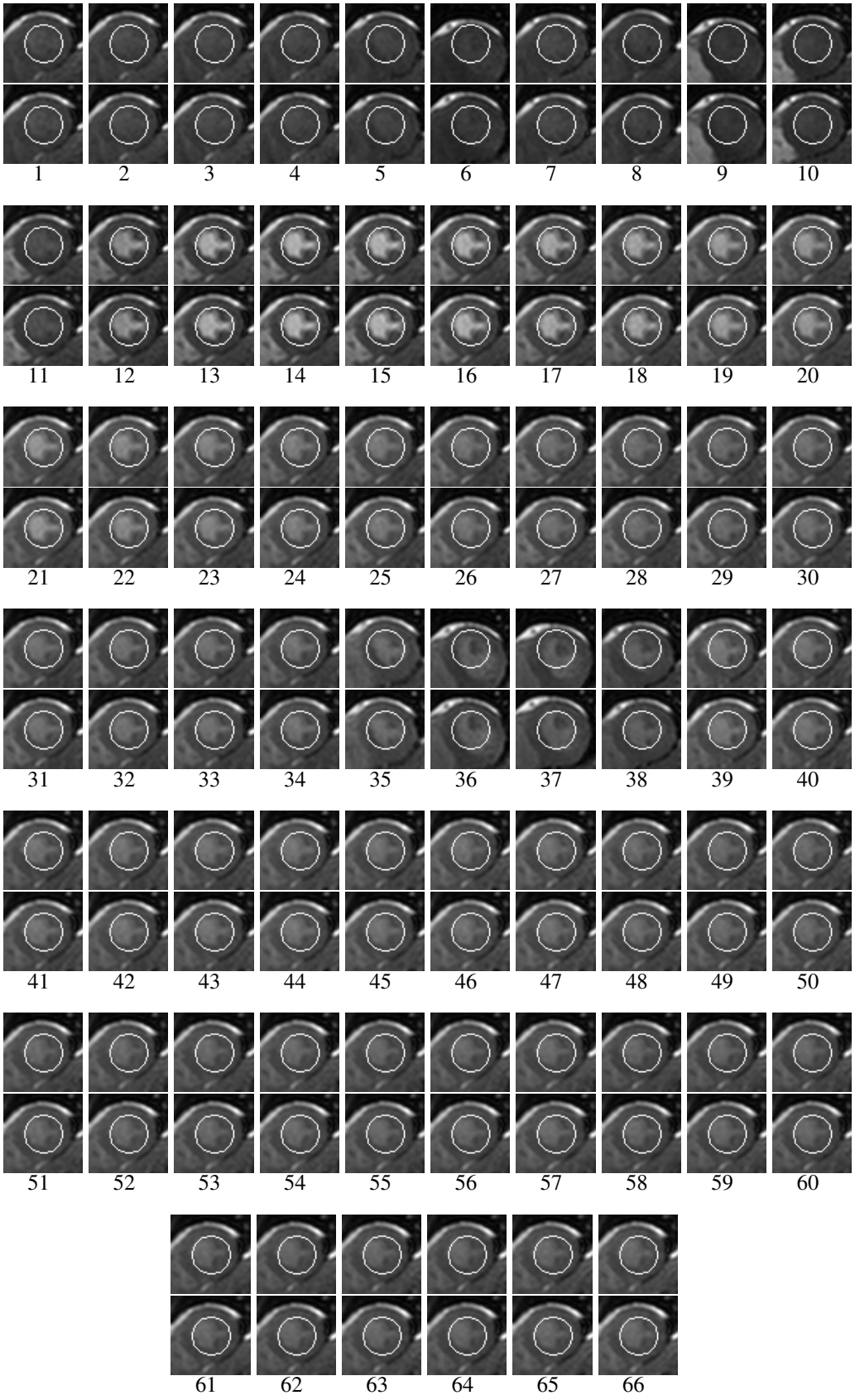

Figure 5.10: Registration Results for Patient 7 under rest conditions.

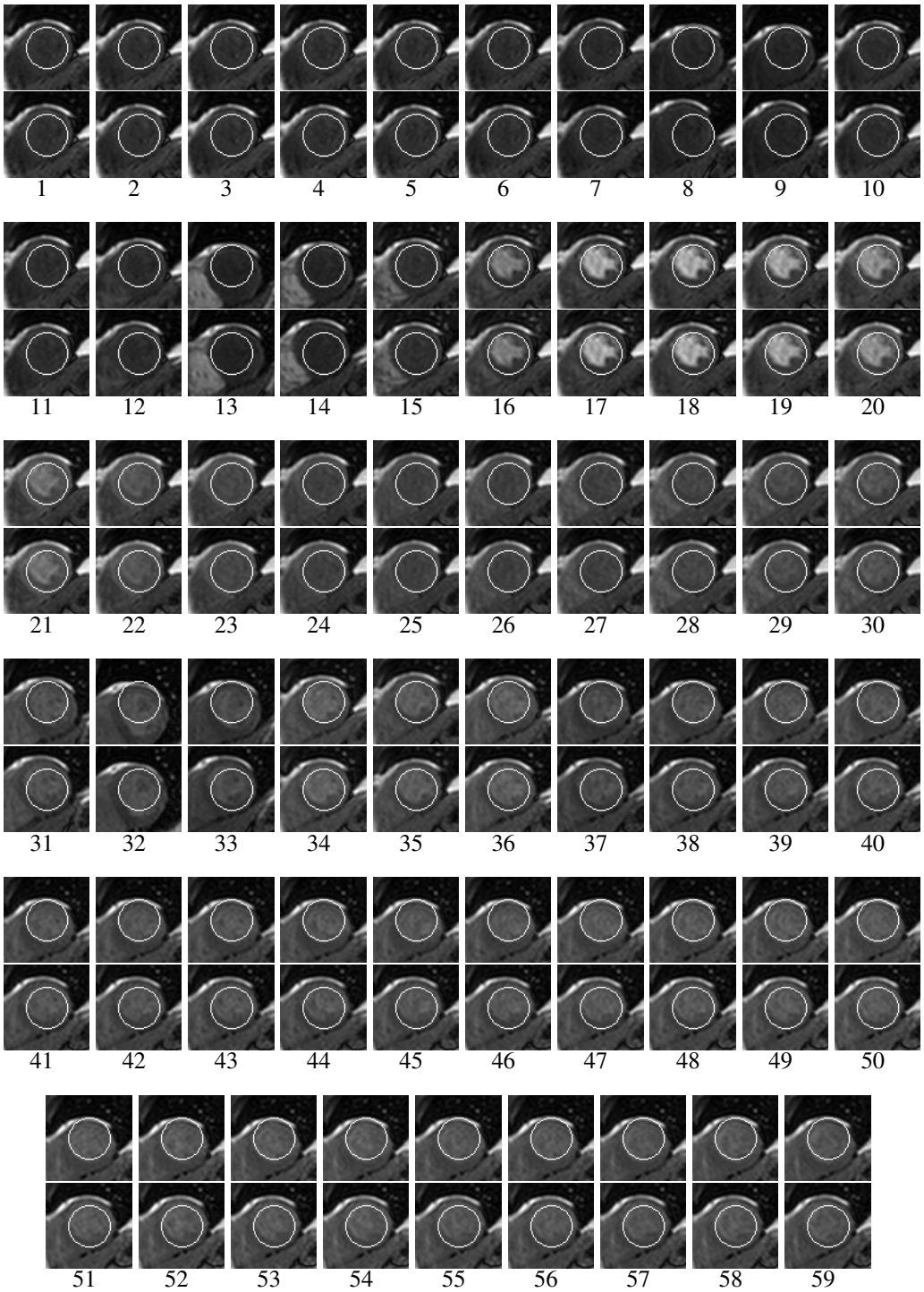

Figure 5.11: Registration Results for Patient 7 under stress conditions.

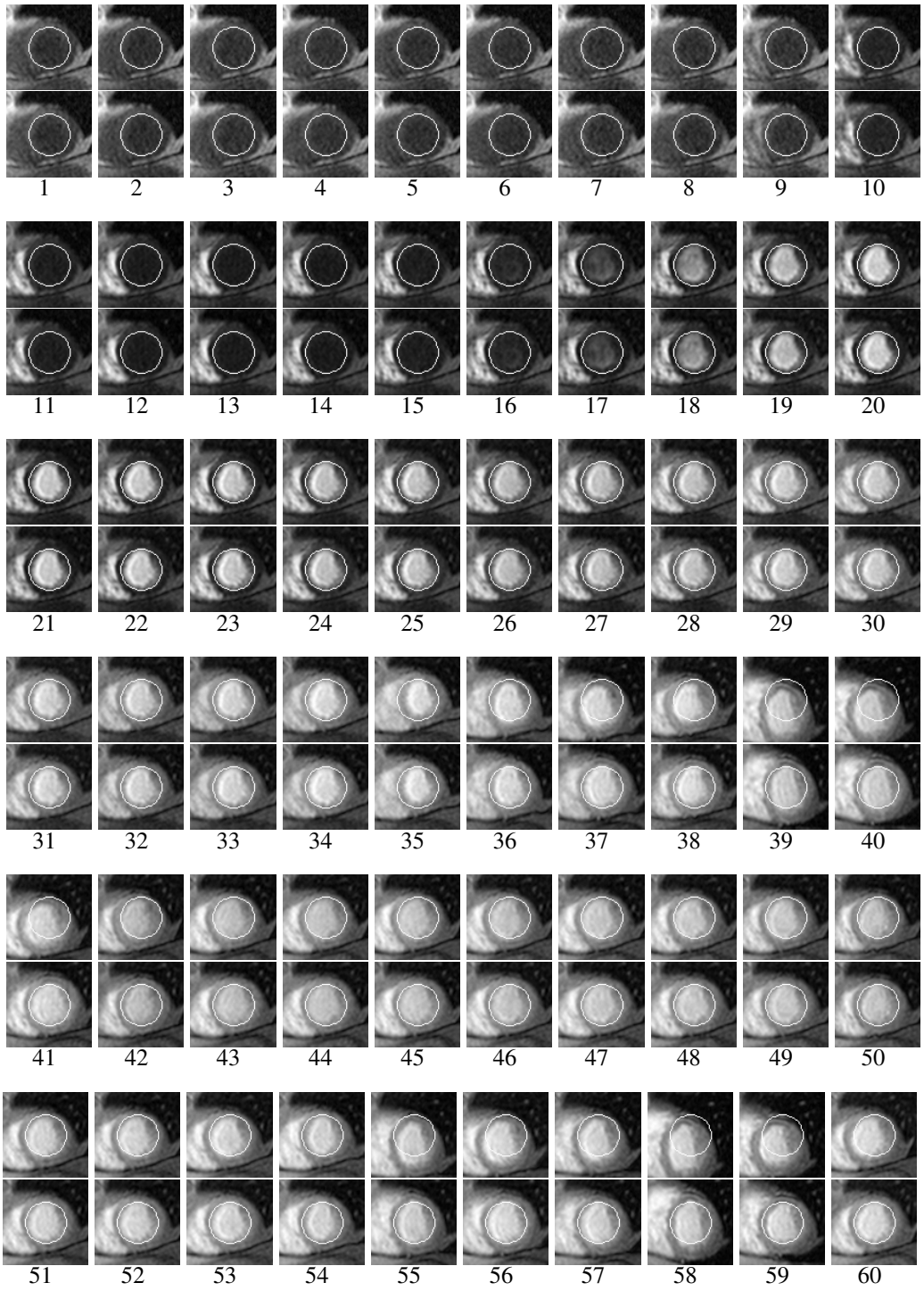

Figure 5.12: Registration Results for Patient 8.

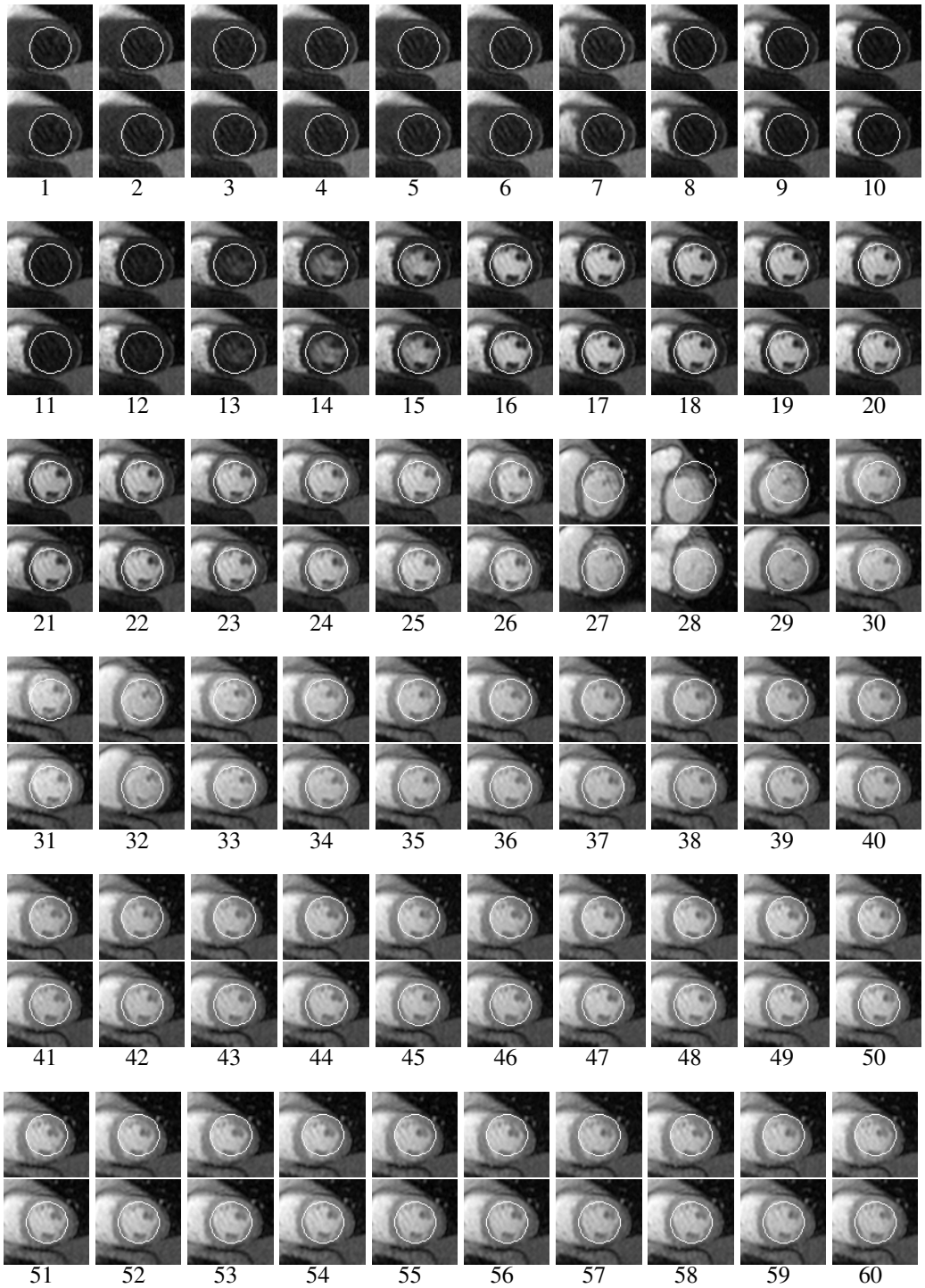

Figure 5.13: Registration Results for Patient 9.

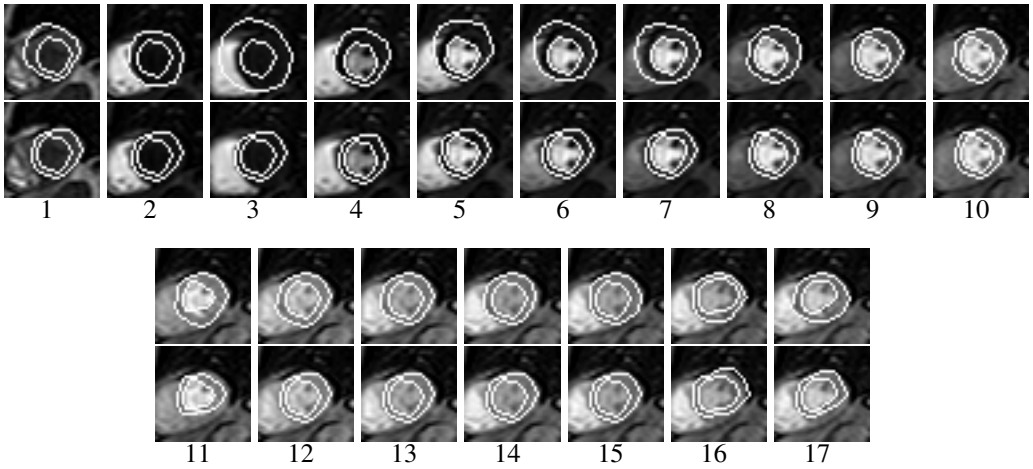

Figure 5.14: Segmentation Results for Patient 1.

Patient 1 (figure 5.14)

The inner contour of the myocardium is correctly detected except at three time steps (11,16,17). For time step 3 the inner contour - which is the default contour for this dataset - is placed inaccurately. This results from the previous inaccurate registration. The outer contour is correctly detected at most time steps (2, 8-17). At the other time steps the contrast between myocardium and background is low. Therefore the outer contour could not be detected reliably.

The refined outer contours provide nearly perfect results. Only time steps with an inaccurate inner contour provide an inaccurate outer contour. This results from the assumption that the thickness of the myocardium is approximately constant over time.

Patient 2 (figure 5.15)

The inner contour of the myocardium is correctly detected except at three time steps (11,21,27). For time step 11 the detection of the inner contour completely fails. For the time steps 21 and 27 the default contour is used. Since the registration for time step 21 failed, the segmentation is inaccurate. At time step 27 the registration corrects the motion artifact at the best but leads still to an inaccurate result. Therefore the default inner contour is placed inaccurately. The outer contour is detected very well except for the three time steps with an inaccurate inner contour.

The final segmentation looks very good except for the three time steps mentioned before.

Patient 3 (figure 5.16)

For this dataset the segmentation step completely fails, although at some time steps 8, 9,11,12,16,18) the inner contour was detected correctly. For the first time steps the segmentation failed caused by inaccurate registration. At the other time steps

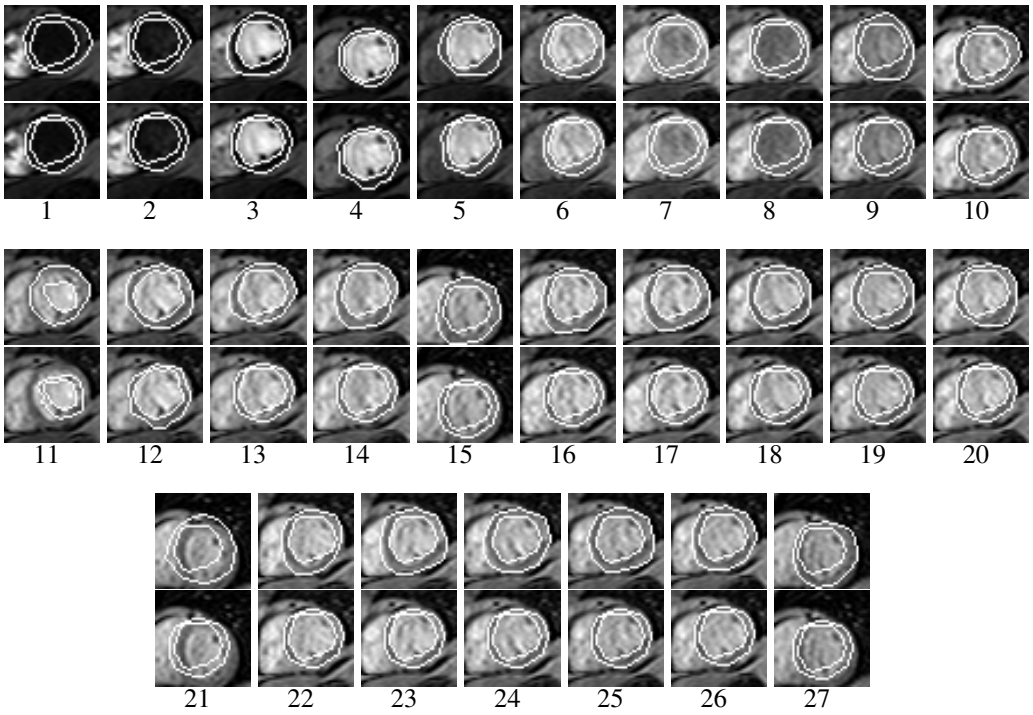

Figure 5.15: Segmentation Results for Patient 2.

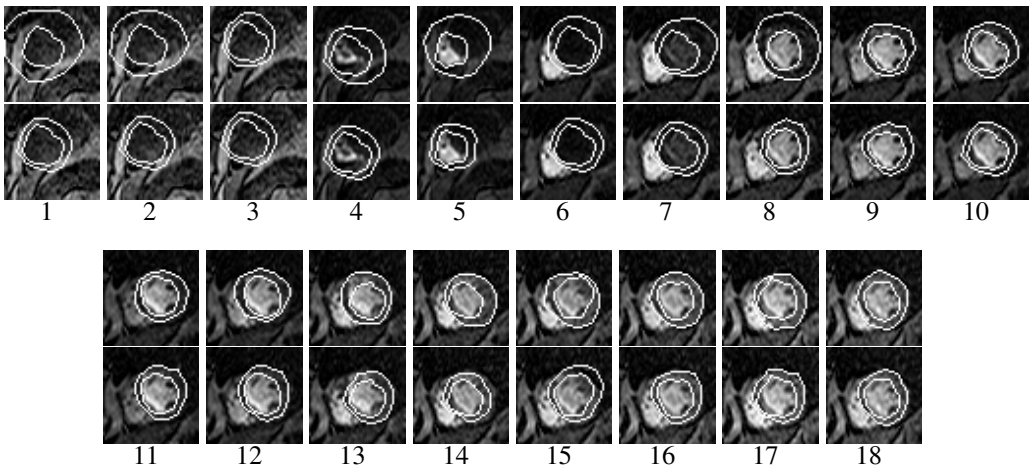

Figure 5.16: Segmentation Results for Patient 3.

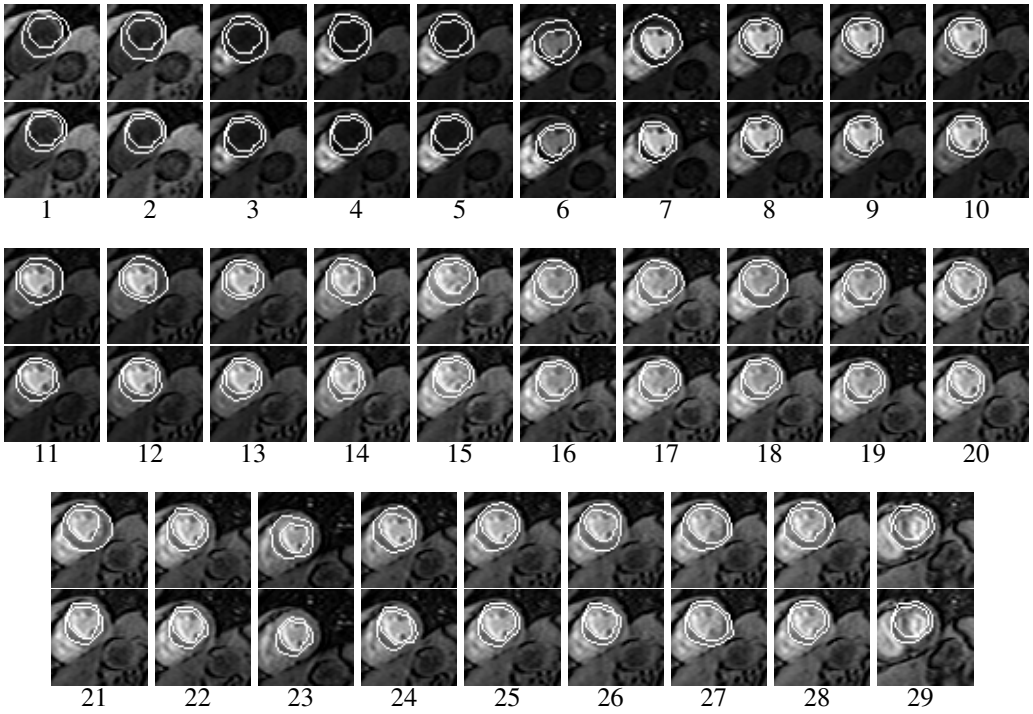

Figure 5.17: Segmentation Results for Patient 4.

poor contrast between myocardium and left ventricle as well as noise lead to an incorrect detection of the inner boundary. The outer boundary is correctly detected at only some time steps (9, 11-13,16). Therefore no satisfying results are gained.

Patient 4 (figure 5.17)

The inner boundary is detected correctly for most time steps. Time step 1 and 2 use the default contour. Because of an imperfect registration they are placed inaccurately. For time step 27 and 29 the segmentation is not perfect but still a good result is achieved. The detection of the outer contour provides good results for time steps where the contrast agent appears in the myocardium.

The final segmentation leads to acceptable results but the thickness of myocardium is mostly too thin. In this dataset the refinement step leads to worse results than without.

Patient 5 (figure 5.18)

The inner boundary is correctly detected for all time steps except time step 16. Sometimes the papillary muscles appear inside and sometimes outside the myocardium. The outer boundary is detected very well except in the first time steps where the contrast between myocardium and background is very low. Due to the good determination of the inner and outer boundaries the final segmentation leads to very good results. Only at time step 16 the segmentation is inaccurate caused by the incorrect detection of the inner boundary.

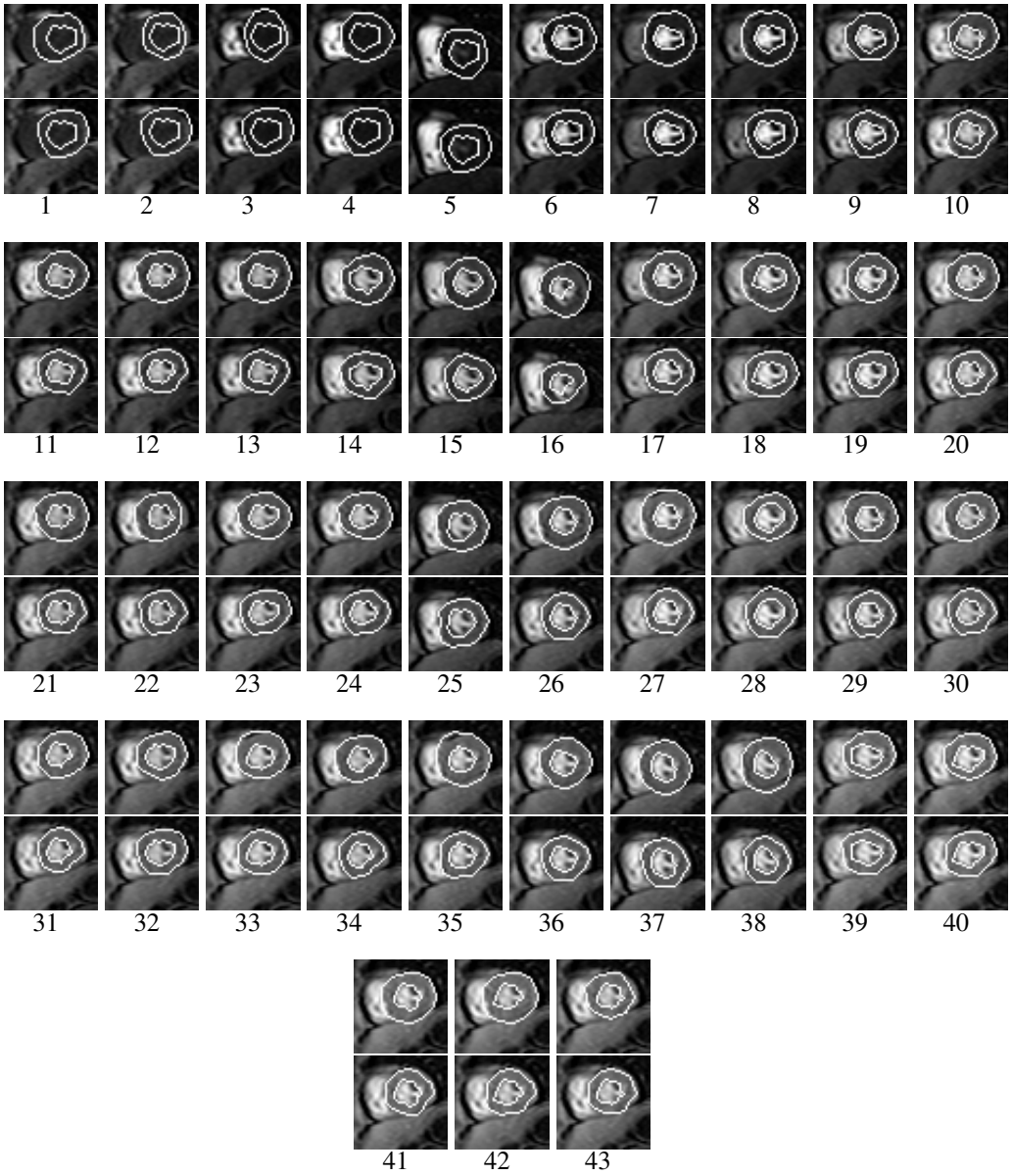

Figure 5.18: Segmentation Results for Patient 5.

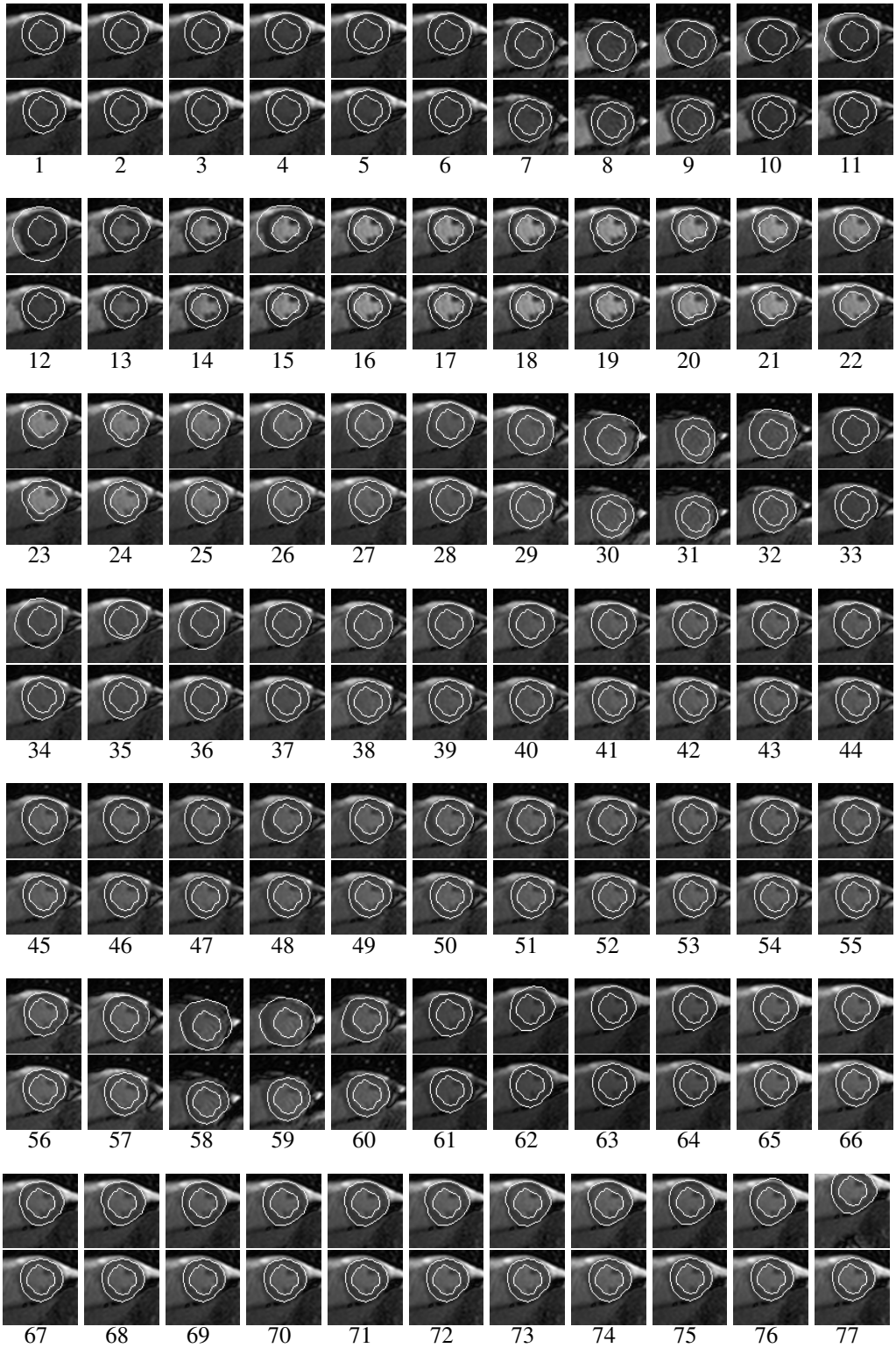

Figure 5.19: Segmentation Results for Patient 6 under rest conditions.

Patient 6 under rest conditions (figure 5.19)

The inner boundary is correctly detected for all time steps. However, sometimes the papillary muscles appear inside and sometimes outside the myocardium. The outer boundary is correctly detected for most time steps. At some time steps (11-13,15,31,32,34,76) a bright structure outside the myocardium is included.

The final segmentation leads to very good results.

Patient 6 under stress conditions (figure 5.20)

The inner boundary is correctly detected for all time steps. The outer boundary is correctly detected for most time steps. At some time steps (22, 42, 56-66) some pixels of the bright structure outside the myocardium are included.

The final segmentation leads to very good results.

Patient 7 under rest conditions (figure 5.21)

The inner contour is correctly detected for all time steps. The outer contour is correctly detected for most time steps. At some time steps (1, 4-6, 13) some pixels of the bright structure outside the myocardium are included. At other time steps (35-39) the contour is not correctly determined according to the low contrast between myocardium and background.

The final segmentation leads to very good results.

Patient 7 under stress conditions (figure 5.22)

The inner contour is correctly detected for all time steps except time step 32. This is caused by an imperfect registration. At many time steps (1-13, 32) the detection of the outer contour failed due to bad contrast between myocardium and background. At some time steps (19, 27) some pixels of a bright structure outside the myocardium are included.

The refinement step leads to very good results except at two time steps (8, 9).

Patient 8 (figure 5.23)

The inner contour is correctly detected for all time steps except time step 39. The outer contour is well detected for all time steps. Therefore the final segmentation leads to very good results.

Patient 9 (figure 5.23)

The inner contour is correctly detected for most time steps. Mostly the papillary muscles appear outside the myocardium but sometimes they appear inside. At the

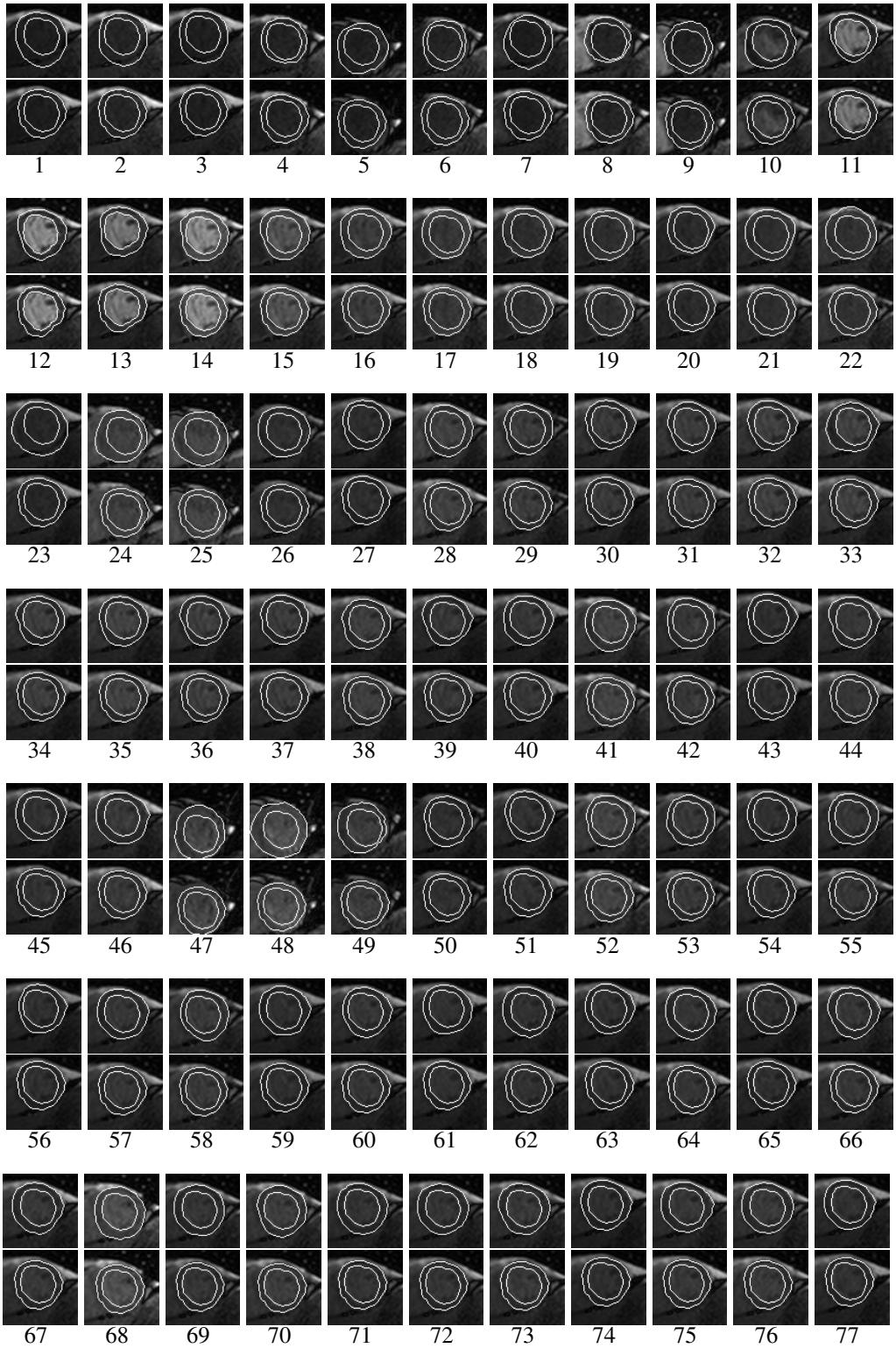

Figure 5.20: Segmentation Results for Patient 6 under stress conditions.

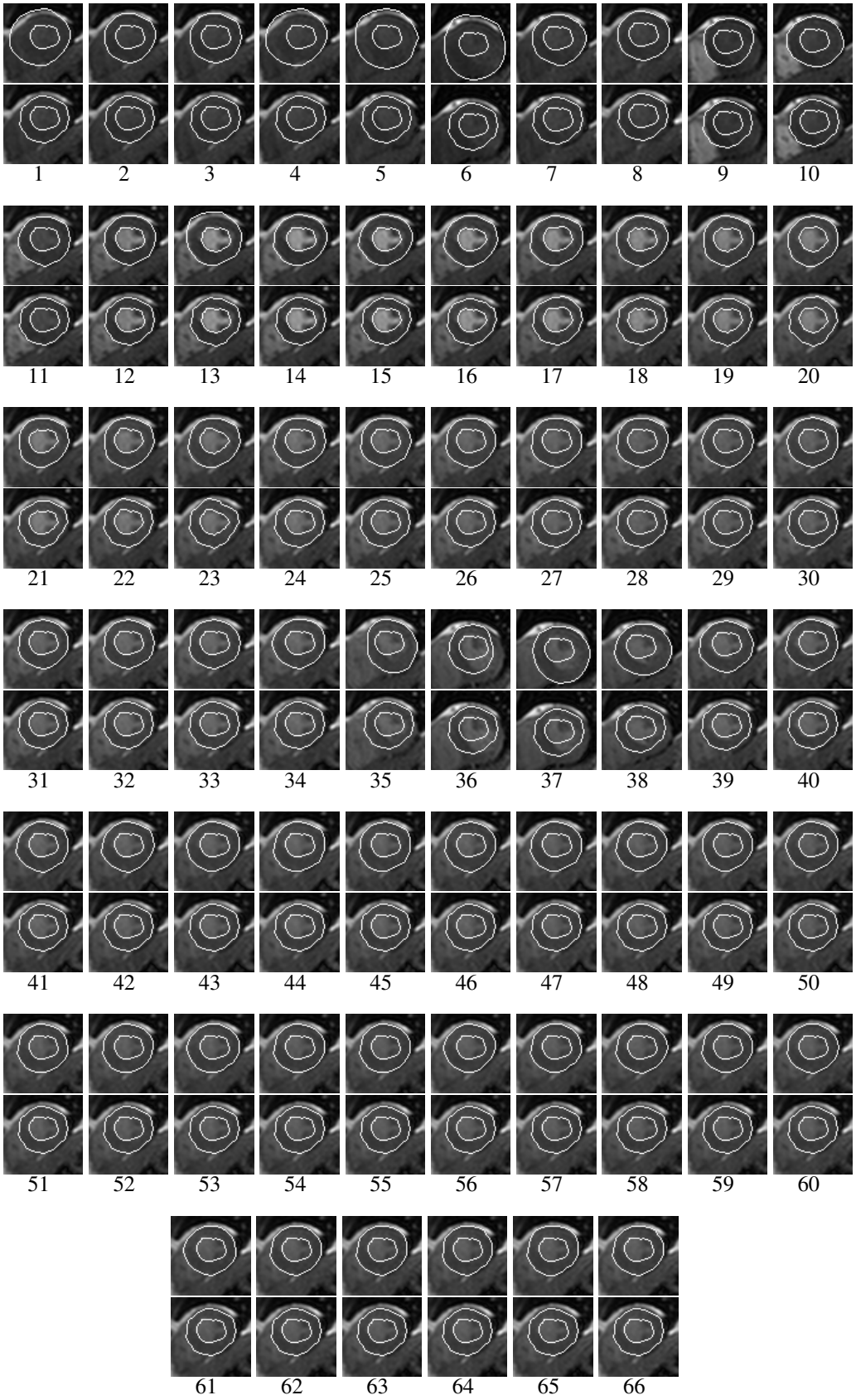

Figure 5.21: Segmentation Results for Patient 7 under rest conditions.

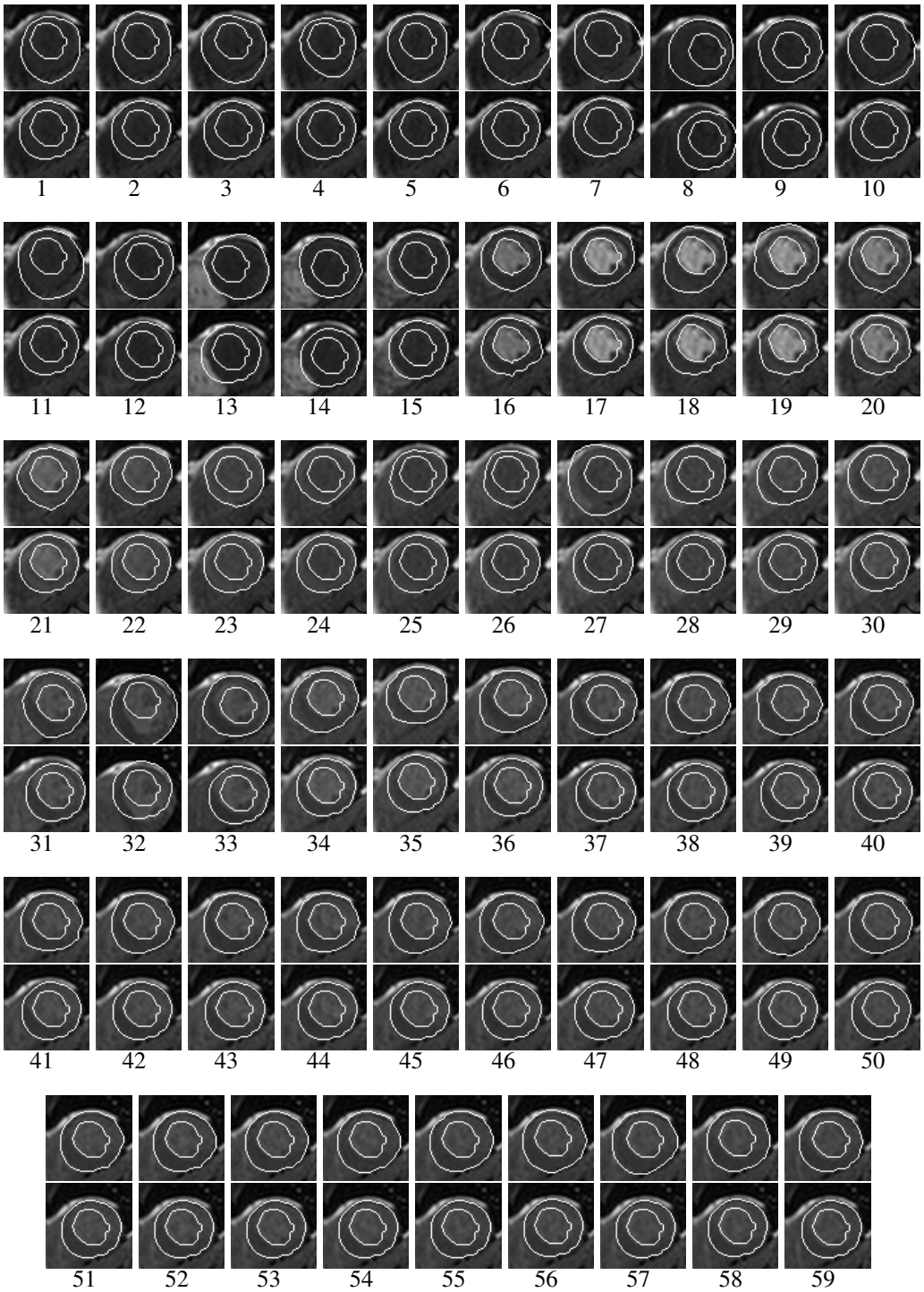

Figure 5.22: Segmentation Results for Patient 7 under stress conditions.

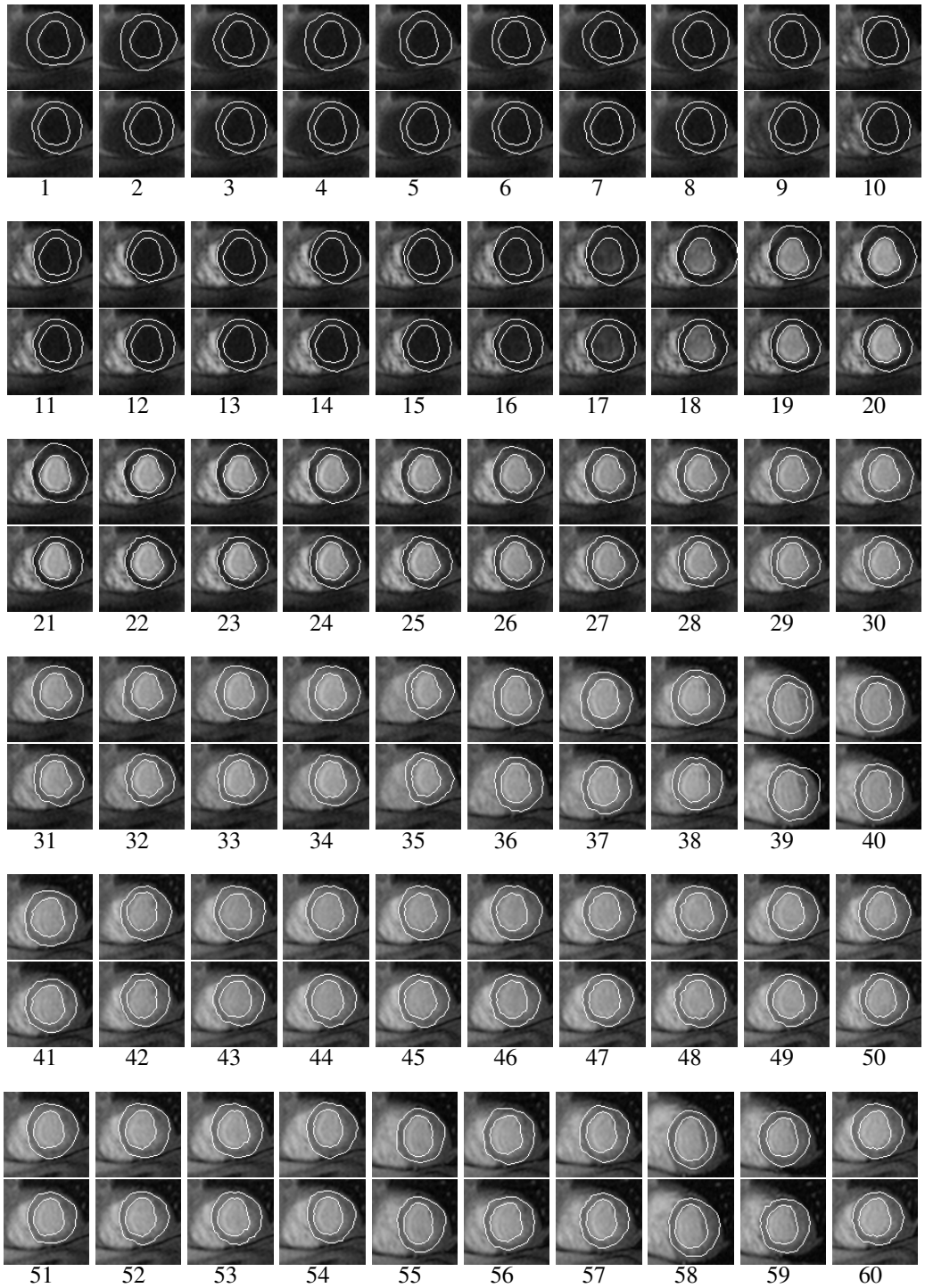

Figure 5.23: Segmentation Results for Patient 8.

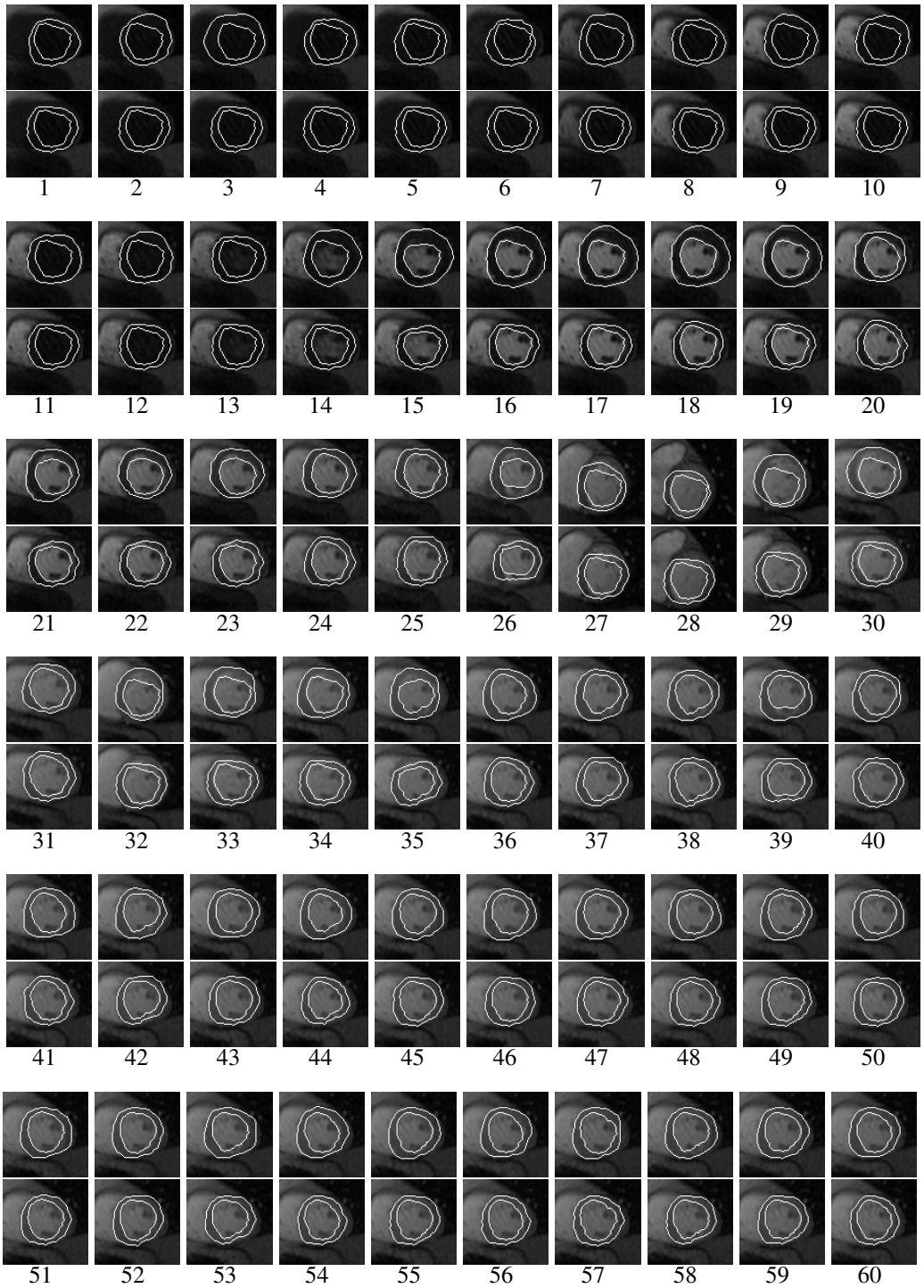

Figure 5.24: Segmentation Results for Patient 9.

time steps 27-29 and 32 the default contour was placed due to bad contrast between left ventricle and myocardium. At this time steps motion artifacts - causing additional shape variations of the left ventricle - are present. Although the motion artifacts were compensated the placed contours become inaccurate therefore. At time step 26 and 35 the detection of the inner contour failed. The outer contours are detected very well where a good contrast between myocardium and background exists. The final segmentation leads to satisfying results except when the inner contour was detected inaccurately.

Summary

The segmentation leads to good results for most datasets. Only for the dataset of patient 3 completely wrong results were obtained. If the previous registration step leads to good results, mostly the inner contour is correctly detected. Low contrast between myocardium and background make it hard to detect the outer contours. Therefore at many time steps the contours are not detected correctly. However the refinement step leads to acceptable results.

Overall 533 images were segmented. After visual inspection the following result has been turned out: About 25 images ($\sim$5%) result in questionable segmentations. Whereas half of them came from the dataset of patient 3. About 50 images ($\sim$10%) result in acceptable segmentations. At the remaining images ($\sim$85%) nearly perfect segmentation results are gained.

5.5 Analysis Results

Figures 5.25 - 5.35 show the results obtained from the analysis step. On the right side the segments of the myocardium are presented in a bull's eye plot. They are color coded according to the maximum upslope in corresponding areas. The color bar on the left side illustrates which color represents which upslope value. Colors appearing further up indicate a higher upslope (black: zero upslope, white: maximum detected upslope). In this thesis the bull's eye plot is extended as follows: The curve in the center of the bull's eye plot shows the mean intensity time curve of the whole myocardium. Furthermore the contrast agent accumulation period is shown (green lines). This period is defined accordingly to the maximum upslope (blue line) of five subsequent time steps. The other curves show the mean intensity times curves for every single segment. Furthermore their maximum upslope (blue line) within the contrast agent accumulation period is shown. At least one segment appears in white because the values of the upslopes are normalized by the highest upslope.

Only the segments at the mid-cavity slice were segmented. Therefore the Bull's Eye plots only illustrate these segments (segments no.7-12, figure 3.4).

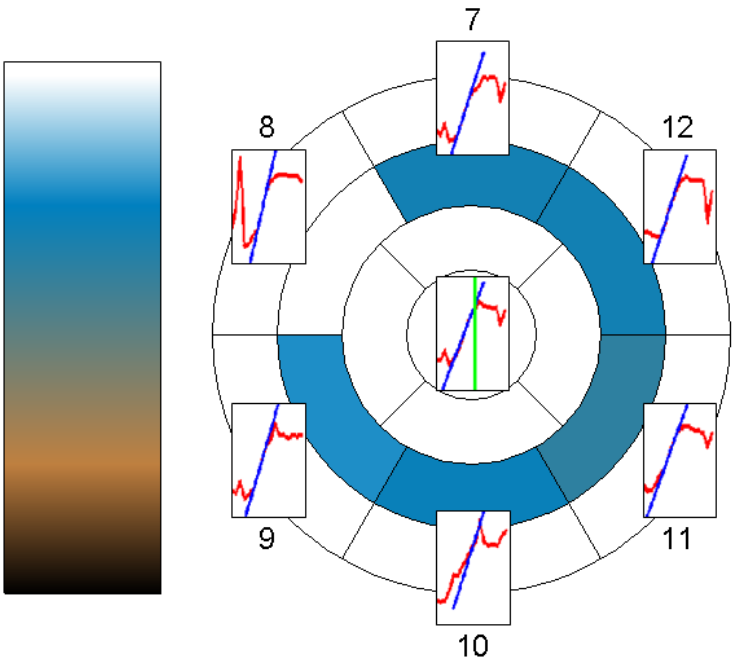

Figure 5.25: Analysis for Patient 1.

Patient 1 (figure 5.25)

The intensity time curve of segment 8 shows a peak at time step 2. This is caused by an inaccurate detection of the myocardial boundaries for this time step. The area corresponding to this segment includes a small amount of pixels from the right ventricle. Since the contrast agent is present in the right ventricle it causes a significant increase of the mean value for this segment. There seems to be no significant perfusion reduction.

Patient 2 (figure 5.26)

The intensity time curves show peaks after the contrast agent accumulation period. These peaks are caused by inaccurate detection of the myocardial boundaries (time steps 11 and 21).

There seems to be no dramatic perfusion reduction anywhere. A minor reduction may be present at segments 7, 8, and 9. This could be caused by a narrowing of the LAD (left anterior descending artery).

Patient 3 (figure 5.27)

The segmentation of this dataset clearly failed. Hence time-intensity curves are clearly wrong and the dataset is not analyzed any further.

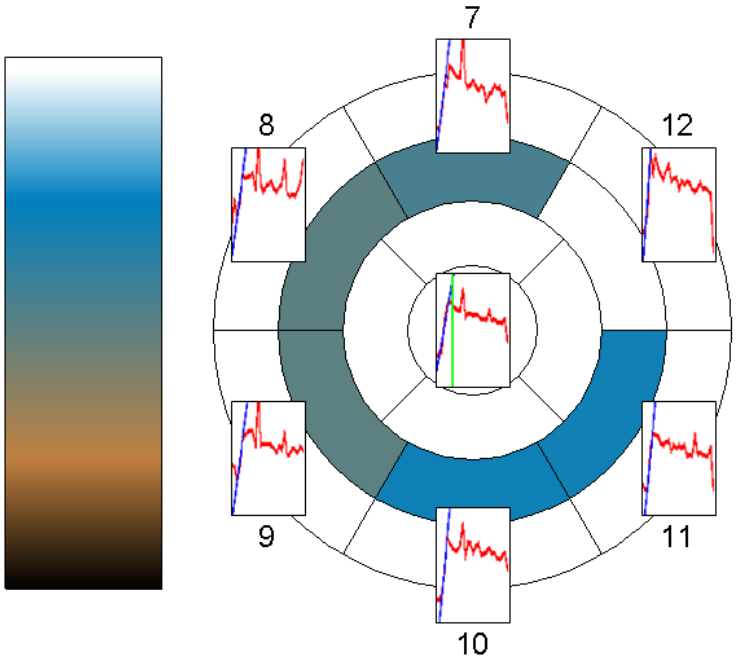

Figure 5.26: Analysis for Patient 2.

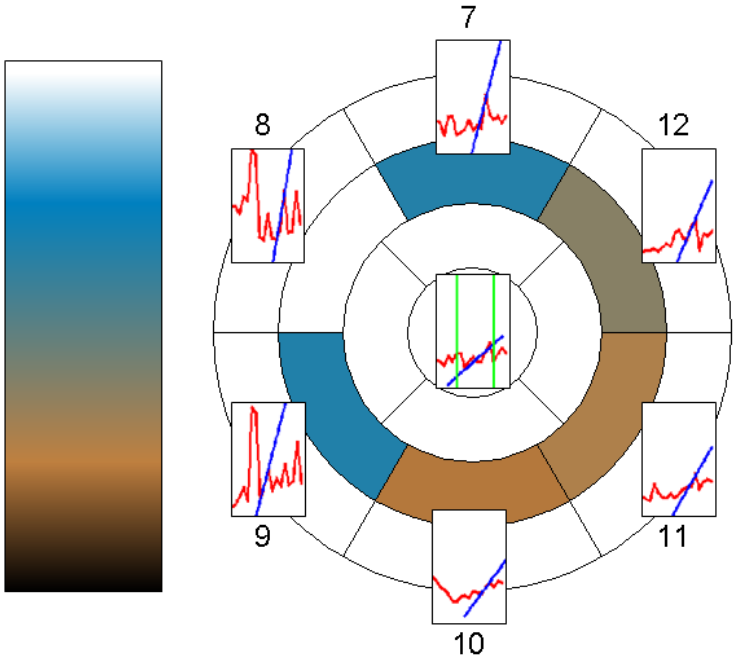

Figure 5.27: Analysis for Patient 3.

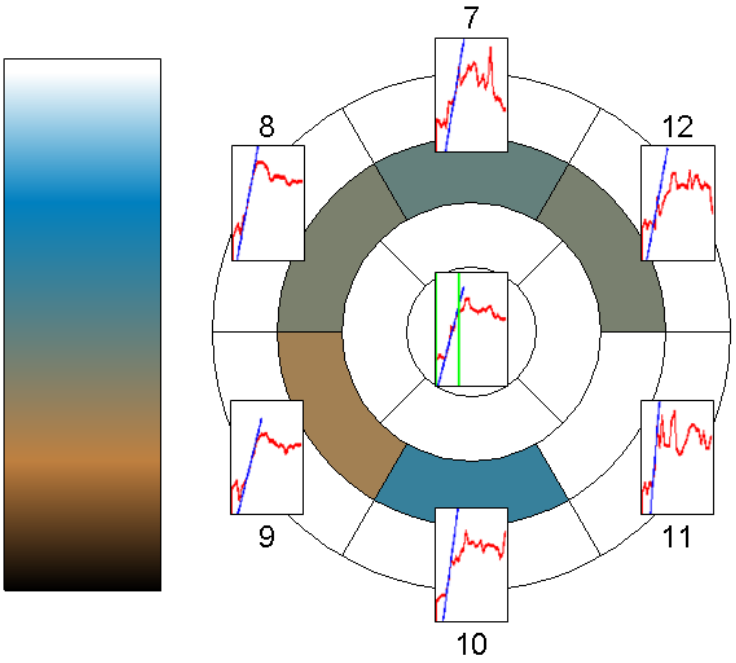

Figure 5.28: Analysis for Patient 4.

Patient 4 (figure 5.28)

The intensity time curves show some peaks and noise after the contrast agent accumulation period. They are caused by an inaccurate detection of the inner boundaries. Sometimes a few pixels belonging to left ventricle show up in the myocardium.

There seems to be a highly reduced perfusion at segment 9. This may be caused by a narrowing of the right coronary artery.

Patient 5 (figure 5.29)

The intensity time curves for the segments 10-12 have high variations. They are caused by an inaccurate segmentation. There the papillary muscles sometimes appear inside and sometimes outside the myocardium. The curves for segments 8 and 9 show high peaks. They are caused by a imperfect segmentation where some pixels of the right ventricle appear in these segments.

When only the color-coded bull's eye plot is considered there seems to be a reduced perfusion in all segments except segment no. 9. But this is not entirely correct. The very high upslope of segment 9 leads to the impression that the others have a low upslope. When additionally considering the intensity time curves of all segments no reduced perfusion is indicated.

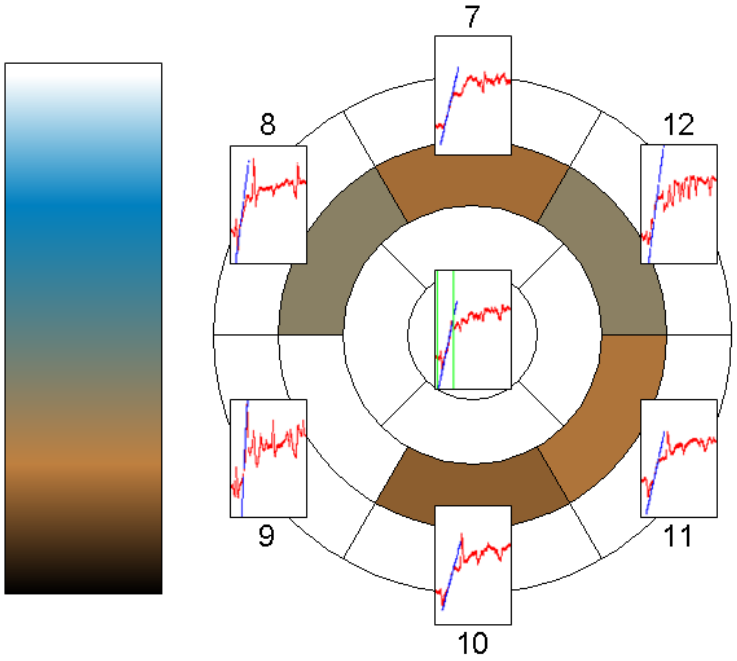

Figure 5.29: Analysis for Patient 5.

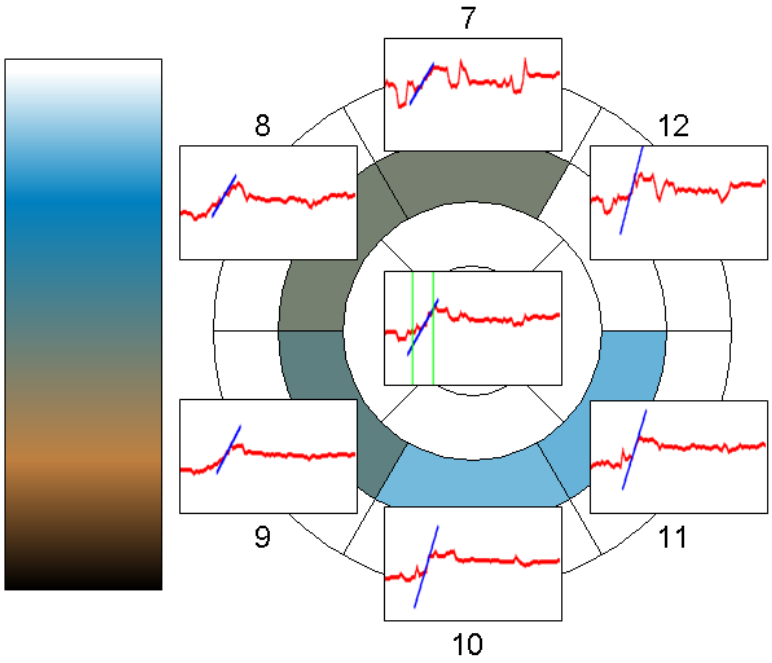

Figure 5.30: Analysis for Patient 6 under rest conditions.

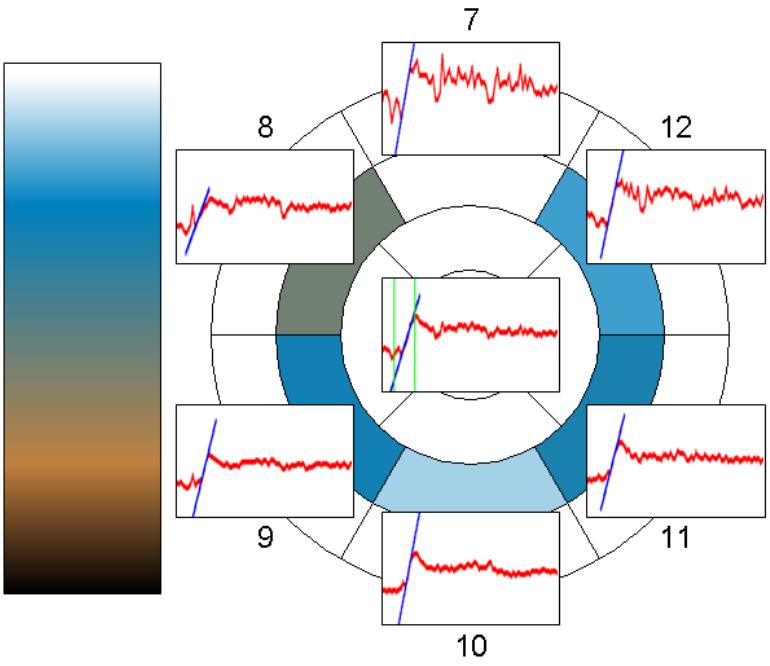

Figure 5.31: Analysis for Patient 6 under stress conditions.

Patient 6 under rest conditions (figure 5.30)

The intensity time curves for segment 7 and 12 show some variations. These variations are caused due to wrongly segmentation of bright regions outside the myocardium.

There seems to be no dramatic perfusion reduction anywhere. A minor reduction could be present at segments 7, 8, and 9. This may be caused by a narrowing of the LAD (left anterior descending artery).

Patient 6 under stress conditions (figure 5.31)

The intensity time curves for segment 7 and 12 show some variations. These variations are caused due to wrongly segmentation of bright regions outside the myocardium. There seems to be no dramatic perfusion reduction anywhere. A minor reduction could be present at segment 8.

Patient 7 under rest conditions (figure 5.32)

The intensity time curve of segment 8 shows a peak before the contrast agent accumulation period. This is caused by an inaccurate segmentation which causes some pixels of the right ventricle appearing in the myocardium. The peaks after the contrast agent accumulation period in every curve are also caused by an inaccurate segmentation.

When only the color-coded bull's eye plot is considered there seems to be a reduced perfusion in all segments except segment no. 12. But this is not entirely

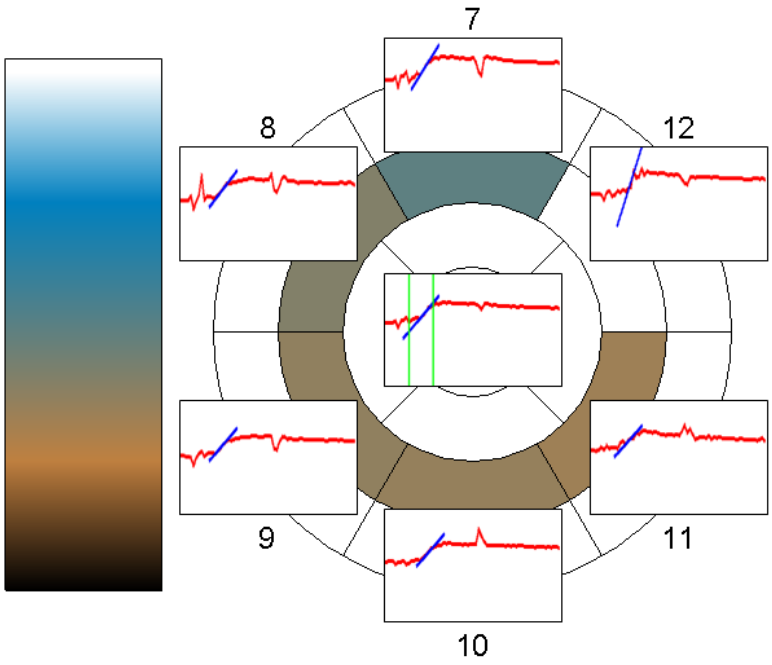

Figure 5.32: Analysis for Patient 7 under rest conditions.

correct. The very high upslope of segment 12 leads to the impression that the others have a low upslope. When additionally considering the intensity time curves of all segments no reduced perfusion is indicated.

Patient 7 stress rest conditions (figure 5.33)

The intensity time curves show peaks before the contrast agent accumulation period. They are caused by an inaccurate segmentation of time step 8 and 9. There seems to be a bad perfusion all over the myocardium. But this is caused by the very high upslope of segment 7. By observing all intensity time curves there seems to be no perfusion reduction.

Patient 8 (figure 5.34)

The intensity time curves have some variation after the contrast agent accumulation period. They are caused because for some segmentations some pixels of the background appear in the myocardium.

There seems to be no perfusion reduction in the myocardium. A minor reduction may be present at segments 11 and 12. This may be caused by a narrowing of the LCX (left circumflex artery).

Patient 9 (figure 5.35)

The intensity time curves exhibit some variation after the contrast agent accumulation period. These variations appear because for some time steps pixels of the back-

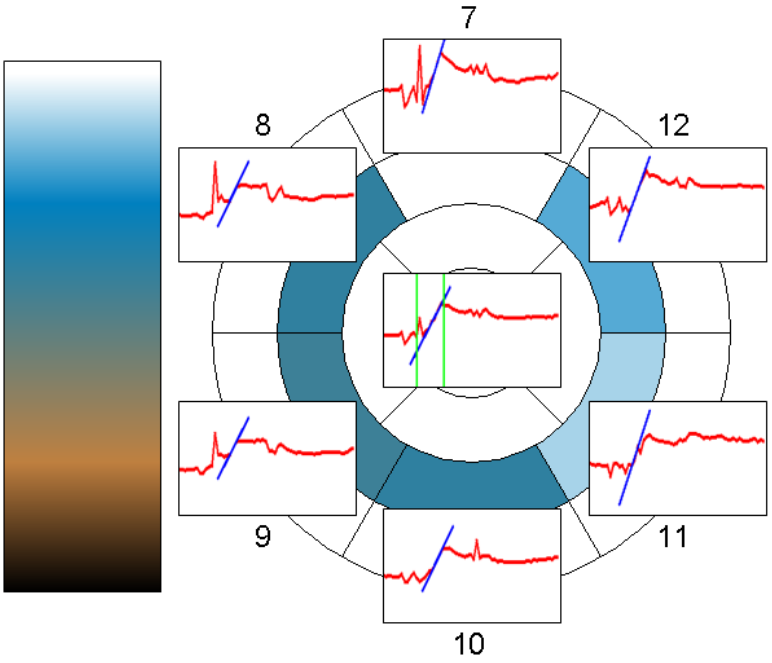

Figure 5.33: Analysis for Patient 7 under stress conditions.

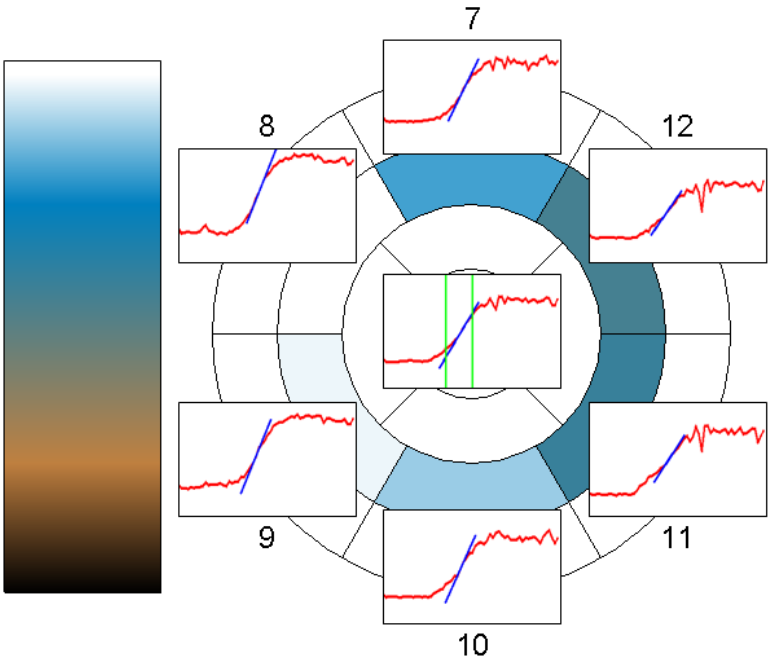

Figure 5.34: Analysis for Patient 8.

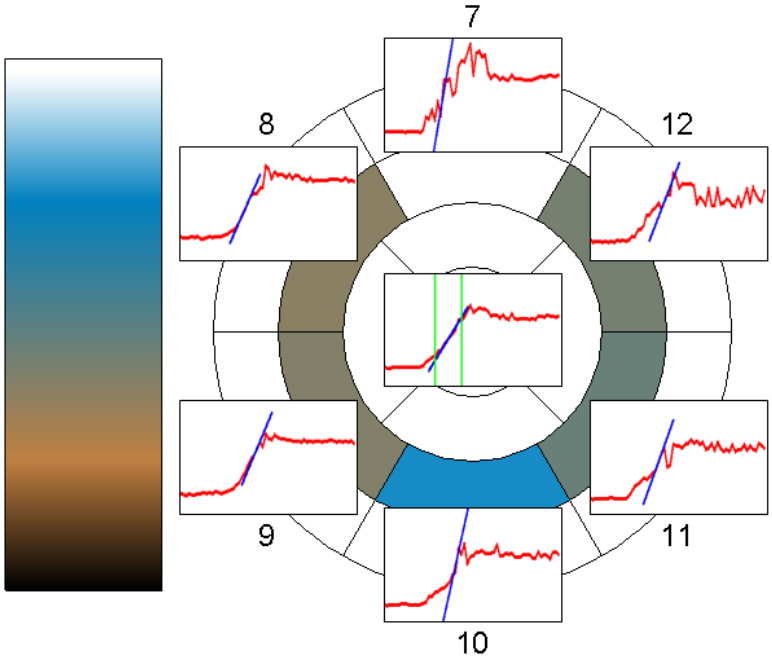

Figure 5.35: Analysis for Patient 9.

ground are included in the segmentation of the myocardium. Furthermore higher variations exist for the curves of segment 7 and 12. They are caused by inaccurate segmentations.

When only the color-coded bull's eye plot is considered there seems to be a reduced perfusion in all segments except segment no. 7. But this is not entirely correct. The very high upslope of segment 7 leads to the impression that the others have a low upslope. When additionally considering the intensity time curves of all segments no reduced perfusion is indicated.

Summary

If the segmentation step provides sufficiently good results the analysis provides meaningful results. Furthermore, by observing only the color coded bull's eye plots incorrect conclusions might be drawn. Therefore additionally the intensity time curves of the single segments should be considered. Finally, this analysis can give only an indication of a bad myocardial perfusion.

5.6 Performance Analysis

The previous sections gave an overview of the accuracy of the method. This section gives an overview of the performance. The tests were carried out on a workstation with an AMD Athlon 64 3400+ (2.4GHz) processor and 2GB RAM. The implementation is not optimized with respect to speed. An improvement of performance should be possible.

		ROI Selection		registration	Segmentation		Analysis	
		variance based	model based		temporal analysis	spatial analysis	segment definition	segment analysis
1	Patient 1	4.1	1.9	0.5	0.2	3.4	0.3	0.2
2	Patient 2	3.5	1.4	3.3	0.01	4.5	1.5	0.3
3	Patient 3	2.3	1.2	0.7	0.03	3.6	0.5	0.2
4	Patient 4	2.1	1.8	1.7	0.1	5	0.7	0.3
5	Patient 5	5.4	2.4	1.8	0.1	7.4	0.4	0.4
6	Patient 6 rest	23.0	3.8	53.9	0.5	43	10.7	3
7	Patient 6 stress	24.6	4.2	78.5	0.7	47.2	16	3
8	Patient 7 rest	17.3	3.7	18.2	0.3	36.5	3.9	2.5
9	Patient 7 stress	15.8	3.5	40.8	0.4	33.1	10.1	2.3
10	Patient 8	4.7	1.6	60.5	0.6	29.5	16.2	1.9
11	Patient 9	5.3	2.6	59.3	0.5	30.1	15.8	1.9

Table 5.2: Performance Overview. Duration of different steps at the algorithm in seconds. The total time of the algorithm for every dataset is shown in figure 5.37

Table 5.2 gives an overview of the performance of the individual tasks of the processing pipeline. The model based ROI selection is up to six times faster than the variance based method. This is effected by two aspects: First, the variance based method deals with the whole 4D-dataset whereas the model based method only operates on a single slice for every time step. Second, the incremental structure of the model based method discards many candidates at every step which reduces computational costs. Furthermore, the registration process depends on the amount of images to register to each other. The dataset of patient 7 under rest conditions seems to be an outlier. The short registration time is achieved by the small ROI which dramatically reduces computational cost for the registration process. Therefore the registration time depends on the amount of images and of the ROI size. The performance for the segmentation depends on the amount of time steps. The performance of the analysis depends on the amount of time steps too.

Figure 5.36 illustrates the relative performance for every individual task of the whole processing pipeline. In Figure 5.36(a) the variance based ROI selection is used whereby in figure 5.36(b) the model based approach is used.

Figure 5.37 illustrates the performance for each individual dataset. The whole analysis process depends on the amount of time steps for each individual dataset. Furthermore, the performance also depends on the resolution of each image.

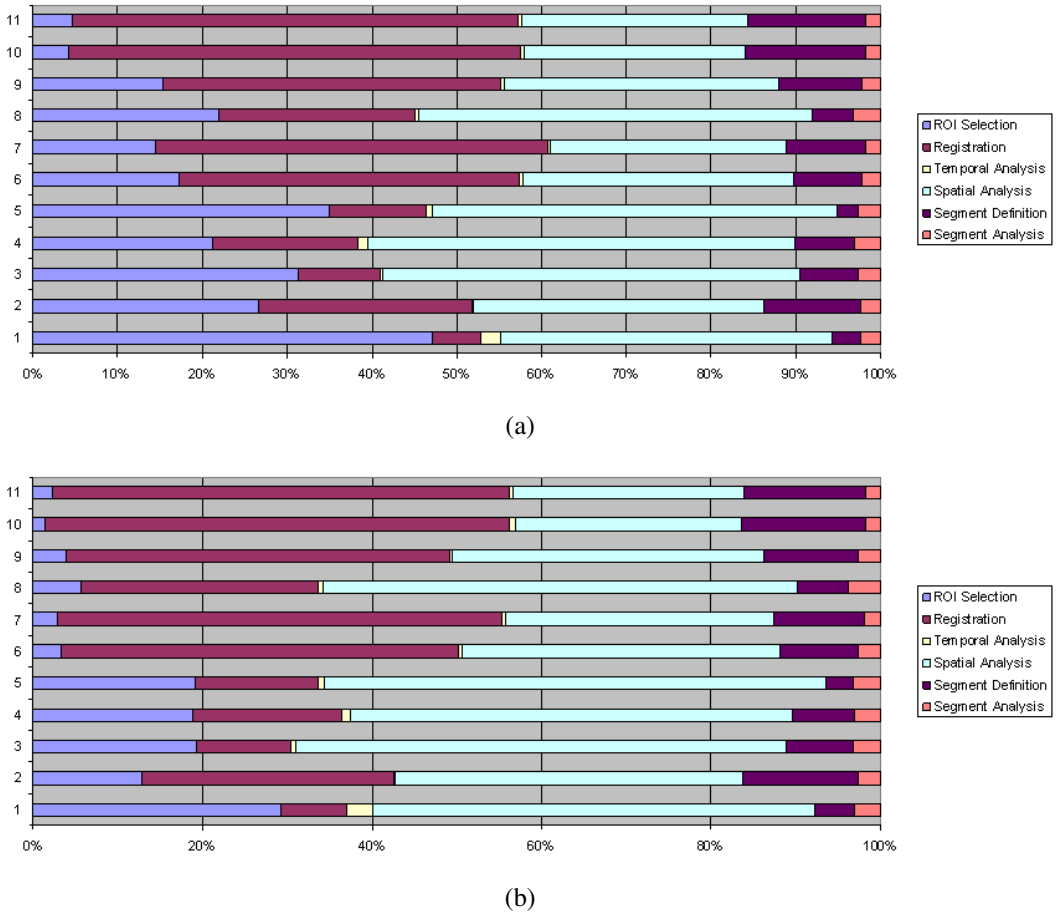

Figure 5.36: Relative Performance. (a) with variance based ROI selection, (b) with model based ROI selection.

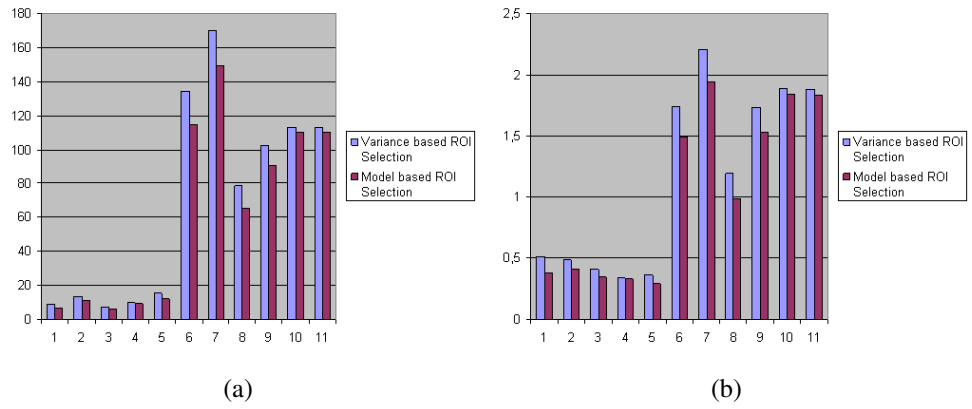

Figure 5.37: Performance on Datasets. (a) performance for the whole dataset, 5.37(b) average performance per slice (in seconds)

Chapter 6

Conclusion and Future Work

In this thesis the automatic analysis of cardiac perfusion MRI data was discussed. The importance of automatic analysis of such data for preliminary detection of coronary artery diseases was outlined. An overview of the anatomy, physiology, and pathophysiology of the heart was given. Coronary artery diseases, consequences, therapeutical interventions, and preliminary detection methods were discussed. A short overview of magnetic resonance imaging was presented. Problems of magnetic resonance imaging causing high image variabilities was pointed out.

The main focus of this thesis lies on automatic segmentation and analysis of cardiac perfusion MRI. The new introduced method was divided into four parts:

- ROI Selection
- Registration
- Segmentation
- Analysis

Every part is self-contained and operates on the output of the previous part. Therefore each part can easily be substituted. This thesis has given a detailed description of all these parts.

It was shown that for the majority of the eleven cardiac MRI datasets good results were achieved. Whereas the achieved results were validated by visual inspection. It has been demonstrated that the adapted variance based approach for the ROI detection [Sörgel and Vaerman, 1997] fails if huge motion artifacts are present. Furthermore it has been demonstrated that the new introduced incremental approach for the detection of the ROI gave very good results. Despite the strong intensity variations the left ventricle was correctly detected in all but one datasets. Mutual Information restricted to the ROI has been applied successfully for compensation of the motion artifacts. A critical task is the accurate detection of the myocardial boundaries which could well be accomplished with the introduced two step approach using an adapted shortest path algorithm [Yeh *et al.*, 2005]. For the analysis of cardiac perfusion it is proposed to consider both: bull's eye plot [Cerqueira

et al., 2002] and characteristic intensity time curves. For this purpose the bull's eye plot and the characteristic curves have been combined in this thesis.

Further improvements of individual steps of the algorithm may be addressed in future work. Some possible improvements are:

- *The use of anatomical information in the registration step:* The information about the position of the lung relatively to the myocardium is known (from the previous step) and can be used. The similarity measurement of the registration can be designed as a combination of Mutual Information and Mean Square Error. Mutual Information can be used for the region of the myocardium and left ventricle because the gray values changes there over time. Mean Square Error can be used for the region of the lung because the gray values are nearly constant there over time.

- *Further improvement step after segmentation:* By a precise observation of the regions covered by the left ventricle and myocardium a conclusion of a correct segmentation may be made.

- *Combination of several measurements for the analysis*

Furthermore an optimization of the implemented method would be desirable to speed up the analysis of cardiac perfusion MRI data.

Finally it should be remarked that the interpretation of medical images is a highly critical task with respect to a patient's health. Therefore an automatic analysis tool should offer an user interface for the operator to make corrections of automatic generated results possibly at every stage of the process.

Bibliography

G. Adluru, E. V. R. Di Bella, and R. T. Whitaker. Automatic segmentation of cardiac short axis slices in perfusion. In *Proceedings of IEEE International Symposium on Biomedical Imaging: From Nano to Macro*, pages 133–136. IEEE, 2006.

AHA. American heart association, 2007. `http://www.americanheart.org`; [Online accessed 04-December-2007].

N. Al-Saadi, E. Nagel, M. Gross, A. Bornstedt, B. Schnackenburg, and C. et al. Klein. Noninvasive Detection of Myocardial Ischemia From Perfusion Reserve Based on Cardiovascular Magnetic Resonance. *Circulation*, 101:1379–1383, 2000.

N. Al-Saadi, M. Gross, A. Bornstedt, B. Schnackenburg, C. Klein, E. Fleck, and E. Nagel. Vergleich verschiedener Parameter zur Bestimmung eines Index der myokardialen Perfusionsreserve zur Erkennung von Koronarstenosen mit kardiovaskulärer Magnetresonanztomographie. *Clinical Research in Cardiology*, 90(11):824–834, 2001.

Allyn & Bacon. Blood flow through the heart, 2004. `http://www.abacon.com/dia/exphys/one.html`; [Online accessed 14-November-2007].

Statistic Austria. Todesursachen, 2006. `http://www.statistik.at/web_de/statistiken/gesundheit/todesursachen/index.html`; [Online accessed 19-November-2007].

Faiza Behloul, Boudewijn P. F. Lelieveldt, Rob J. van der Geest, and Johan H. C. Reiber. A Virtual Exploring Robot for Adaptive Left Ventricle Contour Detection in Cardiac MR Images. In *Proceedings of Medical Image Computing and Computer-Assisted Intervention*, pages 1287–1288. Springer, 2001.

J. Bogaert, S. Dymarkowski, and A.M. Taylor. *Clinical Cardiac MRI*. Springer, 2005.

M. D. Cerqueira, N. J. Weissman, V. Dilsizian, A. K. Jacobs, S. Kaul, W. K. Laskey, D. J. Pennell, J. A. Rumberger, T. Ryan, and M. S. and Verani. Standardized myocardial segmentation and nomenclature for tomographic imaging of the heart: a statement for healthcare professionals from the Cardiac Imaging Committee of the Council on Clinical Cardiology of the American Heart Association. *Circulation*, 105(4):539–542, 2002.

T.F. Christian, D.W. Rettmann, A.H. Aletras, S.L. Liao, J.L. Taylor, R.S. Balaban, and A.E. Arai. Absolute myocardial perfusion in canines measured by using dual-bolus first-pass MR imaging. *Radiology*, 232(3):677–84, 2004.

T. F. Cootes, C. J. Taylor, D. H. Cooper, and J. Graham. Active shape models - their training and application. *Computer Vision and Image Understanding*, 61(1):38–59, 1995.

T. F. Cootes, G. J. Edwards, and C. J. Taylor. Active Appearance Models. *Lecture Notes in Computer Science*, 1407:484–498, 1998.

Robert R. Edelman. Contrast-enhanced MR Imaging of the Heart: Overview of the Literature. *Radiology*, 232:653–668, 2004.

D. T. Gering. Automatic Segmentation of Cardiac MRI. In *Proceedings of Medical Image Computing and Computer-Assisted Intervention*, pages 524–532. Springer, 2003.

S. Graf, A. Khorsand, G. Stix, S. Nekolla, A. Becherer, K. Kletter, R. Dudczak, H. Sochor, G. Maurer, and G. Porenta. Attenuation correction for myocardial perfusion imaging. A comparison between SPECT and PET imaging by polar map analysis. *Nuklearmedizin*, 45(4):171–176, 2006.

B. Kaiser, S. Globits, H. Mayr, M. Mittendorfer, and E. Salomonowitz. Myokardiale First-Pass-Perfusionsdiagnostik mittels Magnetresonanztomographie. *Journal für Kardiologie*, 10:26–31, 2003.

Michael R. Kaus, Jens von Berg, Jürgen Weese, Wiro Niessen, and Vladimir Pekar. Automated segmentation of the left ventricle in cardiac MRI. *Medical Image Analysis*, 8:245–254, 2004.

Anja Kuß. Techniken zur Exploration myokardialer Perfusionsdaten. Master's thesis, Otto-von-Guericke-Universität Magdeburg, 2006.

H. Lippert, D. Herbold, and W. Lippert-Burmester. *Anatomie Text und Atlas*. Urban & Fischer, 2002.

J. Milles, R. J. van der Geest, M. Jerosch-Herold, J. H. C. Reiber, and B. P. F. Lelieveldt. Fully Automated Registration of First-Pass Myocardial Perfusion MRI Using Independent Component Analysis. In *Proceedings of Information Processing in Medical Imaging*, volume 4584, pages 544–555. Springer, 2007.

Steven C. Mitchell, Johan G. Bosch, Boudewijn P. F. Lelieveldt, Rob J. van der Geest, Johan H. C. Reiber, and Milan Sonka. 3-D Active Appearance Models: Segmentation of Cardiac MR and Ultrasound Images. *IEEE Trans. Med. Imaging*, 21(9):1167–1178, 2002.

J. Montagnat and H. Delingette. 4D Deformable Models with temporal constraints: application to 4D cardiac image segmentation. *Medical Image Analysis*, 9(1):87–100, 2005.

Sharon L. Mulvagh, Anthony N. DeMaria, Steven B. Feinstein, Peter N. Burns, Sanjiv Kau, James G. Miller, Mark Monaghan, Thomas R. Porter, Leslee J. Shaw, and Flordeliza S. Villanueva. Contrast Echocardiography: Current and Future Applications. *American Society of Echocardiography Task Force on Standards and Guidelines for the Use of Ultrasonic Contrast in Echocardiography*, 13(4):331–342, 2000.

Eike Nagel, Christoph Klein, Ingo Paetsch, Sabine Hettwer, Bernhard Schnackenburg, Karl Wegscheider, and Eckart Fleck. Magnetic Resonance Perfusion Measurements for the Noninvasive Detection of Coronary Artery Disease. *Circulation*, 108:432–437, 2003.

Steffen Oeltze, A. Kuß, F. Grothues, Anja Hennemuth, and Bernhard Preim. Integrated Visualization of Morphologic and Perfusion Data for the Analysis of Coronary Artery Disease. In *Proceedings of EuroVis06: Joint Eurographics - IEEE VGTC Symposium on Visualization*, pages 131–138. Eurographics Association, 2006.

Steffen Oeltze, Helmut Doleisch, Helwig Hauser, Philipp Muigg, and Bernhard Preim. Interactive visual analysis of perfusion data. *IEEE Transactions on Visualization and Computer Graphics*, 13(6):1392–1399, 2007.

H. Ólafsdóttir. Registration and analysis of myocardial perfusion MRI. Master's thesis, Informatics and Mathematical Modelling, Technical University of Denmark, DTU, 2004.

H. Ólafsdóttir. Nonrigid registration of myocardial perfusion MRI. In *Proceedings of Svenska Symposium i Bildanalys, SSBA 2005, Malmø, Sweden*, 2005.

C. Pluempitiwiriyawej and S. Sotthivirat. Active Contours With Automatic Initialization For Myocardial Perfusion Analysis. In *Proceedings of Engineering in Medicine and Biology Society*, pages 3332–3335. IEEE, 2005.

Charnchai Pluempitiwiriyawej, José M. F. Moura, Yi-Jen Lin Wu, and Chien Ho. STACS: new active contour scheme for cardiac MR image segmentation. *IEEE Transactions on Medical Imaging*, 24(5):593–603, 2005.

Vincenzo Positano, Maria Filomena Santarelli, and Luigi Landini. Automatic Characterization of Myocardial Perfusion in Contrast Enhanced MRI. *EURASIP Journal on Applied Signal Processing*, 2003(5):413–421, 2003.

Willibald Pschyrembel. *Klinisches Wörterbuch*. de Gruyter, 2002.

All refer health. Pictures and Images, 2008. `http://health.allrefer.com/pictures-images/`; [Online accessed 18-Februar-2008].

J. Schwitter, D. Nanz, S. Kneifel, K. Bertschinger, M. Bchi, P.R. Knsel, B. Marincek, T.F. Lscher, and G.K. von Schulthess. Assessment of Myocardial Perfusion in Coronary Artery Disease by Magnetic Resonance. *Circulation*, 103:2230–2235, 2001.

W. Sörgel and V. Vaerman. Automatic heart localization from a 4D MRI dataset. In *Proceedings of SPIE Medical Imaging 1997: Image Processing*, volume 3034, pages 333–344. SPIE, 1997.

L.J. Spreeuwers and M. Breeuwer. Automatic Detection of Myocardial Boundaries in MR Cardio Perfusion Images. In *Proceedings of Medical Image Computing and Computer-Assisted Intervention*, pages 1228–1231. Springer, 2001.

L.J. Spreeuwers and M. Breeuwer. Detection of left ventricular epi-and endocardial borders using coupled active contours. In *Proceedings of Computer Assisted Radiology and Surgery*, pages 1147–1152. Elsevier, 2003.

L.J. Spreeuwers, F. Wierda, and M. Breeuwer. Automatic correction of myocardial boundaries in MR cardio perfusion analysis. In *Proceedings of Computer Assisted Radiology and Surgery*, pages 902–907. Elsevier, 2002.

L.J. Spreeuwers, F. Wierda, and M. Breeuwer. Optimal Myocardial Boundary Estimation for MR Cardio Perfusion Measurements Using Sensitivity Analysis. In *Proceedings of Computers in Cardiology*, pages 197–200. IEEE, 2002.

M.B. Stegmann and H.B.W. Larsson. Motion-Compensation of Cardiac Perfusion MRI Using a Statistical Texture Ensemble. In *Proceedings of Functional Imaging and Modeling of the Heart*, pages 151–161. Springer, 2003.

M. B. Stegmann, H. Ólafsdóttir, and H. B. W. Larsson. Unsupervised motion-compensation of multi-slice cardiac perfusion MRI. *Medical Image Analysis*, 9(4):394–410, 2005.

Y. Sun, M.-P. Jolly, and J. M. F. Moura. Contrast-Invariant Registration of Cardiac and Renal MR Perfusion Images. In *Proceedings of Medical Image Computing and Computer-Assisted Intervention*, pages 903–910. Springer, 2004.

G. Thews, E. Mutschler, and P. Vaupel. *Anatomie Physiologie Pathophysiologie des Menschen*. Wissenschaftliche Verlagsgesellschaft mbH Stuttgart, 1999.

H. C. van Assen, R. J. van der Geest, M. G. Danilouchkine, H. J. Lamb, J. H. C. Reiber, and B. P. F. Lelieveldt. 3D active shape model matching for left ventricle segmentation in cardiac CT. In *Proceedings of SPIE Medical Imaging*, volume 5032, pages 384–393. SPIE, 2003.

Hans C. van Assen, Mikhail G. Danilouchkine, Faiza Behloul, Hildo J. Lamb, Rob J. van der Geest, Johan H. C. Reiber, and Boudewijn P. F. Lelieveldt. Cardiac LV Segmentation Using a 3D Active Shape Model Driven by Fuzzy Inference. In *Proceedings of Medical Image Computing and Computer-Assisted Intervention*, pages 533–540. Springer, 2003.

Hans C. van Assen, Mikhail G. Danilouchkine, Alejandro F. Frangi, Sebastián Ordas, Jos J. M. Westenberg, Johan H. C. Reiber, and Boudewijn P. F. Lelieveldt. SPASM: Segmentation of Sparse and Arbitrarily Oriented Cardiac MRI Data Using a 3D-ASM. In *Proceedings of Functional Imaging and Modeling of the Heart*, pages 33–43. Springer, 2005.

Paul Viola and William M. Wells. Alignment by maximization of mutual information. *International Journal of Computer Vision*, 24(2):137–154, 1997.

WHO. World health organisation, 2007. `http://www.who.int`; [Online accessed 13-Februar-2008].

N. Wilke, M. Jerosch-Herold, Y. Wang, Y. Huang, B.V. Christensen, A.E. Stillman, K. Ugurbil, K. McDonald, and R.F. Wilson. Myocardial perfusion reserve: assessment with multisection, quantitative, first-pass MR imaging. *Radiology*, 204(2):373–84, 1997.

S.D. Wolff, J. Schwitter, R. Coulden, M.G. Friedrich, D.A. Bluemke, R.W. Biederman, E.T. Martin, A.J. Lansky, F. Kashanian, T.K.F. Foo, P.E. Licato, and C.R. Comeau. Myocardial First-Pass Perfusion Magnetic Resonance Imaging: A Multicenter Dose-Ranging Study. *Circulation*, 110:732–737, 2004.

K.K. Wong, E.X. Wu, M.C. Ng, Y. Wu, H.F. Tse, C.P. Lau, G. Lo, and E.S. Yang. Image Registration in Myocardial Perfusion MRI. In *Proceeding of IEEE Engineering in Medicine and Biology*, volume 1, pages 453–454. IEEE, 2005.

Chenyang Xu and Jerry L. Prince. Gradient Vector Flow: A New External Force for Snakes. In *CVPR*, pages 66–, 1997.

G.Z. Yang, P.D. Gatehouse, J. Panting, P. Burger, D.J. Pennell, and D.N. Firmin. Motion analysis for magnetic resonance myocardial perfusion imaging. In *Proceedings of Image Processing and Its Applications*, volume 2, pages 838–842, 1997.

J.-Y. Yeh, J. C. Fu, C. C. Wu, H. M. Lin, and J. W. Chai. Myocardial border detection by branch-and-bound dynamic programming in magnetic resonance images. *Computer Methods and Programs in Biomedicine*, 79(1):19–29, 2005.

S. Zambal, A. Schöllhuber, K. Bühler, and J. Hladůvka. Fast and Robust Localization of the Heart in Cardiac MRI Series. *International Conference on Computer Vision Theory and Applications*, 1:341–346, 2008.